Spring 1-1-2013

Wave Driven Disturbances of the Thermal Structure in the Polar Winter Upper Stratosphere and Lower Mesosphere

Katelynn R. Greer
University of Colorado Boulder, greer.katelynn@gmail.com

Recommended Citation

Greer, Katelynn R., "Wave Driven Disturbances of the Thermal Structure in the Polar Winter Upper Stratosphere and Lower Mesosphere" (2013). *Aerospace Engineering Sciences Graduate Theses & Dissertations*. 73.
https://scholar.colorado.edu/asen_gradetds/73

Wave Driven Disturbances of the Thermal Structure in the Polar Winter Upper Stratosphere and Lower Mesosphere

by

Katelynn R. Greer

B.S., University of Colorado, 2007

M.S., University of Colorado, 2009

A thesis submitted to the

Faculty of the Graduate School of the

University of Colorado in partial fulfillment

of the requirements for the degree of

Doctor of Philosophy

Department of Aerospace Engineering Sciences

2013

This proposal entitled:
Wave Driven Disturbances of the Thermal Structure in the Polar Winter Upper Stratosphere and Lower Mesosphere
written by Katelynn R. Greer
has been approved for the Department of Aerospace Engineering Sciences

Prof. Jeffrey P. Thayer

Prof. Scott E. Palo

Date ____________________

The final copy of this thesis has been examined by the signatories, and we find that both the content and the form meet acceptable presentation standards of scholarly work in the above mentioned discipline.

Greer, Katelynn R. (Ph.D., Aerospace Engineering Sciences)

Wave Driven Disturbances of the Thermal Structure in the Polar Winter Upper Stratosphere and Lower Mesosphere

Thesis directed by Prof. Jeffrey P. Thayer

The polar winter middle atmosphere is a dynamically active region that is driven primarily by wave activity. Planetary waves intermittently disturbed the region at different levels and the most spectacular type of disturbance is a major Sudden Stratospheric Warming (SSW). However, other types of extreme disturbances occur on a more frequent, intraseasonal basis. One such disturbance is a synoptic-scale “weather event” observed in lidar and rocket soundings, soundings from the TIMED/SABER instrument and UK Meteorological Office (MetO) assimilated data. These disturbances are most easily identified near 42 km where temperatures are elevated over baseline conditions by a remarkable 50 K and an associated cooling is observed near 75 km. As these disturbances have a coupled vertical structure extending into the lower mesosphere, they are termed Upper Stratospheric/Lower Mesospheric (USLM) disturbances. This research begins with description of the phenomenology of USLM events in observations and the assimilated data set MetO, develops a description of the dynamics responsible for their development and places them in the context of the family of polar winter middle atmospheric disturbances.

Climatologies indicates that USLM disturbances are commonly occurring polar wintertime disturbances of the middle atmosphere, have a remarkably repeating thermal structure, are located on the East side of the polar low and are related planetary wave activity. Using the same methodology for identifying USLM events and building climatologies of these events, the Whole Atmosphere Community Climate Model *WACCM* version 4 is established to spontaneously and internally generate USLM disturbances. Planetary waves are seen to break at a level just above the stratopause and convergence of the EP-flux vector is occurring in this region, decelerating the eastward zonal-mean wind and inducing ageostrophic vertical motion to maintain mass continuity.

The descending air increases the horizontal temperature gradient at 2 hPa and is responsible for the stratopause warming. Embedded in this planetary wave breaking process is baroclinic instability, as indicated by the Charney-Stern criteria and an EP-flux analysis decomposed by planetary and synoptic-scale waves.

It is recognized that USLM events are part of a family of disturbances that occur in the polar winter middle atmosphere which have the potential to impact the entire atmospheric column. Relationships between USLM events, minor SSWs and major SSWs are examined and displayed through a Venn diagram which looked for events that were linked to each other (or not) by temporal evolution of the polar vortex within 14 days. Critically, every identified major SSW (in both MetO and WACCM) is preceded by a USLM disturbance, and the baroclinic instability that is embedded in the planetary wave breaking of USLM disturbances mark significant disruption to the middle atmosphere, which may aid in the forecast of major SSWs. This leads to the proposal of new *dynamics based* definitions of minor and major SSWs.

Dedication

To Doug and Claudell Greer, my parents. There is so much to thank you for- from allowing science projects in your microwave to setting up a telescope to view the Hale-Bopp comet to little things like patiently listening to my babbling about science. You are my foundation.

To J. Kyle Doyle, my close friend. You are always in my heart and mind. *Consider my promise fulfilled.*

Over the past 6 years I have received support and encouragement from a great number of individuals. Thank you to my sister, Jenna Baumann, who is just similar enough to me that you nearly always understand my motivations but different enough that we can have a roaring good conversation. Thank you to my close friends who have been on this strange project of studying fruit fly sex with me (some have had to bear it longer than others): Scott & Laura Potter, Tyler & Michelle Redick, AJ Lindell, Jaime Redick, Jenn Reiter, Katelynn McCalmont, Tirzah & TJ Seitenbach, and James Everton. Ann Bellows, you have been a constant source of support and have always pushed me to look at the world differently. Russ Brown, thank you for taking an interest in me and helping through the best and the worst times of my life. I would like to thank my lab mates; most especially Steve Mitchell, Matt Hayman & Loren Chang for helping me through challenges, lending a caring ear, and great source of advice. In addition, Robert Stillwell, Vu Nguyen, Cody Vaudrin (hurry up and graduate already!), Vicki Hsu and Greg Lucas for being the best lab mates one could hope for! Thank you to my thesis committee: Prof. Scott E. Palo, Dr. V. Lynn Harvey, Dr. Hanli Liu & Prof. Baylor Fox-Kemper. I would also like to thank Prof. Cora E. Randall for her support and assistance in times of paperwork related crises and Prof. Xinzhao Chu for always encouraging me. Lastly, but certainly not least, I would like to thank Professor Jeffrey P. Thayer. Little did I know that when you taught my junior level thermodynamics course that you would be the catalyst for my love of research and that a mere 7 years later I would still be working with you and learning from you on the way to a PhD. Jeff, thank you so much for your support, your belief in my potential, your patience with me, and all the opportunities you helped make possible- few are as lucky as I have been to have had a first-class PhD advisor *and* extraordinary mentor.

Acknowledgements

This work was supported by NSF grant ATM-0454999 and AGS-0940174. We would like to thank the NASA TIMED mission for providing the ready access to the SABER 1.07 temperature data set. We also appreciate the BADC for supplying access to the UK MetO data: UK Meteorological Office, [Swinbank, R., et al. "Stratospheric Assimilated Data." British Atmospheric Data Centre. 2006. http://badc.nerc.ac.uk/data/assim/ (accessed January 10, 2011).

Contents

Chapter

Appendix

Tables

Table

Figures

Figure

Chapter 1

Introduction

1.1 Research Impact

This thesis focuses on the dynamical mechanisms responsible for thermal structure variability in the polar winter middle atmosphere. Here we establish an observed anomalous thermal structure (Upper Stratosphere Lower Mesosphere $USLM$ disturbances) as re-occurring synoptic weather events and describe the coupled thermal and dynamical mechanisms responsible for its formation. Observations, assimilated data and numerical models have been used to develop criteria for identifying USLM disturbances, establish their climatology, and examine their development within the context of breaking planetary waves, wave-mean flow interactions, vertical indirect circulations and the potential to support baroclinic instabilities in the polar winter middle atmosphere. The tangible impacts of this work include three publications [84][25][26] and contribute to advancing the field of aeronomy by providing a deeper understanding of the mechanisms of natural variability in the polar winter middle atmosphere. This research will contribute to an overarching goal of the community to improve prediction of the large scale restructuring of the polar vortex during active winters.

The outcomes of this research include:

- Identified the USLM thermal structure as a synoptic-scale feature of polar wintertime disturbances that are dynamically driven by planetary waves
- Established criteria for identifying USLM events in observations, assimilated data sets and

models; showing that Whole Atmosphere Community Climate Model (WACCM) spontaneously and internally generates USLMs that match the observed characteristics

- Developed climatologies detailing frequency of occurrence, duration, geographical preference, composited structure and morphology in assimilated data and the WACCM model in both hemispheres
- Determined breaking planetary waves near 49 km altitude could produce conditions to support baroclinic instability on the East side of the polar vortex. This is established as the likely mechanism leading to front-like behavior in the polar middle atmosphere
- Identified critical relationships of USLM disturbances with minor and major SSWs and may assist in the prediction of major SSWs. Propose an initial iteration of dynamics-based definitions of SSWs. This will advance ability to predict large-scale disturbances of the entire atmospheric column from the troposphere to the thermosphere and ionosphere
- Associated mesosphere coolings (separated mesopause) and stratopause folds with USLM events

1.2 Geophysical Dynamics of the Polar Winter Middle Atmosphere

The polar winter middle atmosphere is dominated by the highly variable polar vortex; a belt of high-speed Westerlies that setup each winter and separates warm air of the mid-latitudes from the cold polar air. The vertical temperature structure of the winter polar middle atmosphere is a balance between net long wave radiation cooling and net heat transport (plus local temperature changes due to adiabatic heating). Air from the warm summer pole rises and drifts toward the winter pole, generating a meridional circulation. This meridional circulation is driven by eddies and helps balance the differential heating caused by the tilt of Earth's axis [3]. In general, temperature increases with altitude throughout the stratosphere until the stratopause (which is highly variable in altitude); after which the temperature decreases with altitude in the mesosphere. The wintertime polar stratopause is created by the indirect dynamic circulation of the polar vortex and adiabatic heating of air sinking over the pole [50]. The existence of the polar vortex is a function of the rotation rate of earth and the temperature gradient between the pole and the equator. In the winter, when the temperature gradient is especially strong, the westerly zonal mean flow feeds eddies and local instabilities[3]. Typically, there is also an associated area of weak high pressure, known as the Aleutian High[28]. Under typical winter conditions, a strong polar vortex sits over the pole and extends vertically through the stratosphere and mesosphere.

1.3 Disturbances of the Polar Winter Middle Atmosphere

Periodically throughout the polar wintertime, the middle atmosphere becomes disturbed. The Aleutian High may amplify, displacing the polar vortex off of the pole. The temperature structure may also be altered; portions of the stratosphere may become warmer than normal and regions of the mesosphere may become cooler than normal. The strongest disturbance to the middle atmosphere is a major Sudden Stratospheric Warming, which may disturb the entire atmospheric column, from the troposphere to the thermosphere on a planetary scale. During major Sudden Stratospheric Warmings, the polar vortex is extremely disturbed, may be strongly displaced off the pole, split into two smaller vortices or completely broken up. It can take several weeks for the vortex to recover to nominal conditions after a major Sudden Stratospheric Warming. Other known disturbances include minor Sudden Stratospheric Warmings, in which the thermal structure of the middle atmosphere is strongly disturbed but the polar vortex remains intact, Canadian warmings in which the Aleutian high becomes anomalously strong, and Final warmings where the polar vortex breaks down in the spring as the middle atmosphere transitions to summer conditions. Upper Stratosphere Lower Mesosphere (USLM) disturbances are synoptic-scale disturbances in which the thermal structure is defined by an anomalously hot stratopause located at the low altitude of 42 km (2 hPa), a separated mesopause near 75 km, and an intact polar (although disturbed) vortex. Major Sudden Stratospheric Warmings are believed to require pre-conditioning; minor Sudden Stratospheric Warmings are believed to be a required precondition and USLM disturbances are also a required pre-condition.

1.4 Observational Challenges

Traditional measurements of the stratosphere and mesosphere temperatures have included radiosondes, Michelson interferometers (OH*), rockets, and lidar. Although there is an extensive network of radiosonde launches, they do not reach altitudes greater than 30 km. The OH* airglow measured by the Michelson interferometer is confined to discrete altitudes in the mesosphere, around 87 km. Rockets are expensive, infrequently launched, and only launched in specific geographic locations. Although lidars can take continuous measurements with excellent vertical resolution, they are generally ground based and therefore provide geographic point profiles of the atmosphere. Given these observation sets, while still of great value, the data coverage is generally sporadic in space and time.

Global coverage of stratospheric and mesospheric data sets with good vertical resolution (less than 5 km) have only recently become available. These are in the form of satellite measurements leading to improved assimilated data sets. Assimilated data sets use observations from a variety of sources and models to produce a three-dimensional state of the atmosphere.

Also recently available are sophisticated atmospheric models that extend from the ground into the thermosphere (over 110 km in altitude). These comprehensive models include atmospheric chemistry, oceans, solar inputs and even gravity wave parameterizations. Models may be forced by re-analysis data or run freely allowing the atmosphere to evolve autonomously.

Data from ground-based observations, space-based systems, assimilated data set and models will be used in this thesis.

1.5 Thesis Overview

This thesis comprises 8 chapters of the following content:

- **Chapter 1:** Statements of the motivation and purpose of this thesis, impacts and contributions to the aeronomy field, as well as a brief overview of background of the polar winter dynamics, structure and challenges of this research.

- **Chapter 2:** This chapter contains more detailed descriptions of the geophysical fluid mechanics of the polar winter middle atmosphere, starting with the primitive equations and developing them toward the quasi-geostrophic system. Potential vorticity, waves, EP-flux and instabilities are also mathematically developed. The historical context of disturbances to the polar winter atmosphere and the various types of weather events experienced by the polar winter middle atmosphere are also described.

- **Chapter 3:** This chapter contains description of the data and methodologies used in this thesis. Observational data includes Lidar measurements, rocketsonde data, and observations from the Thermosphere-Ionosphere Mesosphere Energetics and Dynamics (TIMED) satellite's instrument Sounding of the Atmosphere using Broadband Emission Radiometry (SABER) instrument. The UK Meteorology Office stratospheric assimilated data (MetO or UKMO) extends up to 0.1 hPa on 66 pressure surfaces daily since December 1991. The model used is the Whole Atmosphere Community Climate Model (WACCM), version 4, which is a global chemistry climate model developed by the National Center for Atmospheric Research (NCAR).

- **Chapter 4:** This chapter describes the characteristics of USLM disturbances (including a case study), the USLM event identification algorithm for daily data sets, and climatological features of USLM events.

- **Chapter 5:** This chapter develops the coupled thermal and dynamical mechanisms responsible for the development of USLM disturbances using both assimilated and model data. USLM disturbances are baroclinic instabilities embedded within a breaking planetary wave in the lower mesosphere which results in indirect circulation and extreme temperatures at the stratopause level of 42 km. EP-flux divergence of USLM disturbances separated into planetary and synoptic scale components is used to disentangle planetary wave activity from baroclinic instability activity.

- **Chapter 6:** This chapter develops the relationships between minor Sudden Stratospheric Warming, major Sudden Stratospheric Warming and USLM events. Venn diagrams are used to illustrate relationships and required preconditioning for different disturbances.
- **Chapter 7:** This chapter contains descriptions and analysis of phenomena associated with USLM disturbances that impact the structure and dynamics of the winter polar middle atmosphere, specifically, mesospheric cooling, vertical transport of chemically active tracers, and stratopause folds.
- **Chapter 8:** This chapter summarizes the thesis and provides an outlook for future work to continue the development toward deeper understanding of the natural variability of the polar winter middle atmosphere.

Chapter 2

Background

2.1 Introduction: Description of the Middle Atmosphere

The middle atmosphere is generally regarded as the portion of Earth's atmosphere between the tropopause and the homopause, or between approximately 10 km and 110 km in altitude above the surface of Earth. This region encompasses the stratosphere and the mesosphere.

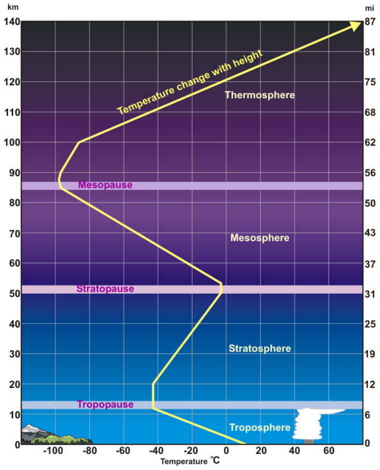

Figure 2.1: Temperature profile of the standard atmosphere with height during nominal conditions (This figure has been adapted from [95]).

The atmosphere is divided into layers based on temperature gradient. Figure 2.1 is a general depiction of the temperatures and different regions of our atmosphere from the surface to 140 km in altitude. The region of interest to this study is the stratosphere and mesosphere, which will include both the stratopause (generally at a winter altitude of approximately 50 km and temperature of approximately 260 K) and mesopause (generally located in the winter at an altitude of 100 km and 210 K).

The vertical temperature structure of the winter Arctic middle atmosphere is a balance between net long wave radiation cooling and net heat transport (plus the local temperature change due to adiabatic heating). Air from the warm summer pole rises and drifts toward the winter pole, generating a meridional circulation. This meridional circulation is driven by eddies and helps balance the differential heating caused by the tilt of Earth's axis [3]. In general, temperature increases with altitude throughout the stratosphere until the stratopause (which is highly variable in altitude); after which the temperature decreases with altitude in the mesosphere. The wintertime Arctic stratopause is created by the interhemispheric residual circulation, indirect circulation of the polar vortex and adiabatic heating of air sinking over the pole [50]. The dynamic structure of the winter Arctic middle atmosphere is dominated by the polar vortex, which can be quite variable in the Northern Hemisphere. The existence of the polar vortex is a function of the rotation rate of earth and the temperature gradient between the pole and the equator. In the winter, when the temperature gradient is especially strong, the westerly zonal mean flow feeds eddies and instabilities [3]. Typically, there is also an associated area of weakly high pressure, known as the Aleutian High in the Northern Hemisphere. Under typical winter conditions, a strong polar vortex sits over the pole and extends vertically through the upper troposphere, the stratosphere and mesosphere.

Periodically throughout the polar wintertime, the middle atmosphere becomes disturbed. The Aleutian High may amplify, displacing the polar vortex off of the pole; some scientific communities refer to this as amplification of planetary wave 1 (S1). The temperature structure may also be altered; portions of the stratosphere may become warmer than normal and regions of the mesosphere may become cooler than normal. Ageostrophic vertical circulations may also become enhanced during these times resulting in regions of adiabatic heating and cooling.

The atmosphere, as a fluid, may support a great variety of wave types. Waves are usually classified by their restoring force: 'gravity waves' have gravity or buoyancy as a restoring force, while the restoring force for Rossby waves (also generally referred to as 'planetary waves' for their planetary scale) is the conservation of potential vorticity. Other waves, such as acoustic waves, are of such small scale and high frequency that they are not of interest here. In the troposphere, planetary waves can be seen in the kinks of the polar jet stream. In the middle atmosphere, amplification of planetary wave 1 is usually observed as an amplification of the Aleutian high and the displacement of the polar vortex off of the pole. The polar winter middle atmosphere also has the potential to generate instabilities. An instability is a perturbation which may amplify or decay, and is the tendency of the atmosphere to support vertical motion.

2.2 Geophysical Fluid Mechanics in the Polar Winter Middle Atmosphere

2.2.1 Development of the Governing System of Equations

Geophysical fluid mechanics generally concerns all naturally occurring fluid motions. While the scales and compositions of oceans, rivers and the atmosphere vary, they can all be described by the same set of equations. This set of equations includes the momentum, continuity and thermodynamic equations. These equations can be further simplified by using the appropriate assumptions for the fluid; in this work the fluid is the middle atmosphere. The fluid here is assumed to be compressible gas on a rotating sphere, that the fluid is shallow and that the distance anywhere in the atmosphere to the center of the earth a is roughly equivalent to the radius of the the earth r. Since this work is concerned with large scale motions, the vertical momentum equation may be replaced by the hydrostatic balance and the horizontal component of the Coriolis force is small compared to the vertical component and may also be neglected.

The spherical coordinates used are longitude λ, latitude ϕ (+90 at the North Pole), and a vertical coordinate of 'log-pressure height'. See appendix A for a list of symbols. The use of log-pressure height instead of geometric height simplifies as

$$z \equiv -H \ln(\frac{p}{p_s}) \tag{2.1}$$

Where H is the scale height, p is the pressure and p_s is a standard pressure. Using log-pressure height and spherical coordinates the *primitive equations* are written as [3]

$$\frac{Du}{Dt} - (f + \frac{u \tan \phi}{a})v + \frac{\Phi_\lambda}{a \cos \phi} = X \tag{2.2}$$

$$\frac{Dv}{Dt} + (f + \frac{u \tan \phi}{a})u + \frac{\Phi_\phi}{a} = Y \tag{2.3}$$

$$\Phi_z = H^{-1} R\theta \exp^{-\kappa z/H} \tag{2.4}$$

$$\frac{u_\lambda + (v \cos \phi)_\phi}{a \cos \phi} + \frac{(\rho_0 w)_z}{\rho_0} = 0 \tag{2.5}$$

$$\frac{D\theta}{Dt} = Q \tag{2.6}$$

These equations represent the zonal momentum equation (2.2), meridional momentum equation (2.3), the hydrostatic balance or vertical momentum equation (2.4), continuity equation(2.5) and thermodynamic equation (2.6). Subscripts denote partial derivatives, while D/Dt is a total derivative (sum of advection and local change) representing the total time rate of change following the fluid motion. X and Y represent nonconservative forces such as friction; Q is the diabatic heating. However, in the polar winter night for periods less than 7 days, the diabatic cooling may be neglected and studies of large scale motions may also neglect friction. f is the Coriolis parameter which results from the rotation of the Earth.

A further simplification may be realized by considering the scale of the phenomena of interest. As currently written, these equations may capture everything from tiny sound waves to great curves of the jet stream. However, some studies may be unnecessarily complicated (and computational expensive) by the inclusion of sound waves and other (relatively) small phenomenon. A further complication arises from the appearance of density ρ in the primitive equations. Since both pressure and density decrease monotonically throughout the atmosphere, the ideal gas relation can be used to replace density in the equations. Where pressure is used as the vertical coordinate, the vertical motion will be denoted as $\omega = \frac{\partial p}{\partial t}$. While midlatitude systems assume a disturbance centered at a latitude of 45°, the polar structures studied here are generally located nearer to $\phi_0 = 65°$. Using this, an f-plane approximation of the Coriolis force can be expressed as

$$f_0 = 2\Omega \sin\phi_0 \cong 10^{-4}s^{-1} \tag{2.7}$$

It turns out that the f-plane approximation is not significantly changed by this latitude; the value is accurate to within one order of magnitude. Assuming an f-plane allows for the additional geometric simplification of replacing spherical coordinates (λ, ϕ) by eastward and northward Cartesian coordinates (x, y), which restricts the motion to the area near the latitude ϕ_0. Using a Taylor's expansion, the Coriolis force can be expressed as

$$f = f_0 + \frac{\partial f}{\partial y}y = f_0 + \beta y = 2\Omega \sin\phi_0 + \frac{2\Omega}{a}\cos(\phi_0)y \tag{2.8}$$

And the primitive equations can be expressed in isobaric, Cartesian coordinates as

$$\frac{Du}{Dt} - fv + \Phi_x = X \tag{2.9}$$

$$\frac{Dv}{Dt} + fu + \Phi_y = Y \tag{2.10}$$

$$\Phi_p = \frac{-RT}{p} \tag{2.11}$$

$$\frac{\partial u}{\partial x} + \frac{\partial v}{\partial y} + \frac{\partial \omega}{\partial p} = 0 \tag{2.12}$$

$$\frac{D\theta}{Dt} = \frac{\partial T}{\partial t} + \frac{\partial T}{\partial x} + \frac{\partial T}{\partial y} - S_p\omega = Q \tag{2.13}$$

Where the last term on the right hand side of equation (2.13) is adiabatic heating and the static stability parameter $S_p = -T\frac{\partial \ln\theta}{\partial p}$.

Geostrophic balance is an extreme simplification for large-scale, low-frequency, extra-tropical flows where the Coriolis terms $(-fv, fu)$ in equations (2.9) and (2.10) are exactly balanced by the horizontal gradients of geopotential (Φ_x, Φ_y) and there is no geostrophic vertical wind. This balance requires that the ageostrophic velocities (V_a) be significantly smaller than the geostrophic velocities (V_g), or

$$|V_a| \,/\, |V_g| \sim O(Ro) \tag{2.14}$$

and approximately of the order of the Rossby number (Ro). The Rossby number is a non-dimensional number and may be defined several ways, but the most intuitive explanation is that it is the ratio of the relative magnitude of the acceleration of the flow to the Coriolis acceleration(acceleration due the rotation of Earth). Thus, when the Rossby number is small, rotation effects are important[88]. The characteristic scales of the motion of interest based on observations for a high-latitude synoptic system are[31]

$2\Omega \sim 1.4 * 10^{-4} s^{-1}$	Earth rotation
$U \sim 15 m s^{-1}$	horizontal velocity scale
$V \sim 1.5 m s^{-1}$	horizontal velocity scale
$W \sim 10^{-2} m s^{-1}$	vertical velocity scale
$L \sim 10^6 m$	length scale
$H \sim 7 * 10^3 m$	depth scale
$X \sim 10^{-4} m s^{-2}$	zonal non-conservative forcing scale
$Y \sim 10^{-4} m s^{-2}$	meridional non-conservative forcing scale
$Q \sim 5 * 10^{-5} K s^{-1}$	adiabatic heating rate scale
$\delta P/p \sim 10^3 m^2 s^{-2}$	horizontal pressure fluctuation scale
$L/U \sim 10^5 s$	time scale

The time scale is based on the synoptic advective time scale and the horizontal pressure change is normalized by the density to account for the exponentially decreasing pressure and density with increasing height in the atmosphere. Applying these scales to find the Rossby number by taking the ratio of the acceleration of the flow to the acceleration due to the Coriolis force results in

$$Ro \equiv (U^2/L)/(2\Omega U) = U/(2\Omega L) \sim 0.1 \tag{2.15}$$

The high-latitude middle atmosphere scales indicate that the the Rossby number is less than one ($R_o < 1$), meaning that the rotation term dominates the nonlinear advection terms in the zonal momentum equations. When the Rossby number is very small, the flow generally is in geostrophic balance. The wind may be separated into geostrophic and ageostrophic portions as $u = u_g + u_a$, $v = v_g + v_a$, and $\omega = \omega_a$ (there is no vertical wind under geostrophic balance). In addition, the Rossby radius of deformation is between 1000 km and 2000 km. Using geostrophic balance, the horizontal momentum balance may be written as

$$u_g = -\frac{1}{f_0}\Phi_y \tag{2.16}$$

$$v_g = -\frac{1}{f_0}\Phi_x \tag{2.17}$$

Because the horizontal geostrophic velocities are non-divergent and the Coriolis parameter is accounted for by the constant f_0, we can also introduce a geostrophic stream function ψ where

$$\psi \equiv f_0^{-1}\left(\Phi - \Phi_0\right) \tag{2.18}$$

and

$$u_g = -\psi_y; v_g = \psi_x \tag{2.19}$$

However, geostrophic motion is restrictive and diagnostic only; it lacks a time derivative and therefor cannot be used to predict motion. Using a variation of the simplifications and scaling arguments for geostrophic motion, another system can be derived in which the motion is *quasi-geostrophic*. Again assuming that the Rossby wave number is small (on the order of 0.1), the ratio of the time derivatives to the Coriolis terms in equations (2.9) and (2.10) are small, that the second term in the Taylor series expansion of the Coriolis parameter be small ($\beta L << f_0$) and finally that friction is small, the quasi-geostrophic system of equations is written as

$$\frac{D_g u_g}{Dt} - f_0 v_a - \beta y v_g = X \tag{2.20}$$

$$\frac{D_g v_g}{Dt} + f_0 u_a + \beta y u_g = Y \tag{2.21}$$

$$\frac{\partial u_a}{\partial x} + \frac{\partial v_a}{\partial y} + \frac{\partial \omega}{\partial p} = 0 \tag{2.22}$$

$$\frac{\partial T}{\partial t} + u_g \frac{\partial T}{\partial x} + v_g \frac{\partial T}{\partial y} - \left(\frac{\sigma p}{R}\right) \omega = Q \tag{2.23}$$

where

$$D_g \equiv \frac{\partial}{\partial t} + u_g \frac{\partial}{\partial x} + v_g \frac{\partial}{\partial y} \tag{2.24}$$

is the geostrophic time derivative and $\sigma \equiv -RT_0 p^{-1}$. T_0 is a basic state temperature. The quasi-geostrophic system was first developed by Charney [1948], but Holton [2004] and Andrews, Holton & Leovy [1987] also give excellent (and more complete) derivations of the quasi-geostrophic system.

Although the system now includes time evolution, strictly speaking, it is not suitable for a prediction system. For this purpose, the evolution of the potential vorticity has been found to be extremely useful. Vorticity is a measurement of the microscopic spin (or rotation) in a fluid and is mathematically defined as the curl of the velocity ($\nabla \times V$). In a rotating reference frame vorticity can be split into two components: absolute vorticity η and relative vorticity ζ. Both relative and absolute vorticity are dominated by their vertical components, so only that component will be retained here. Given Earth's rotation, the absolute vorticity is the sum of the relative vorticity (local u and v) and the Coriolis parameter

$$\zeta = \frac{\partial v}{\partial x} - \frac{\partial u}{\partial y} \tag{2.25}$$

$$\eta = \frac{\partial v}{\partial x} - \frac{\partial u}{\partial y} + f \tag{2.26}$$

Potential vorticity is a concept where given adiabatic frictionless conditions, the quantity is conserved following the motion of the fluid. Using isentropic surfaces, potential vorticity is the ratio of the absolute vorticity to the separation of isentropic surfaces. Quantitatively, it can be defined in multiple vertical coordinate systems, here it will be defined using isentropic (potential temperature) surfaces because of potential vorticity's conservation properties in this coordinate.

$$IPV = -g\left[f + \frac{\partial v}{\partial x} - \frac{\partial u}{\partial y}\right] / \frac{\partial p}{\partial \theta} \tag{2.27}$$

The derivation of this form of potential vorticity applies the hydrostatic approximation but makes no assumption of balanced geostrophic flow. However, potential vorticity can also be approximated using the Rossby number and quasi-geostrophic flow. Taking the curl of equations (2.20) and (2.21) and using the quasi-geostrophic continuity equation (see Holton [2004] or Andrews, Holton & Leovy [1987]for more detailed description of the derivation) the quasi-geostrophic potential vorticity is written in terms of the stream function and pressure as a vertical coordinate as

$$q = \underbrace{f}_{A} + \underbrace{\frac{\partial^2 \psi}{\partial x^2} + \frac{\partial^2 \psi}{\partial y^2}}_{B} + \underbrace{\frac{\partial}{\partial p}\left(\frac{f_0^2}{\sigma^2}\frac{\partial \psi}{\partial p}\right)}_{C} \tag{2.28}$$

On the right side of equation (2.28), term A is the planetary vorticity, term B is barotropic vorticity, and term C is baroclinic vorticity. The σ^2 variable acts in a manner similar to the Brunt-Vaisala frequency N^2 in equations where potential temperature is used as the vertical coordinate, here $\sigma^2 = -\frac{R}{c_p}\frac{p}{p_0}^{\kappa}\frac{\partial\overline{\theta}}{\partial p}$, where p_0 and $\overline{\theta}$ are reference pressures and reference potential temperatures, respectively.

Further value of using potential vorticity in meteorology is in following atmospheric disturbances and predicting the flow. Using the curl of geostrophic horizontal momentum equations (2.20) and (2.21), the time evolution equation of the potential vorticity can be derived. Once the tendency of the potential vorticity is found for a future time, it can be inverted to determine the patterns of temperature and geopotential heights.

The preceding discussion forms the foundation of the required fluid mechanics needed for the study of mean flows, waves and instabilities in the polar winter middle atmosphere.

2.2.2 Waves

The atmosphere, as a fluid, supports a great variety of wave types. Waves are usually classified by their restoring force: ‘gravity waves’ have gravity or buoyancy as a restoring force, while the restoring force for Rossby waves is the conservation of potential vorticity. Other waves, such as acoustic waves, are of such small scale and high frequency that they are not of interest here.

Gravity waves have a variety of sources, wave numbers and interactions with other waves. A gravity wave source could be a large convective cell in the troposphere or flow over orography such as a mountain. They are extremely important for the momentum budget in the mesosphere, where they break and have consequences for the structure and dynamics of the region. They may also interact non-linearly with other waves and tides.

Development of equations governing waves is typically done using the perturbation method. In the perturbation method, all field variables are divided into two parts, the mean and the perturbation. For example,

$$\Psi(x,t) = \overline{\Psi} + \Psi'(x,t) \tag{2.29}$$

The quantity with the over bar is the mean state (or basic state) while the primed quantity is the perturbation (the wave part). This method assumes that the perturbation is small compared to the mean. Perturbations may be in time or space (although we will generally note time means as $\langle X \rangle$). Assuming that the perturbations are small, these equations can be linearized by presuming that a perturbation times a perturbation is small enough to be neglected. Pure internal gravity waves are due to buoyancy forces only, however waves with frequencies large compared to f are modified by the Coriolis force and are called inertial-gravity waves. We will start with pure internal gravity such that when linearizing the primitive equations, $f = 0$ (also neglecting friction and diabatic effects and assuming vertical wavelengths are smaller than the scale height H).

$$u'_t + \Phi'_x = 0 \tag{2.30}$$

$$v'_t + \Phi'_y = 0 \tag{2.31}$$

$$u'_x + v'_y + \rho_0^{-1}\left(\rho_0 w'\right)_z = 0 \tag{2.32}$$

$$\Phi'_{zt} + N^2 w' = 0 \tag{2.33}$$

Here, N is a constant($N^2 = \frac{R}{H}\frac{\partial\theta_0}{\partial z}\exp(-\kappa z/H)$). Assuming waves of the form

$$\psi' = A_\psi Re\left\{\exp\left(i(kx + ly + mz - \sigma t)\right)\right\} \tag{2.34}$$

Where Re is the real component of the complex number, A_ψ is an amplitude constant, k is the zonal wave number, l is the meridional wave number, m is the vertical wave number and σ is the frequency (different from the atmospheric stability parameter). The field variables are

$$(u', v', w', \Phi') = A_{u,v,w,\Phi} Re\left\{\exp\left(i(kx + ly + mz - \sigma t)\right)\right\} \tag{2.35}$$

Substituting these field variables into the linearized primitive equations yields the following system of equations

$$A_u = \frac{k}{\sigma}A_\Phi \tag{2.36}$$

$$A_v = \frac{l}{\sigma}A_\Phi \tag{2.37}$$

$$A_w = -\frac{\sigma m}{N^2}A_\Phi \tag{2.38}$$

Solving for σ, the resulting dispersion relation may be expressed as

$$\sigma = \frac{N\sqrt{k^2 + l^2}}{m} \tag{2.39}$$

Following the same procedure but with a non-zero f, the inertial-gravity wave dispersion relation is simply

$$\sigma^2 = f^2 + \frac{N^2(k^2 + l^2)}{m^2} \tag{2.40}$$

However, as a consequence of the inertial-gravity wave dispersion relation, $|f| \leq |\sigma| << N$. All things being equal, inertial-gravity waves tend to propagate more horizontally than pure internal gravity waves[3].

In the troposphere, planetary waves (Rossby waves of a planetary scale) can be seen in the kinks of the polar jet stream. At tropospheric altitudes, the polar jet stream is dominated by planetary wave numbers 5 through 7, meaning that there are between 5 and 7 kinks in the jet stream around a latitude circle. The middle atmosphere also has a polar jet stream (which surrounds the core of the polar vortex) but it is dominated by planetary wave numbers 1 and 2; the higher wave numbers have been filtered out as they propagated vertically through the troposphere and stratosphere. Planetary wave 1 (S1) is usually observed as an amplification of the Aleutian high and the displacement of the polar vortex off of the pole while planetary wave 2 (S2) is observed qualitatively as an elongation or splitting of the polar vortex.

Waves can be further categorized as forced or unforced. Free traveling planetary waves are unforced, global-scale normal modes [3]. Well known examples include the 5-day westward traveling disturbance of S1 and the 2-day S3 wave. However, here we are interested in forced planetary waves with low frequencies, i.e. 'quasi-stationary.' These waves are typically forced from below, in the troposphere by topography or sometimes diabatic heating conditions. Essentially, a planetary wave may be explained as a chain of air parcels, that when displaced in latitude (such as by a mountain range), it experiences a restoring force due to the beta-effect (the meridional gradient in potential vorticity, see equation (2.8)). These forced planetary waves may be quasi-stationary, but as they propagate vertically their amplitudes grow exponentially with height. Eventually, the wave will become non-linear and unstable, breaking and depositing its momentum. Figure 2.2 shows SABER observations of a planetary wave disturbing the middle atmosphere. This is a longitude-log(p) plot around the 70N latitude circle. The color contours indicate the temperature perturbations while the solid (dashed) line contours indicate positive (negative) perturbations in geopotential height. This clearly shows a planetary wave 1 with strong westward tilt below approximately 0.1 hPa. Above this level, the tilt begins to vanish, suggesting that wave is breaking and dumping

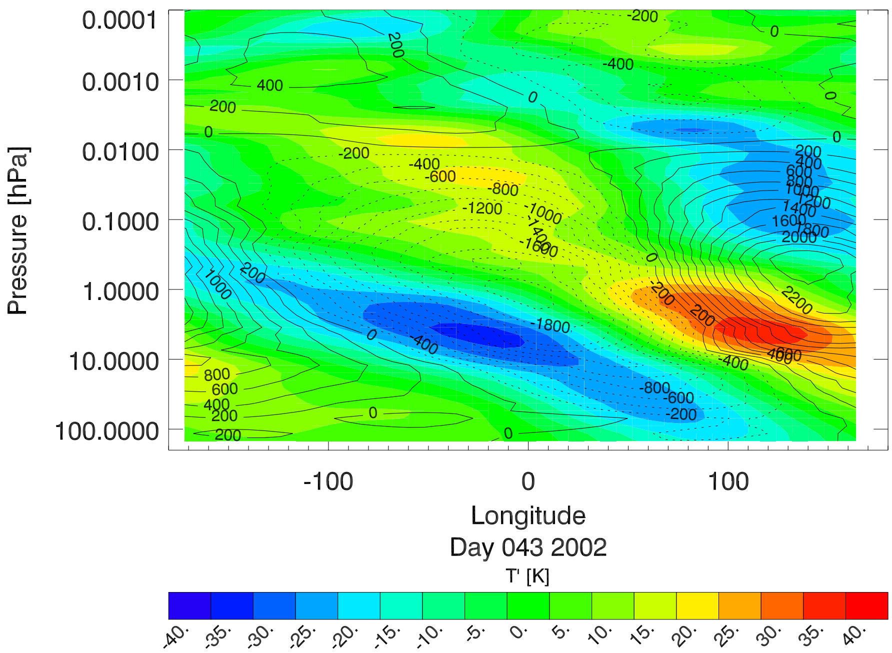

Figure 2.2: Following Salby [2002], S1 and S2 planetary wave perturbations around the 70N latitude circle of temperature (in color, see color bar) and geopotential height (positive perturbations are shown in solid lines while negative perturbations are shown in dashed lines) using TIMED/SABER data for the case study date of 13 February 2002. A strong westward tilt below the nominal mesopause is observed suggesting planetary wave interactions with the mean flow. This TIMED/SABER data has been processed by taking a whole day's worth of satellite passes and interpolating to a regular grid of longitude and log-pressure by the inverse-distance method. At each pressure level, the mean and first 12 wave components are calculated. The perturbations at each pressure level are found by subtracting the summed 12 wave components from the mean.

its momentum. The perturbations of temperature and geopotential are also out of phase signaling baroclinic conditions.

The flow is governed by quasi-geostrophic potential vorticity, equation (2.28), such that the absolute vorticity following the flow is conserved $D(\zeta + f)/Dt = 0$. For a β-plane,

$$\zeta_t + u\zeta_x + v\zeta_y + \beta v = 0 \tag{2.41}$$

Using the perturbation method ($u = \overline{u} + u'$,$v = v'$,$\zeta = \zeta'$), linearizing and recalling that the stream function is $u = -\psi_y$ and $v = \psi_x$, equation (2.41) is [32]

$$\left(\nabla^2\psi'\right)_t + \overline{u}\left(\nabla^2\psi'\right)_x + \beta\psi'_x = 0 \tag{2.42}$$

Where $\nabla^2\psi' = \psi'_{xx} + \psi'_{yy} = \zeta'$ and assuming solutions of the form

$$\psi' = A_\psi Re\left\{\exp\left(i(kx + ly + mz - \sigma t)\right)\right\} \tag{2.43}$$

Plugging this into equation (2.42) and solving for the dispersion relation σ:

$$\sigma = \overline{u}k - \frac{\beta k}{k^2 + l^2} \tag{2.44}$$

The zonal phase speed is defined to be $c_x = \sigma/k$ and for this dispersion relation becomes

$$c_x = \overline{u} - \frac{\beta}{k^2 + l^2} \tag{2.45}$$

As a consequence of this dispersion relation and phase speed, the zonal phase propagation of planetary waves is always westward relative to the zonal mean wind and the phase speed increases with decreasing wave numbers. For low wavenumbers (common in the middle atmosphere), the phase speed is frequently large enough to balance the eastward advection by the zonal mean wind such that the wave appears stationary relative to the surface of the earth; these are *quasi-stationary planetary waves* and are of greatest interest here.

As the planetary waves propagate vertically, they may encounter critical layers or their amplitudes become so large that they become non-linear, break and deposit their momentum into the mean flow. McIntyre and Palmer [1985] established that planetary wave breaking occurs when the IPV contours become irreversibly contorted, cascading from large scale down to smaller scales[57]. The standard method for diagnosing planetary wave breaking is to look for regions of reversals in the meridional gradient of IPV (equation(2.27)) on isentropic surfaces (for the Northern Hemisphere):

$$\frac{\partial}{\partial y}(IPV) = g\left(\frac{\partial}{\partial y}\left[p_\theta^{-1}\left(f + v_x - u_y\right)\right]\right) < 0 \tag{2.46}$$

The *Eliassen-Palm Flux* (E-P flux) vector give rises to a suite of diagnostic tools that may be used to investigate wave interactions with the mean flow. A derivation of the Eliassan-Palm flux will not be shown here, but a good derivation is given by Andrews, Holton & Leovy [1987] using residual circulations in the Transformed Eulerian-Mean (TEM) system of equations. The vector $\mathcal{F}$ is the E-P flux; this vector has components in the meridional and vertical directions, and in spherical coordinates defined as[72]

$$\mathcal{F}^{(\phi)} \equiv \rho_0 a \cos\phi \left(\frac{\partial \overline{u}}{\partial z} \frac{\overline{v'\theta'}}{\partial\overline{\theta}/\partial z} - \overline{v'u'} \right) \tag{2.47}$$

$$\mathcal{F}^{(z)} \equiv \rho_0 a \cos\phi \left(\left[f - \frac{1}{a\cos\phi} \frac{\partial}{\partial\phi} (\overline{u}\cos\phi) \right] \frac{\overline{v'\theta'}}{\partial\overline{\theta}/\partial z} - \overline{w'u'} \right) \tag{2.48}$$

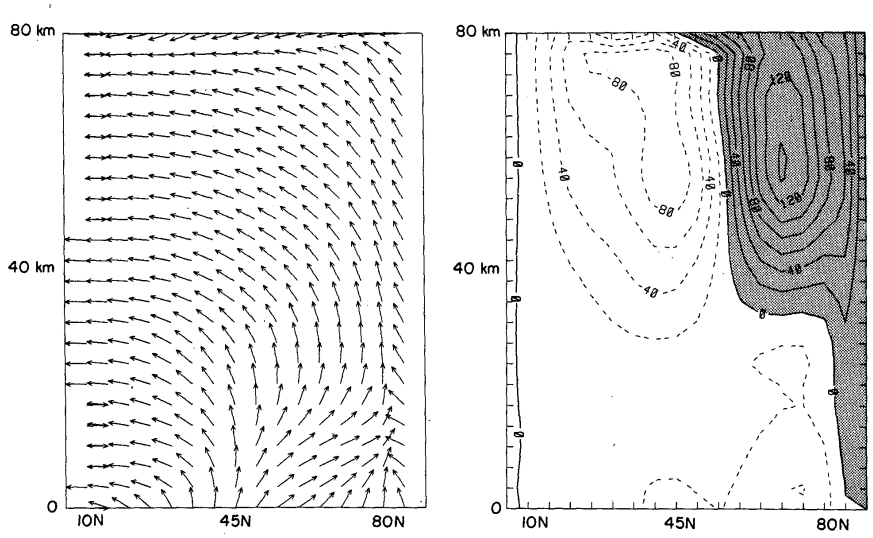

FIG. 3. (a) Direction of F_G, the quasi-geostrophic Eliassen-Palm flux, in the height–latitude plane. (b) Divergence of F_G. For consistency with other authors (e.g. Geller et al., 1983) the divergence is divided by a cosϕ. Units are 10^{-6} m s^{-2}.

Figure 2.3: An example of the Eliassen-Palm flux reproduced from Robinson [1986].

An example of an Eliassen-Palm flux calculation is shown in figure 2.3, reproduced from Robinson [1986]. On the left is the meridional plane (axes of latitude and height) showing the EP-flux vectors; on the right is the shading of the divergence of the EP-flux vectors. Shaded contours indicate flux divergence, a positive PV flux, and eastward flow acceleration.

This vector has the unique attribute that the eddy (wave) forcing terms appear explicitly. The meridional eddy momentum flux is $\overline{v'u'}$, while the meridional eddy heat flux is $\overline{v'\theta'}$. Instead of using potential temperature, θ, these equations can be written in terms of temperature T [32] or buoyancy $\flat$ [88]. The direction and magnitude of $\mathcal{F}$ determine the relative importance of eddy momentum flux and eddy heat flux. For example, when $\mathcal{F}$ is in the vertical direction, meridional heat flux dominates. The quasi-geostrophic EP-Flux vector is somewhat simpler, but we will use the full expression in this work for completeness; the quasi-geostrophic EP-flux can be found in Andrews, Holton & Leovy [1987].

The *divergence* of the E-P flux vector is a very useful quantity expressing acceleration/deceleration of the zonal mean flow due to wave-mean flow interaction (including both gravity waves and planetary waves). The divergence in the EP-flux can be calculated directly as

$$\nabla \cdot \mathcal{F} \equiv \frac{1}{a\cos\phi}\frac{\partial}{\partial\phi}\left(\cos\phi\mathcal{F}^{(\phi)}\right) + \frac{\partial\mathcal{F}^{(z)}}{\partial z} \tag{2.49}$$

The resulting scalar value is typically reported in units of $[m/s/day]$. It is also of note that in the quasi-geostrophic system, $\nabla \cdot \mathcal{F}$ can also be found using quasi-geostrophic potential vorticity q. A formal description of deriving this can, again, be found in Andrews, Holton & Leovy [1987].

$$\rho_0\overline{v'q'} = \nabla \cdot \mathcal{F} \tag{2.50}$$

This equation directly implies that the divergence in EP-flux is proportional to the poleward flux of quasi-geostrophic potential vorticity; a divergence in this value occurs in regions where the eddies act to accelerate the zonal mean wind[71].

2.2.3 Instabilities

An instability is a perturbation (or wave) which may amplify or decay in time, and also indicates the tendency of the atmosphere to support vertical motion. As a planetary wave breaks in the middle atmosphere, local conditions may be modified by secondary instabilities: inertial, barotropic, or baroclinic. Barotropic instability is associated with strong horizontal shear in the mean flow, while baroclinic instability is associated with strong vertical shear in the mean flow, or equivalently, with strong horizontal temperature gradients. Both types of shear may occur at the same location, although one type of instability typically dominates. Inertial instabilities are regions of negative (positive) potential vorticity from the Southern Hemisphere (Northern Hemisphere) which has been advected into the Northern Hemisphere (Southern Hemisphere); this type of instability is not significant during the times and regions of interest here. The stability properties of the fluid may be described by a normal modes approach [65]. Based on quasi-geostrophic theory, the Charney-Stern necessary conditions for instability [12][65] are derived from a normal modes analysis wherein a single Fourier mode is introduced into the flow with a complex phase velocity. Four necessary conditions for baroclinic instability are inferred from this; only one of the conditions must be met.

Charney-Stern-Pedlosky necessary conditions [88]:

(1) The meridional gradient in quasi-geostrophic potential vorticity changes sign within the interior

(2) The meridional gradient in quasi-geostrophic potential vorticity is the opposite sign to the zonal wind gradient with height at the upper boundary

(3) The meridional gradient in quasi-geostrophic potential vorticity is the same sign as the zonal wind gradient with height at the lower boundary

(4) The sign of the zonal wind gradient with height is the same at the upper and lower boundaries

The relevant condition in the middle atmosphere is condition (1). Except under very specific circumstances (including when isentropic surfaces are coincident with isobaric surfaces, which is not valid during middle atmospheric disturbances with sharp gradients), quasi-geostrophic potential vorticity q is generally not the same quantity as Ertel's IPV [34]. The origin of isobaric q is shown in section (2.2.1). In spherical isobaric coordinates the meridional gradient of q is:

$$\frac{1}{a}\frac{\partial q}{\partial \phi} = \beta + \frac{1}{a}\frac{\partial}{\partial \phi}\left[\frac{1}{f_0 a^2 \cos^2\phi}\frac{\partial^2 \Phi'}{\partial \lambda^2}\right]$$

$$+\frac{1}{a^3\cos\phi}\frac{\partial}{\partial\phi}\left[\cos\phi\frac{\partial}{\partial\phi}\left(\cos\phi\frac{\partial}{\partial\phi}(f_0^{-1}\Phi')\right)\right] \tag{2.51}$$
$$+\frac{1}{a}\frac{\partial}{\partial\phi}\left[\frac{\partial}{\partial p}\left(\frac{f_0^2}{\sigma^2}\frac{\partial}{\partial p}(f_0^{-1}\Phi')\right)\right]$$

When identifying a barotropic or baroclinic instability, not only should the Charney-Stern criteria be satisfied, but it will be of a synoptic scale (as opposed to planetary scale).

2.3 Polar Winter Middle Atmosphere Weather Events

2.3.1 Historical Context

Some of the earliest continuous observations of the stratosphere began with Richard Scherhag in the early 1950's using radiosondes. These radiosondes typically reached heights no greater than 30 km (approximately 10 hPa) in altitude, but allowed for observations of the structure of the lower stratosphere. In 1952 Scherhag observed the first recorded major Sudden Stratospheric Warming (SSW) over Berlin [76] [77] as anomalous conditions in the winds and temperatures. SSWs are one of the most spectacular and disruptive types of variability seen the polar winter middle atmosphere and can impact the entire atmospheric column, from the troposphere [4] to the thermosphere and ionosphere [23][13].

As the troposphere experiences many weather disturbances because of baroclinic instabilities that develop at the polar jet stream, some of the earliest attempts at describing the mechanisms of disturbances in the polar winter middle atmosphere employed baroclinic instability. In 1974 Simmons used an idealized model to examine the possibility of baroclinic instabilities at the stratopause and mesopause. He determined that while conditions were favorable for baroclinic instability at the stratopause, their growth rates were small and exhibited wave numbers of 5 through 9[79], clearly not displaying the observed behavior of the rapidly developing and planetary scale of SSWs[31].

As it turns out, while the troposphere is primarily thermally driven, the middle atmosphere is driven by waves. Matsuno proposed that SSWs were the result of planetary waves propagating up from the troposphere and interacting with the mean-flow. In 1971, Matsuno used a numerical model to reproduce SSWs by his proposed mechanism [53]. Although this proposed mechanism originally competed with the baroclinic instability mechanism, it is now the generally accepted as the underlying cause of stratospheric warmings.

2.3.2 Sudden Stratospheric Warmings

The growth of upward propagating planetary waves from the troposphere and subsequent interaction with the mean flow in the middle atmosphere is now understood to be the key mechanism of sudden stratospheric warmings. The interaction of the transient Rossby wave with the mean flow results in a deceleration of the mean flow past the point of flow reversal. This also induces a downward circulation in the stratosphere and upward circulation in the mesosphere resulting in adiabatic heating and cooling [44]. The transient planetary wave is surmised to be caused by resonant Rossby waves [87] or alterations in the refractive index such that the generation and propagation of the necessary planetary waves are favored[64].

It is further believed that the atmosphere must be 'pre-conditioned' in order for a major SSW to develop. Limpusuvan et al. [2004] reports that pre-conditions of SSWs include planetary wave activity that is focused toward the polar vortex, that the zonal flow is displaced polewards and that circulation anomalies in the polar vortex are drawn poleward and downward.

Sudden Stratospheric Warmings (SSW) are somewhat awkwardly defined. Andrews et al. [1987] uses the definition of Sudden Stratospheric Warmings of being events where the *zonal mean temperature increases poleward from 60° latitude and the zonal mean zonal wind reverses below at 10 hPa or below.* It is considered a **major SSW** if both conditions are met or a **minor SSW** if only the temperature condition is met[3]. However, the World Meteorological Organization (WMO) incorporates a temporal requirement in their definition as the latitudinal gradient of the 10 hPa zonal-mean temperatures between 60° and 85° be positive for more than 5 days and that the wind reverses at 10 hPa at 65°. There are additional suggested definitions such as those by McInturff (1978) and Labitzke (1982) that use combinations of polar cap temperatures, temperature gradients, wind reversals, timing or structure (dominant wave numbers). However, using a zonal mean fails to capture the nature of many synoptic features in the stratosphere. In addition, the 10 hPa threshold is a legacy from the era of radiosonde measurements and may not be the optimal level for determining anomalous behavior in the stratosphere. Here, we will employ the definition Andrews et al. [1987] for its widespread use in literature, making it easier to compare results.

Major and minor SSW events have been identified and cataloged since 1964 by groups such as Labitzke [1982] and Charlton & Polvani [2007]. The conditions for major SSWs are generally not met every winter, and in fact, only happen in about half of the winters in a given decade, although there was an unusually cold period in the Northern Hemisphere (NH) between 1990 and 1998[48] without major SSWs. Much work has been put into understanding the mechanisms, conditions and morphology of SSWs through observations, analyses and models. The earliest models were numerical, such as that of Matsuno. In the 1980's the first mechanistic models of the stratosphere using the primitive equations were developed, such as by Butchart [1982] and Smith [1992] who tested different realistic initial conditions and their impact on the development of SSWs. While simple models are still sometimes employed to examine middle atmospheric phenomenon, the trend has been toward complex models that incorporate chemistry, oceans, solar activity and have top-boundaries well above 100km. There has only been one recorded major SSW in the SH, which occurred in September of 2002 [89][5][2] and was very unexpected due to the cold and strong polar vortex that generally dominates in the SH [51]. It is believed that the stratosphere must meet certain preconditions in order to develop a SSW[58]. While the definition of major SSW is not frequently met, other types of middle atmospheric disturbances are observed up to several times per winter season and may be part of the required pre-conditioning of the middle atmosphere.

2.3.3 Definitions, Classifications & a Continuum of Disturbances

In addition to the noted minor and major Sudden Stratospheric Warmings of the previous section, there are still other types of middle atmospheric warmings. A **Canadian Warming** occurs when the Aleutian high intensifies and displaces the polar vortex off of the pole; the temperature gradient at 10 hPa may reverse but does not result in a break down of the polar vortex[41][30]. A **Final Warming** is said to mark the transition from the cold winter vortex to the weak summer anti-cyclone and is a warming that is not followed immediately by the reformation of the vortex.

Classification of warmings is a topic of current debate given the assortment of definitions using a variety of criteria and the modern availability of observations of the entire atmospheric column. The 10 hPa criteria level is no longer considered sacrosanct, and an optimal level based on dynamics is desired[90][29]. There are new attempts to objectively create criteria for middle atmospheric disturbances using mathematical techniques such as K-means clustering[14] and geometric moments[27], which try to avoid any preconceived classifications. The K-means clustering study performed by Couglin and Gray [2009] concluded that the polar winter stratosphere exists in two (and only two) natural well-separated states and that all polar winter middle atmospheric disturbances simply exist on a continuum of the disturbed state. The Hannachi et al. [2011] group supports the existence of three well-defined states of the polar stratosphere (undisturbed, vortex displacement disturbance and vortex split disturbance) and firmly reject the continuum of disturbances proposed by Couglin & Gray [2009]. However, the Coughlin & Gray [2009] study used zonally averaged variables dismissing synoptic scale disturbances and the Hannachi et al. [2011] study limited their scope to stratospheric levels between 30 hPa and 10 hPa (approximately 23 km to 30 km in altitude) when the optimal dynamical level may be higher in the stratosphere or mesosphere.

The focus of this work is on a type of disturbance that has the distinct feature of an anomalously warm stratopause located near 42 km in altitude (approximately 2 hPa). On 11 December 2000 the ARCLITE facility's Rayleigh lidar instrument captured an example of this peculiar type of event over Sondrestrom, Greenland, as shown in figure 2.4 [85]. For comparison purposes, the standard MSIS model temperature profile is shown for the same altitudes. During this event, the stratopause lowered to approximately 42 km and warmed an amazing 50 K. Neither MSIS or the NCEP reanalyses were able to capture this event, although NCEP did nearly capture the stratopause altitude correctly. A few days earlier the same phenomenon had been observed over another lidar site in Andoya, Sweden (cf. [85]) and it is believed that this event advected into the Sondrestrom lidar's field of view. However, this was certainly not the first observation of an event

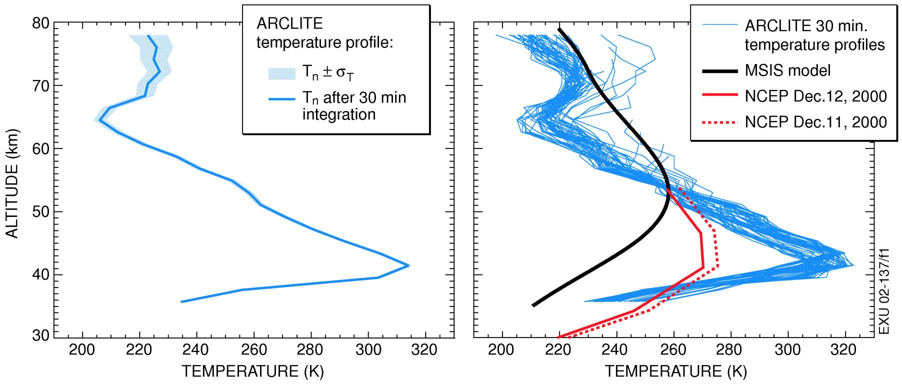

Figure 2.4: The left panel shows an average temperature profile and its error derived from the ARCLITE lidar in Sondrestrom, Greenland on 11 December 2000. The right panel shows each 30 minute integration. The black line is the MSIS profile for this date and location. The lidar profiles deviate from standard models and NCEP fields with the stratopause 50 K warmer and located at approximately 42 km in altitude.[85]

of this type, as von Zahn et al. discerned an event of this type in 1998 and others have indicated such structure in earlier sounding rockets experiments [90]. It was also noted that these events were phenomena distinct from well known major or minor Sudden Stratospheric Warmings, but they do not neatly fit into any other definitions proposed in the last 60 years.

Chapter 3

Data Sources & Methodology

3.1 Observational Data

3.1.1 SABER

The Thermosphere-Ionosphere Mesosphere Energetics and Dynamics (TIMED) satellite was launched on 7 December 2001[35]. The TIMED satellite is in a 625 km circular orbit with a 74.1° inclination. Approximately every 60 days, the spacecraft executes a yaw maneuver which allows its instruments to focus on an opposite hemisphere in turn. Originally a two-year mission, the TIMED mission has been extended several times, and, at the time of this writing, is still operating. The mission objective of the satellite is to understand the MLT (Mesosphere-Lower-Thermosphere) region's response to the energy input of the sun (JHU/APL 2009). The TIMED satellite carries four main instruments to achieve this objective: Global Ultraviolet Imager (GUVI), Solar Extreme Ultraviolet Experiment (SEE), TIMED Doppler Interferometer (TIDI), and Sounding of the Atmosphere using Broadband Emission Radiometry (SABER).

SABER is a limb viewing instrument that observes vertical radiance profiles in nine spectral bands between 1.27 μm and 17 μm. The radiances are processed to produce vertical profiles of temperature, density, O_3, H_2O, CO_2, and volume emission rates from O_2 (1.27 μm), OH (2.1 μm) and NO (5.3 μm). Additionally, the radiances can be used to determine cooling rates, solar heating rates, chemical heating rates, and airglow losses[35]. Given the yaw maneuver, SABER views either 52°S to 83°N or 52°N to 83°S with daily global coverage.

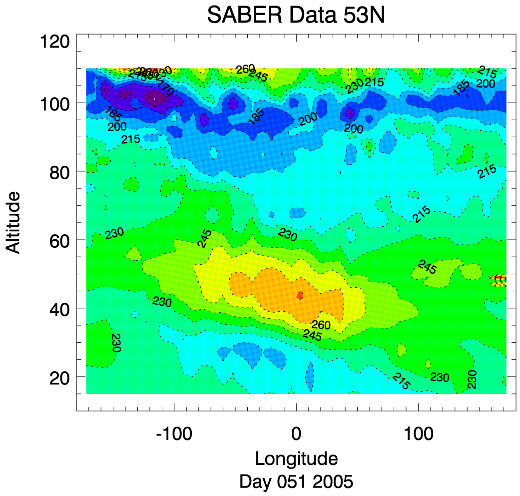

Figure 3.1: Longitude-Altitude plot around the 53°N latitude circle of temperature during a USLM event in February 2005.

SABER scans Earth's limb from 400 km to 'below' the solid surface in 10-channels (the CO_2 14.9 μm band is used twice for calibration purposes). The radiation transmission through the atmosphere is dependent on the spectral band, mixing ratio of the specific constituent, temperature and pressure. Data inversion is conducted on the ground to obtain a variety data products; most relevant here are temperature, pressure and geopotential height. Temperature is determined from the CO_2-14.9 μm channel[35]. Here we use the Level 2A data products: routine observed geophysical parameters, which can be obtained at http://saber.gats-inc.com/. Temperatures are generally available from approximately 10 km to 105 km in altitude, with an accuracy of at least 1.5 K and precision of at least 0.7 K[35]. An example of SABER data is shown in Figure 3.1.

3.1.2 Ground Based Systems

Ground-based instruments used in this study include radiosondes, lidar and OH airglow measurements.

Radiosondes are instrument packages tethered to weather balloons that measure (at the very least) temperature, pressure, humidity and wind. They are regularly released around the globe, typical every 12 to 24 hours and collect information deep into the stratosphere (approximately 30 km in altitude). Radiosonde launches are generally occur over land locations.

Lidar (LIght Detection and Ranging) uses the Rayleigh scattering of photons by air molecules in the atmosphere to derive temperatures. Pulses of a specific wave-length of light (typically 532 nm) are shot into the sky and a telescope collects reflected light (photons); the time of flight determines the altitude from which the photon was reflected. A detailed description of the temperature retrieval method is given in Thayer et al. [1997]. A high powered Rayleigh lidar can produce profiles from the mid-stratosphere into the deep mesosphere (approximately 30 km to 80 km in altitude); coupling it with low altitude lidars can extend the profile to the ground.

A Michelson interferometer may be used to measure nightly kinetic temperatures of airglow, which is confined to discrete altitudes. Mesospheric OH airglow is typically located at 87 km. Nielsen et [2001] describes the methodology and variations of temperature during the polar winter.

Figure 3.2 shows a time series plot of an Upper Stratosphere Lower Mesosphere (USLM) disturbance in December 2001 that combines radiosonde, lidar and OH airglow measurements over the Sondrestrom research station at 67°N and 50.7°W (figure from Thayer & Livingston [2008]). Combining the measurements of all three instruments allows for viewing of the event as it occurs overhead from the ground to approximately 87 km.

The advantages of ground-based observational instruments include their historical validity, long records, high temporal and vertical resolution, and calibration. Their main drawback is that these instruments only observe what is occurring directly overhead and require synoptic, hemispheric or even global context. For example, in figure 3.2, it may appear that the warm temperature anomaly forms and descends while in actuality it is more likely that the anomaly advected into the instruments' field of view. Additionally, there are few if any of these types of observations over oceans and sparsely populated areas.

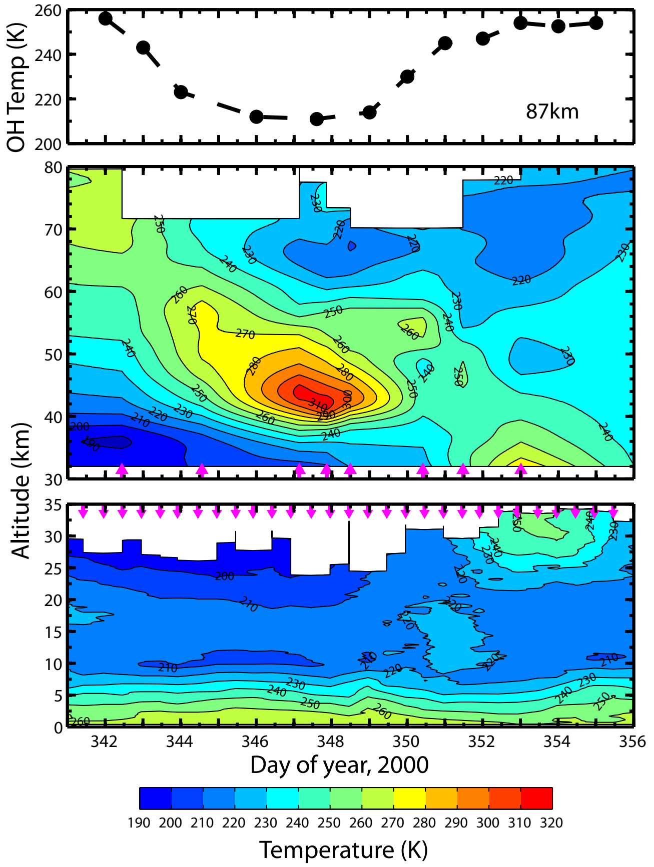

Figure 3.2: Altitude-time plot of temperature at Sondrestrom from 6-21 December 2000 as derived from radiosonde balloons (bottom panel), Rayleigh lidar (middle panel), and OH airglow measurements (top panel). Arrows indicate the midpoint times of data available from balloon and lidar data. Lidar profile averages vary from 2-6 hr integration and OH measurements are nightly averages. From Thayer & Livingston [2008].

3.2 Assimilated Data

Assimilated data sets incorporate observational data with models of the underlying dynamics of the atmosphere. These products produce excellent global coverage and realistic estimations of state variables in areas where no in-situ or remote sensing observations are available.

The UK Met Office assimilated data set (referred to as MetO, but sometimes as UKMO) was developed as part of the UK Met Office's operational weather forecasting system for NASA's Upper Atmosphere Research Satellite (UARS). Once daily (12Z) temperature, winds, and geopotential heights at 2.5° latitude by 3.75° longitude resolution are obtained on 22 pressure surfaces extending from the 1000 to 0.3 hPa (26 pressure surfaces up to 0.1 hPa after late 2003)[83]. The assimilation scheme also incorporates satellite soundings from ATOVS (Advanced TIROS Operational Vertical Sounder) data from the NOAA-15 satellite in addition to TOVS (TIROS Operational Vertical Sounder) data from NOAA-14[46]. However, the assimilated data is independent of TIMED/SABER data and does not incorporate any data from TIMED/SABER instrument. Prior to November 2000, the assimilation used an analysis-correction scheme as described by Lorenc et al. [1991]. Mid-November 2000 and late October 2003 mark major changes in the MetO analyses with the former involving the implementation of 3-D variational assimilation[46] and the latter a new dynamical core in the Unified Model[15]. These periods of change to the MetO assimilation scheme involving 3D var and a new dynamical core were compared to the Northern Annular Mode (NAM) index [e.g. Waugh & Polvani, 2010] to check for consistency. It is seen that in years experiencing NAM values corresponding to a strong polar vortex the MetO database showed diminished winter disturbances [e.g. Manney et al., 2005]. This indicates the assimilation scheme shows variability on a decadal scale and should be satisfactory for our use of the database. This work is based on MetO temperature, horizontal winds, and geopotential height data on pressure surfaces. The isobaric data are interpolated to potential temperature surfaces ranging from 330 to 2000 K in order to compute isentropic potential vorticity (IPV) and to calculate the edge of the polar vortices using the method described by Harvey et al. [2002]. Restricted access to the data is available at http://badc.nerc.ac.uk/browse/badc/ukmo-assim.

An example of MetO assimilated data is displayed in Figure 3.3. Isotherms (dotted lines) and lines of geopotential height (solid lines) contours on the 2.154 hPa pressure surface from MetO data for the case study date of 13 Feb 2002. Of particular interest is that the polar vortex has been displaced off the pole (the geopotential height low, located at approximately 30°E 70°N), the Aleutian high has strengthened (approximately 170°E 65°N), and the anomalously warm air located on the East side of the low in a region of strong geopotential height gradients.

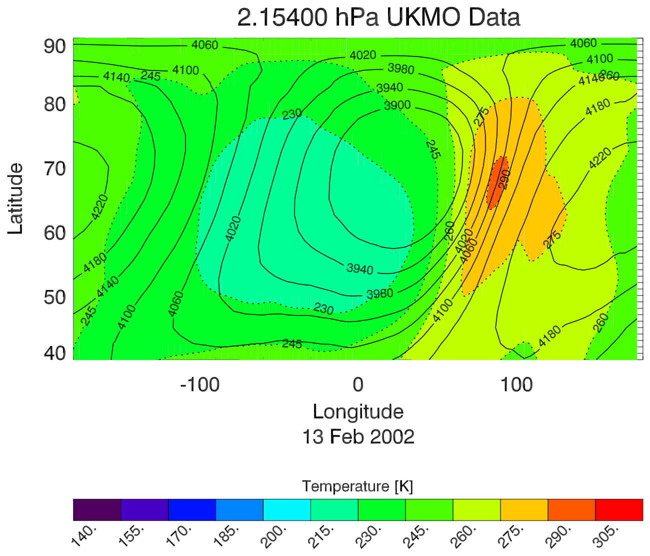

Figure 3.3: Isotherms (dotted lines) and lines of geopotential height (solid lines) contours on the 2.154 hPa pressure surface from MetO data for the case study date of 13 Feb 2002.

3.3 Models

Models range from the very simple to the very complex. Advantages of models include variable spatial and temporal resolution, global coverage with variable altitude ranges, and the ability to quantify variables that are difficult to measure in observations. However, models may not be truly representative of atmospheric conditions and must be verified with observations. Because measurements of the middle atmosphere have, historically, been difficult to come by, mechanistic models have been very useful for understanding the dynamics of the middle atmosphere. One of the first models that made use of detailed primitive equations was created by Butchart et al. [1982]. More recently, Liu and Roble [2002] used another sophisticated model to examine the impact of major SSWs on the lower thermosphere.

The Whole Atmosphere Community Climate Model (WACCM) is a global chemistry climate model developed by the National Center for Atmospheric Research (NCAR). For the work described here, WACCM version 4 (WACCM4) was run in the Community Earth System Model (CESM) framework; i.e., WACCM4 was specified as the atmospheric component set of CESM. CESM is based on the Community Climate System Model version 4 (CCSM4), for which the atmospheric component is the Community Atmosphere Model version 4 (CAM4) [18]. WACCM4 uses a finite-volume dynamical core [42], and extends from the surface of the Earth to the lower thermosphere (approximately 145km). The model uses a hybrid vertical scale with 66 levels that are isobaric above 100 hPa; the vertical resolution increases from about 1.1 km in the troposphere to 1.75 km around 50 km to 3.5 km above approximately 65 km [21]. The horizontal resolution for the run used here is 1.9° latitude by 2.5° longitude. The chemistry module of WACCM4 is based on the Model for Ozone and Related Chemical Tracers version 3 (MOZART3), which is described in Kinnison et al. [2007]. The gravity wave parameterization employed in WACCM4 is described by Richter et al. [2010]. Briefly, orographic gravity waves are parameterized based on McFarlane [1987]; the parameterization includes the efficiency with which they are launched. Non-orographic gravity waves are parameterized according to the formulation of Lindzen [1981]; they are launched through either a convective or frontal source parameterization[70]. For the simulation in this work sea surface temperatures and surface emissions were prescribed based on year 2000 conditions. Solar irradiance and auroral energetic particle input were parameterized as described in Marsh et al. [2007], with a 10.7 cm radio flux index (f10.7) of 210 (appropriate for solar maximum conditions), and a geomagnetic Kp index of 4. A simulation of 42 repeating years was performed; the first two years were removed to account for spinup, leaving 40 years for statistical analyses. An example of WACCM data is shown in Figure 3.4.

The advantage of WACCM is that the model spans from the surface into the thermosphere and incorporates dynamics, chemistry and physics. However, this also makes the model very complex. It is actually comprised of three coupled individual models of the atmosphere. The NCAR Community Atmosphere Model 4 (CAM4) provides the finite volume dynamical core and solves the primitive equations using a a two time-level flux-form semi-Lagrangian scheme[62]. The Model for OZone and Related chemical Tracers (MOZART) includes 51 computed chemical species in addition to N_2, 127 gas-phase reactions, photolytic reactions and ion-neutral/recombination

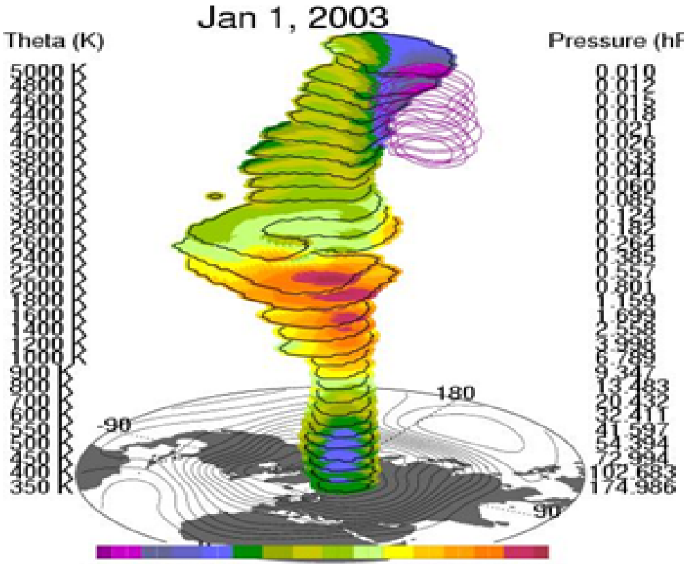

Figure 3.4: An example of WACCM output displaying the 3D polar vortex [c.f. V. L. Harvey.]

reactions[62]. The physics of the mesosphere and thermosphere are modeled with TIME-GCM.

Chapter 4

Characteristics and Identification of USLM Events

Of particular focus for this work are synoptic-scale disturbances, on the order of 1000-2000 km, near the polar winter stratopause and mesosphere. Evidence has been accruing over the years that synoptic-scale disturbances in the polar middle atmosphere can significantly alter the state properties of the upper stratosphere and mesosphere [e.g., Labitzke, 1972; von Zahn et al., 1998; Thayer and Livingston, 2008] and may play an integral part in the evolution of planetary-scale SSWs [e.g., Fairlie et al., 1990; Manney et al., 1994, 2008]. These disturbances have been associated with the production of stratopause temperatures enhanced by 50 K at an atypical low altitude of 42 km and a concomitant cooling in the middle mesosphere by 40 K near 75 km altitude. These synoptic-scale disturbances have been referred to as stratopause warmings [17][8], stratosphere temperature enhancements [59] and upper stratosphere / lower mesosphere (USLM) disturbances [49]. The USLM disturbance moniker is used here to identify this type of disturbance as it captures the notion that changes are occurring in both the upper stratosphere and lower mesosphere. From the collection of temperature and wind observations, these synoptic-scale disturbances often occur prior to the onset of SSWs, cause dramatic changes to the upper stratosphere and lower mesosphere temperature and winds with little change to the lower stratosphere, and are regionally confined[85]. Although USLM disturbances have only been intermittently captured in observations[40][90][85] over the last 40 years, no comprehensive investigation of the their origins, phenomenology and impact on the polar vortex has previously been undertaken. This research chapter seeks to address this gap in the field of aeronomy.

4.1 2002 USLM Case Study

This section is partially adapted from Thayer, Greer & Harvey [2010].

Observations of the polar middle atmosphere have increased significantly over the years with improved spatial and temporal resolution, particularly in the mesosphere, provided by ground-based and space-based techniques. The current NASA satellite missions of Aura and TIMED, along with new data assimilation schemes, have been exceptionally beneficial in studying the complete evolution of SSWs at much improved resolution through the mesosphere [see Manney et al., 2008]. Consequently sub-planetary scale features of the polar middle atmosphere can also be investigated better than ever before.

Analysis of zonally averaged fields of the polar middle atmosphere is a common approach to study planetary-scale disturbances. However, this approach is not adequate to view synoptic-scale disturbances that are embedded in the planetary-scale circulation. Furthermore, synoptic-scale disturbances are not simply superpositions onto the planetary circulation but are interacting with the planetary circulation and altering the state properties of the polar middle atmosphere. The novel capabilities of the Sounding of the Atmosphere using Broadband Emission Radiometry (SABER) instrument on the NASA TIMED satellite are employed. By also employing the U.K. Meteorological Office assimilated stratospheric data fields (referred to as MetO) we can identify these synoptic-scale disturbances in the upper stratosphere and investigate more completely their temporal progression by the regularity and coverage of temperature and geopotential provided by MetO data. This section will focus on a single USLM disturbance that began on 12 February 2002 with the recognition that the common characteristics and findings of this case study are representative of other USLM events. The specific date for our event was identified by searching the MetO polar wintertime temperature fields near 2 hPa for times when temperatures exceeded 290 K. This level of temperature enhancement cannot be caused by typical thermal properties or thermal advection and suggests that strong vertical circulations exist.

Figure 4.1 shows pressure-longitude plots of SABER temperature along the 70° N latitude

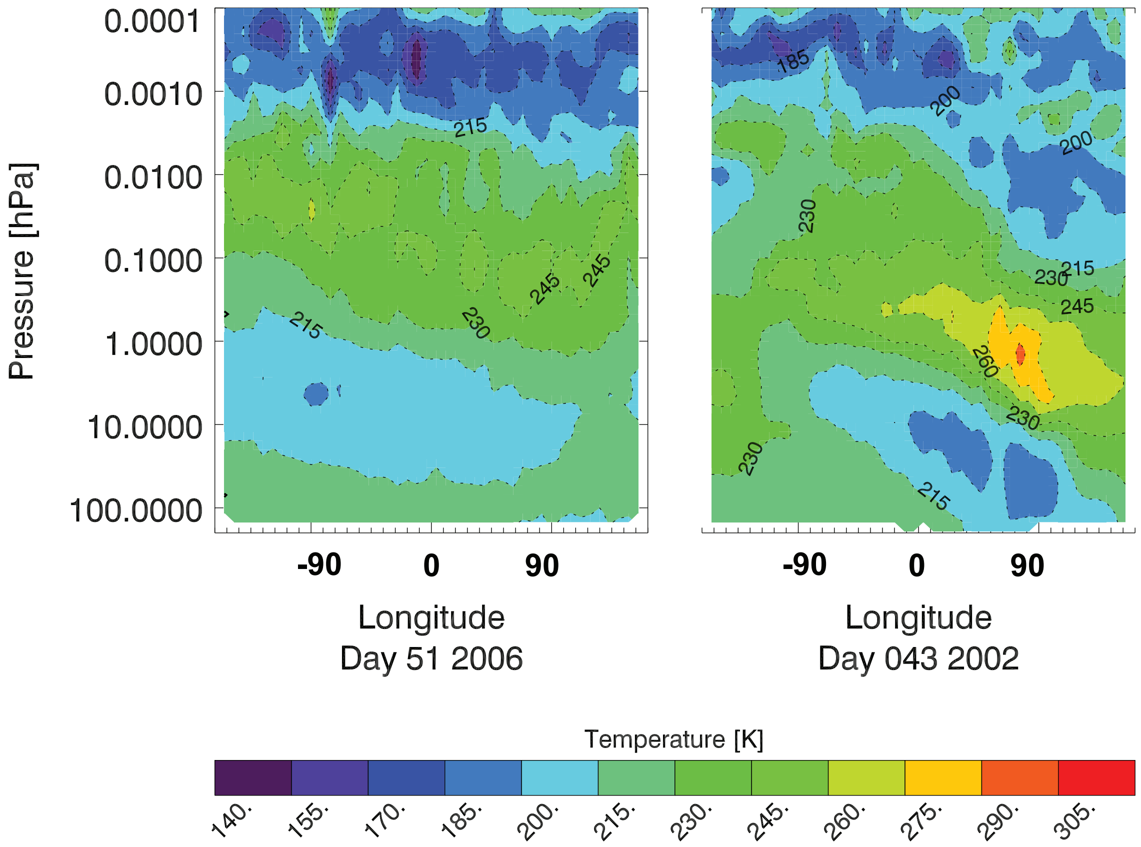

Figure 4.1: Daily maps of SABER temperatures of the polar wintertime middle atmosphere displayed in pressure versus longitude coordinates on a latitude circle of 70 N for a quiet (on left) and a disturbed (on right) day [84].

circle. These plots were constructed by interpolating one-day of data onto a regular grid of longitude at 8° spacing and log-pressure at 0.25 hPa spacing. The data is further smoothed by including only the first 12 wave components around a latitude circle on each pressure surface. Two different days are presented in Figure 1 to contrast a strongly established vortex on 20 February 2006 (left) and our disturbed case of 13 February 2002 (right). The cold lower stratosphere, the warm stratopause, and the cold mesosphere are clear features on both days. The polar vortex was intact on both days. On planetary scales, the 13 February 2002 temperatures are inclined significantly to the west and indicative of a dominant zonal wave number 1 perturbation in the middle atmosphere. The 13 February 2002 SABER data was also shown by Remsberg et al. [2003] as a demonstration of

SABER's capability to capture synoptic scale features and are in good agreement with MetO data in the stratosphere.

On regional or synoptic scales for 13 February 2002, the stratopause temperature on the east side of the polar low is enhanced over background conditions near an altitude of 42 km, and an associated anomalous cooling in the middle mesosphere occurs near 75 km. This cooling in the middle mesosphere is distinctly separated from the nominal wintertime mesopause near 100 km and is related to the stratopause disturbance. The SABER observations provide an estimate of the horizontal scale size of the disturbance to be on the order of 1000-2000 km and a vertical scale between maximum and minimum temperatures of about 35 km. Clearly a second mesopause below the nominally formed wintertime mesopause at 100 km is identified in the SABER data. These 2-D features of the disturbed middle atmosphere observed by SABER are precisely those documented by individual temperature profiles recorded by rockets and lidars [e.g. Labitzke, 1972; von Zahn et al., 1998; Thayer and Livingston, 2008]. The magnitude of the anomolous temperatures recorded by SABER are not as extreme as those recorded by these other methods and is most likely due to the narrow distribution of the feature in longitude, the geometric viewing of the SABER instrument through the atmosphere, and the orbit-by-orbit longitudinal smoothing that occurs in gridding the SABER data on a daily map. In the lower stratosphere, the day of 13 February 2002 does not satisfy the WMO definition of a major stratospheric warming but clearly the middle atmosphere is strongly disturbed. This behavior is a common occurrence for USLM disturbances.

To further describe the features of the USLM disturbance on 13 February 2002, a cross-sectional view in latitude and longitude of SABER data in temperature and geopotential at two select pressure surfaces is displayed in Figure 4.2. The chosen pressure surfaces refer to the levels where the temperature extrema occur in mesosphere cooling and stratopause warming. The stratopause warming region is confined to about 50° of longitude (centered at 90° E) and is limited in latitude from about 50° N to 70° N. The mesosphere cooling region is similarly confined in longitude but extends to lower latitudes. The opposite temperature structure is observed on the west side of the polar low with cooler than normal stratopause temperatures and a warmer mesosphere.

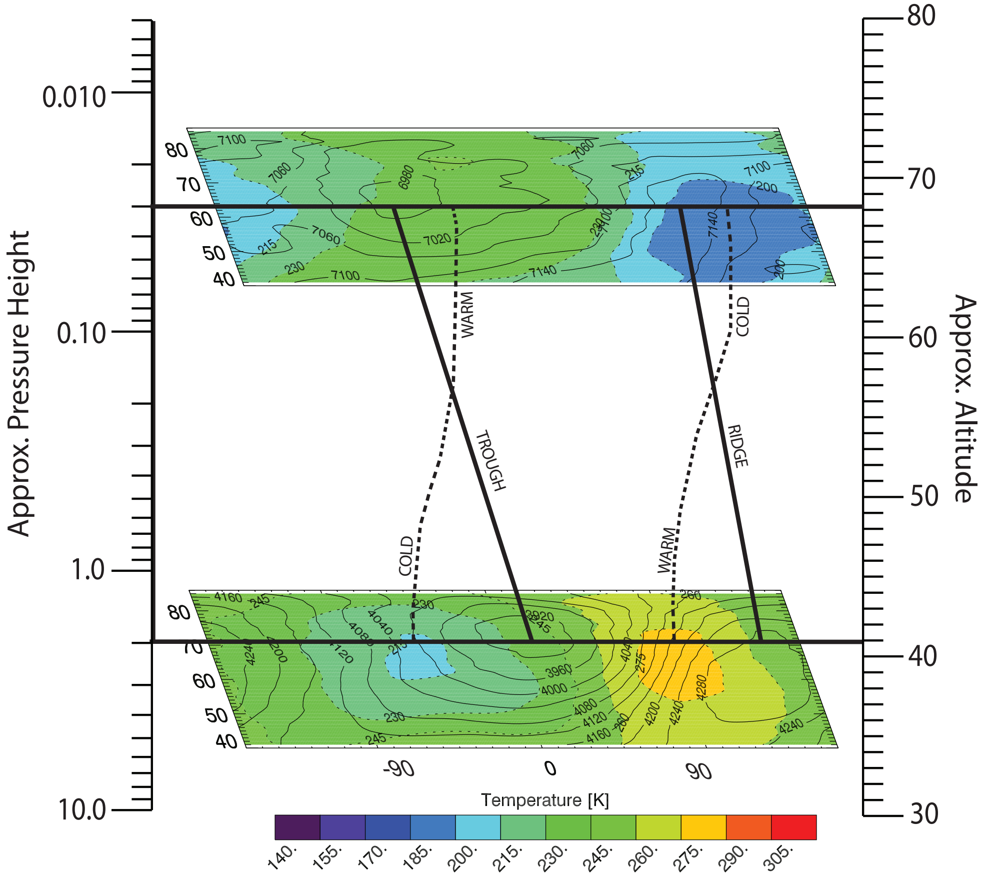

Figure 4.2: A vertical cross-section through the synoptic disturbance on 13 February 2002. Thick vertical solid lines are ridge and trough axes; dashed vertical thick lines are temperature extrema. Two pressure levels are shown (2.0 hPa and 0.03 hPa) on the longitude-latitude plot of geopotential height (thin solid lines) and temperature (colors and thin dashed lines)[84].

Also indicated on the figure are the axes of the polar low and high displaying a westward tilt with decreasing pressure and the axes of temperature extrema (i.e. connecting temperature maxima to temperature minima) that tilts east with decreasing pressure.

The configuration of the temperature and geopotential with pressure in Figure 4.2 is reminiscent of the classic description of an amplifying, midlatitude, synoptic-scale baroclinic disturbance in the troposphere, c.f. Holton [2004]. Tropospheric midlatitude, synoptic-scale disturbances grow through baroclinic instability where small perturbations in the presence of strong vertical wind shear can amplify by drawing energy from the mean flow. A requirement for the generation of perturbation energy through baroclinic instability is systematic poleward transport of warm air and equatorward transport of cold air. Similar behavior can clearly be seen in Figure 4.2 as cold air under the polar low at the 2 hPa level is advected equatorward while warm air under the polar high at the 2 hPa level advects poleward. A baroclinic disturbance may amplify as the cold air advection under the polar low tends to deepen the low while warm air advected under the polar high tends to build the ridge.

In developing baroclinic waves, the combination of differential thermal and vorticity advection lead to amplification of the disturbance. Furthermore, ageostrophic flow is associated with baroclinic disturbances in order to maintain quasi-geostrophic and hydrostatic balance. These same characteristics likely occur in the middle atmosphere. The westward tilt of the middle atmosphere polar low provides the available potential energy from which the synoptic-scale perturbation can extract energy. The static stability of the stratosphere and the thermosphere serve as “semi-rigid” boundaries through which vertical air motion is redirected horizontally - similar to the role of the ground and tropopause in troposphere synoptic-scale disturbances - resulting in a 3-D ageostrophic circulation within the USLM. Baroclinic instability is most effective at intermediate scales that are on the order of the Rossby radius of deformation, which is about 1000 km in the mesosphere. The synoptic scale size of the observed USLM disturbance is about 1000-2000 km. Also, the USLM disturbance evolves on the east side of the polar low, analogous to synoptic scale disturbances in the troposphere.

The available 3-D fields of MetO temperature, geopotential height, and horizontal wind data in the upper stratosphere enable a kinematic analysis of the flow for characterization of the conditions under which the SABER-observed USLM disturbance developed. Figure 4.3 displays a latitude-longitude plot of geopotential height and temperature from the MetO analysis for the 2.154 hPa pressure surface on 13 February 2002. Lines of constant geopotential height and temperature on this pressure surface are displaced from one another and their gradients have regions that are significantly oblique indicating strongly baroclinic conditions. In fact, in the region of the stratopause warming on the east side of the low, the atmosphere is strongly baroclinic. This is

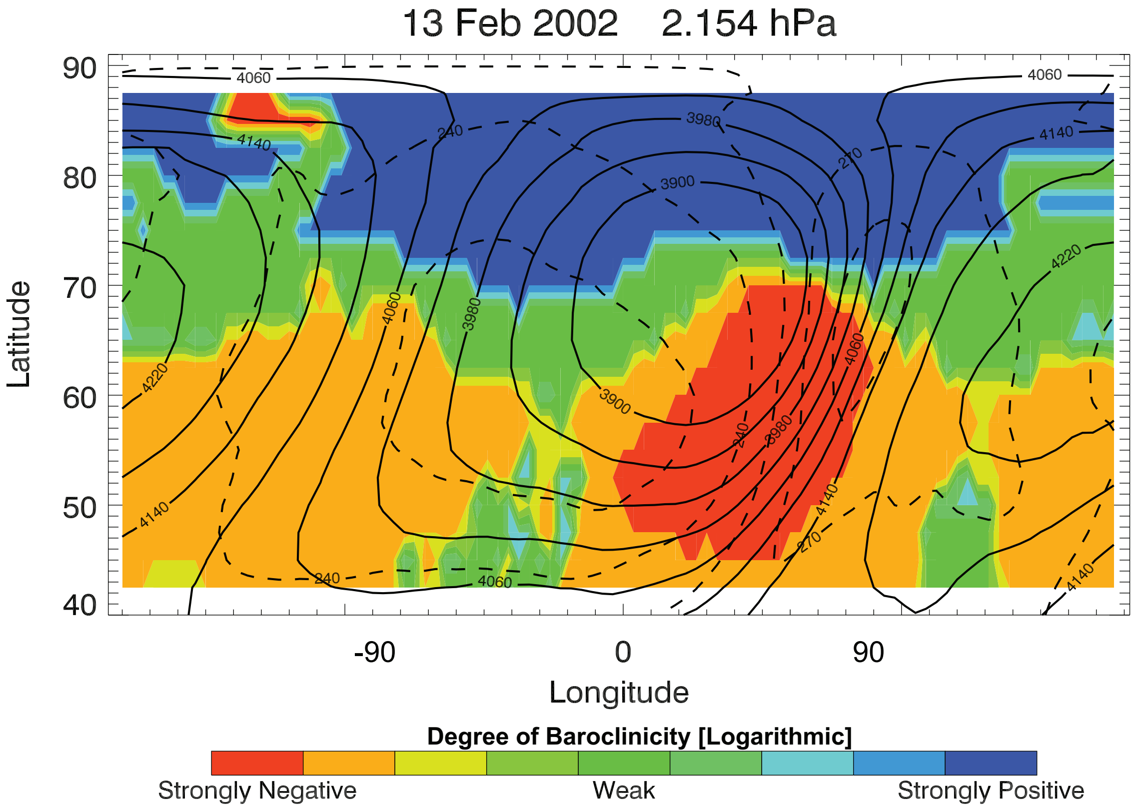

Figure 4.3: Longitude-latitude plot of geopotential height (solid contours) and temperature (dashed contours) from the MetO 2.154 hPa pressure surface on 13 February 2002. Color shading represents the relative degree of baroclinicity [s^{-2}] on a logarithmic scale where the top and bottom 10% values indicate regions of strong baroclinicity [84].

demonstrated by the color contours quantifying the degree of baroclinicity with strong negative baroclinicity occurring in the proximity of the synoptic-scale disturbance. The degree of baroclinicity is proportional to the solenoidal term in the vorticity equation and contributes to the amount of vorticity generated in the region in units of s^{-1} [88]. The solenoidal term is frequently expressed as

$$B \equiv \frac{1}{\rho^2}\left[\nabla\rho \times \nabla p\right] \tag{4.1}$$

The vector B is defined purely in the $\hat{k}$ direction and can be positive or negative (ρ is density and p is pressure). Using the MetO assimilated data, only fields of temperature T and geopotential height Φ are available. Using the ideal gas law and the hydrostatic law, the baroclinicity vector B can be rewritten in terms of these fields as

$$B \propto -\nabla \frac{1}{T} \times \nabla \Phi \tag{4.2}$$

This vector is calculated for every point on the MetO grid on the selected pressure surface and then normalized by the greatest absolute value of B to give the relative assessment of sign and strength of baroclinicity presented in Figure 4.3. The contours in Figure 4.3 are on a logarithmic scale to account for the large dynamic range in baroclinic values, with strong baroclinicity indicating values from the top 10% of both signs in B.

The divergence and tilting terms in the vorticity equation also contribute to vorticity generation but a separate term analysis estimates these to be secondary to the solenoidal term in this localized region. The mesosphere does not generate as strong a solenoidal term but, in combination with weaker winds, may support the physical requirement for baroclinic instability of differential vorticity advection between pressure surfaces.

Whether baroclinic instability is active in USLM disturbances requires an evaluation of criteria for instability. The necessary conditions for baroclinic instability are discussed in section 2.2.3, requiring any one of four criteria be satisfied. These criteria involve the relationship between the vertical wind shear and the meridional gradient of potential vorticity. Figure 4.4 illustrates the potential vorticity distribution and its meridional gradient on the 1600 K isentropic surface on 13 February 2002. The thick black and white contours mark the edge of the Arctic vortex and Aleutian anticyclone, respectively. The numerical algorithm presented by Harvey et al. [2002] was used to identify the vortices. This potential temperature surface is close to 2 hPa and serves as the lower boundary of the USLM disturbance. Two necessary conditions for baroclinic instability are satisfied in the vicinity of the synoptic disturbance. One necessary condition is the meridional gradient in potential vorticity is the same sign as the vertical gradient in the zonal wind at the

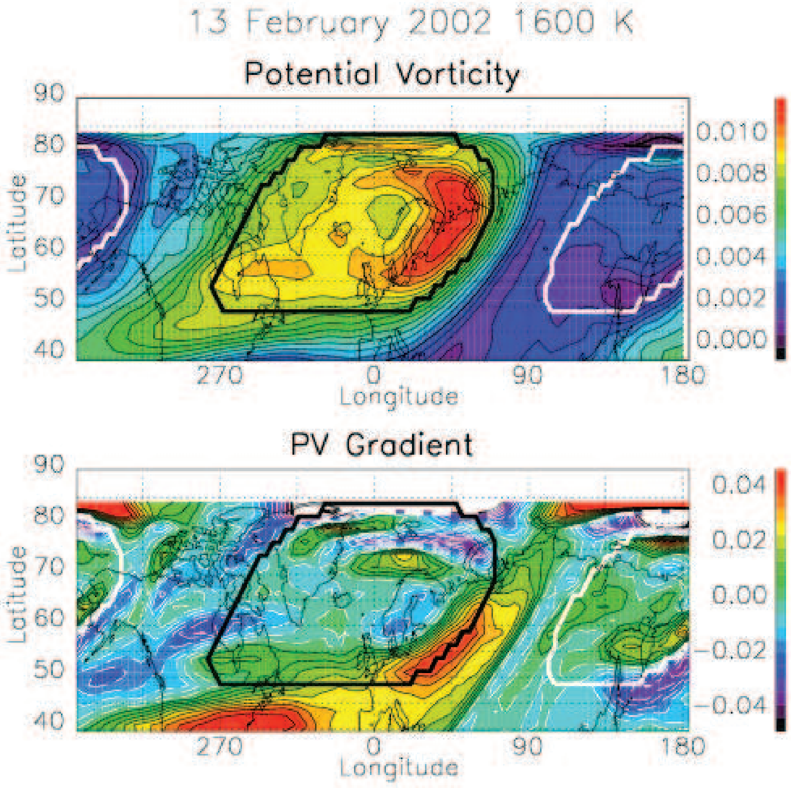

Figure 4.4: Potential vorticity and its meridional gradient on the 1600 K isentropic surface for 13 February 2002. The thick black (white) line depicts the position of the polar vortex (Aleutian anticyclone)[84].

lower boundary. Based on the horizontal temperature distribution at the lower boundary shown in Figure 4.2, both of these gradients are strongly positive in the vicinity of the disturbance. Another necessary condition for instability is for the meridional gradient in potential vorticity to change sign. This occurs within the northwest portion of the regional disturbance.

An ageostrophic circulation would be expected to be established during a disturbance like this February 2002 event to maintain quasi-geostrophy and hydrostatic balance. The circulation is divergent and continuity requires vertical motions resulting in a closed three-dimensional flow. Given the strong static stability of the stratosphere, vertical motions are particularly effective in the thermodynamic energy equation in producing significant changes in temperature. A technique used in tropospheric meteorology to characterize vertical air motions on a pressure surface is known as the Q-vector analysis [33][32]. This type of analysis has been applied to developing fronts in the troposphere to qualitatively assess the associated vertical flow field [74]. Thayer and Livingston [2008] have applied this analysis technique to the middle atmosphere, where it can be computed using geopotential height and temperature fields.

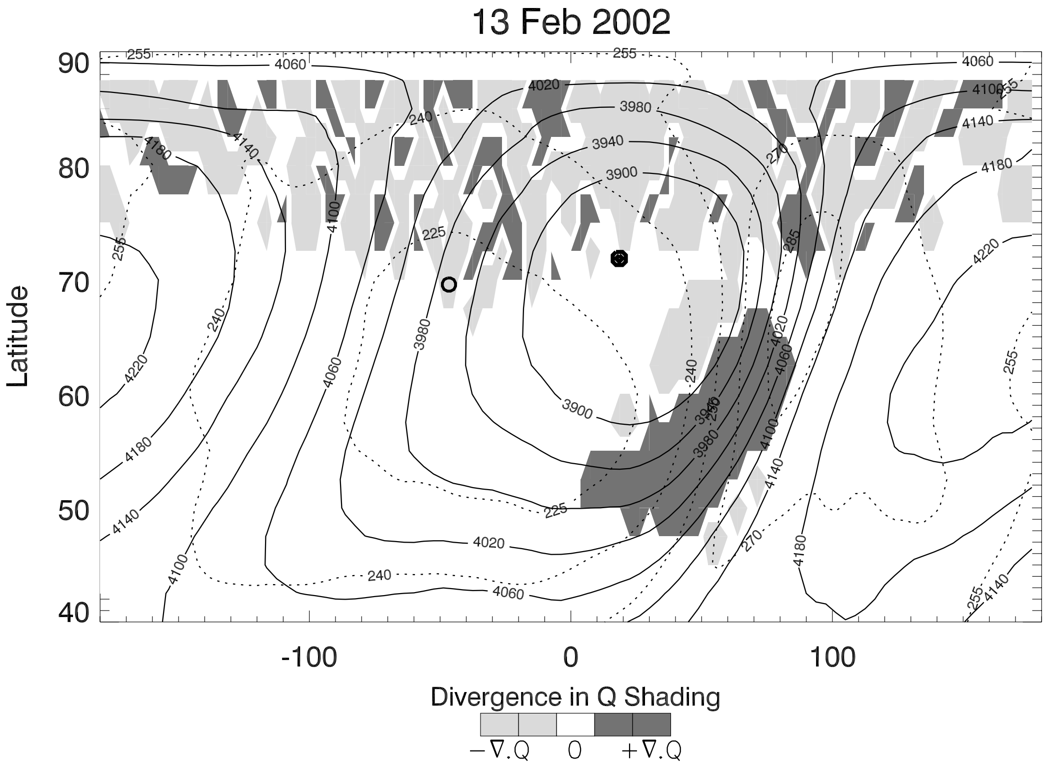

Figure 4.5: Same as Figure 4.3, except the shading refers to the sign of divergence in the Q-vector in regions of strong baroclinicity [84].

The same Q-vector analysis may be applied to the present case; details of the analysis can be found in Thayer and Livingston [2008]. Figure 4.5 presents the Q-vector analysis based on the MetO fields at 2.154 hPa on 13 February 2002, where gray shading identifies regions of divergence in the Q-vector. A divergent Q-vector is directly proportional to downward vertical motion. The significant divergence in the Q-vector is in proximity to the synoptic scale disturbance whose association with downward motion supports the argument that the stratopause warming is attributed to adiabatic compressional heating. This Q-vector configuration was similarly observed for the two USLM cases analyzed by Thayer and Livingston [2008] and is a common feature of USLM disturbances. It should be noted that the Q-vector analysis is susceptible to minor inflections in geopotential and temperature as their gradients and dot products of these gradients are required to estimate the divergence in the Q-vector. Thus, the Q-vector can be quite noisy in regions of weak baroclinicity. However, the analysis is reliable in regions of strong baroclinicity, thus, the Q-vector analysis in Figure 4.5 was masked for regions where only strong baroclinicity prevailed.

As has been applied in tropospheric weather maps, the Q-vector analysis can be used qualitatively to identify regions of vertical motion in the vicinity of baroclinic zones. The application to the USLM disturbance shows a similar utility and identifies vertical motion that is concomitant with the thermal structure and dynamics of the middle atmosphere synoptic feature.

Given the importance of dynamical interactions to the energetics of the middle atmosphere, it is necessary to examine planetary wave behavior throughout the event. In the same manner as Salby et al. [2002], the geopotential and temperature fields from SABER data for 13 February 2002, presented in Figure 4.1, are separated into their zonal mean and perturbation wave components. The dominant wave components are zonal wave numbers 1 and 2 (S1 and S2) and are used to display the perturbation data in Figure 4.6 on a longitude-pressure grid at 70° N. The color scale indicates the temperature perturbation and clearly shows the 40-50 K departure from zonal mean temperatures during this event. The planetary wave structure can be identified in the wave geopotential contours with S1 being the dominant feature in the wave geopotential. Negative and positive eddy geopotential contours are associated with the Arctic polar vortex and Aleutian anticyclone, respectively. Changes in wave geopotential are tied to changes in wave temperature through the perturbation hydrostatic law in a manner expressed by Salby et al. [2002] as $\frac{\partial T'}{\partial z} = \frac{H}{R}\frac{\partial^2 \Phi}{\partial z^2}$. Thus, where the wave geopotential has a strong positive curvature, the perturbation lapse rate, i.e. the negative of the vertical wave temperature gradient, will be strongly positive; where the wave geopotential has a strong negative curvature, the perturbation lapse rate will be strongly negative.

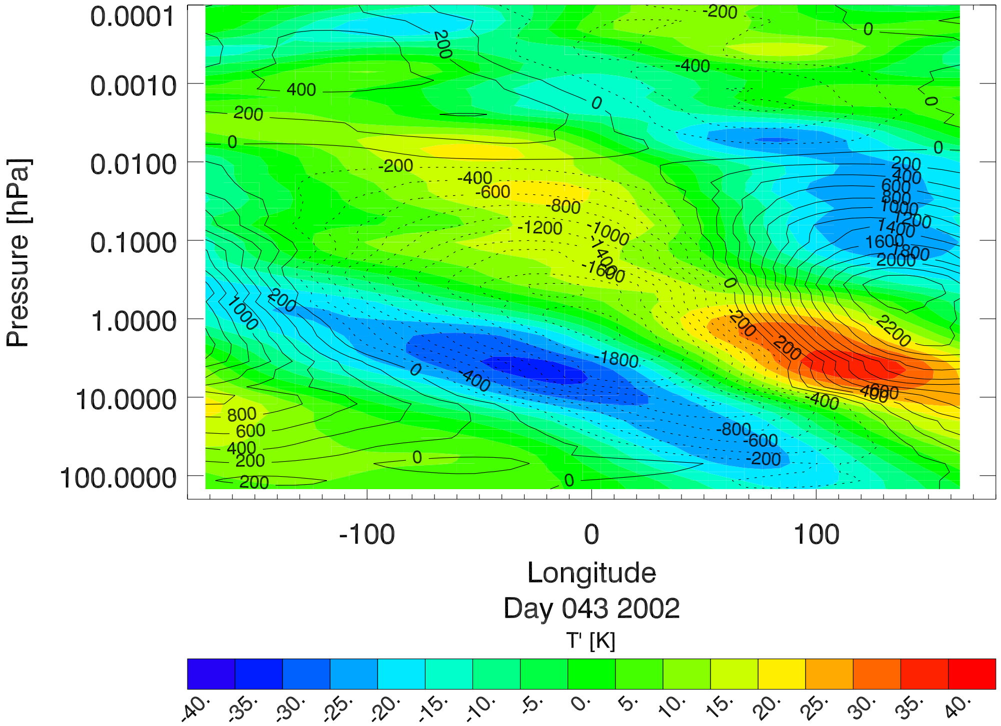

Figure 4.6: Zonal wavenumbers 1 and 2 (S1 and S2) planetary wave perturbations around the 70° N latitude circle on 13 February 2002. SABER temperature is in color and geopotential height is contoured (positive values are solid lines while negative values are dashed) [84].

This is clearly observed in Figure 4.6 at longitudes near 140° E and -20° E, respectively.

The wave geopotential amplifies with height through the lower stratosphere taking on a westward tilt and maximizing near the 1 hPa pressure level. The westward tilt is indicative of vertically propagating planetary waves and the increased availability of potential energy. Above this level, the wave geopotential begins to decrease and displays little tilt with height. This is indicative of planetary wave absorption or breaking in the upper stratosphere and the transfer of eddy momentum flux to the mean flow. Therefore, planetary wave absorption occurs in the upper stratosphere during this event, primarily at wavenumber 1 due to the vortex and the anticyclone, and appears to be the wave-driven source for the ageostrophic circulation. It should be noted that it is difficult to separate from the resultant temperature and geopotential perturbations the degree of contribution that originated from planetary wave absorption alone or through subsequent perturbation growth due to a baroclinic instability. The available potential energy comes from, and is replenished by, planetary wave transience and is converted to kinetic energy to drive the indirect ageostrophic circulation. The subsequent adiabatic heating and cooling may promote baroclinic instability by which amplifies the disturbance.

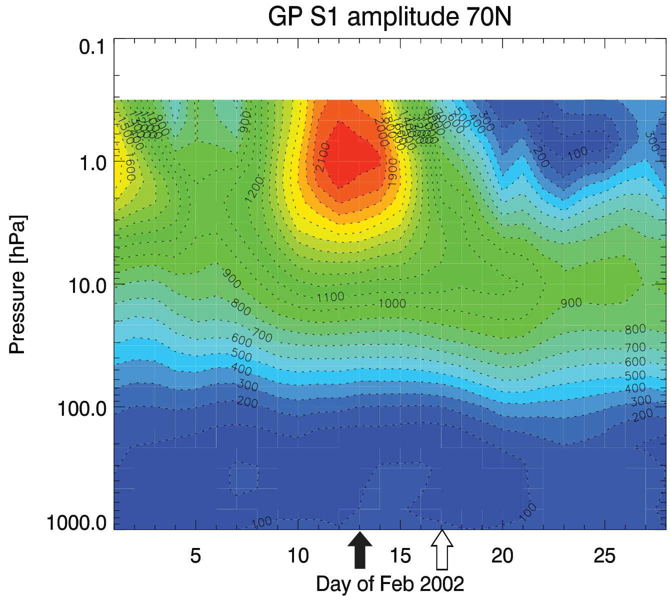

Figure 4.7: Using MetO assimilated temperature fields, the zonal wavenumber 1 planetary wave amplitudes at 70° N are shown for the days leading up to the case study event date on 13 February 2002 (solid black arrow). The perturbation amplitudes reach a maximum near 1 hPa around 12 February 2002. An SSW event has been identified on 17 February 2002 by Charlton and Polvani [2005] and is indicated by a white arrow [84].

For this particular case study, an amplification of planetary wave S1 was observed leading up to the event (13 February 2002). The S1 planetary wave amplitude with time is shown in Figure 4.7. Maximum amplification is located near 1 hPa and temporally peaked on 12 February 2002, the day before our analyzed event. Subsequent to the event, the S1 amplitude subsides significantly by 15 February 2002 and the polar middle atmosphere takes on a much more complex form, with higher frequency harmonics, as a major stratospheric warming begins on 17 February 2002[10]. Our identified event precedes the major warming and this is a common observational occurrence [e.g. von Zahn et al., 1998; Manney et al., 2008; Thayer and Livingston, 2008].

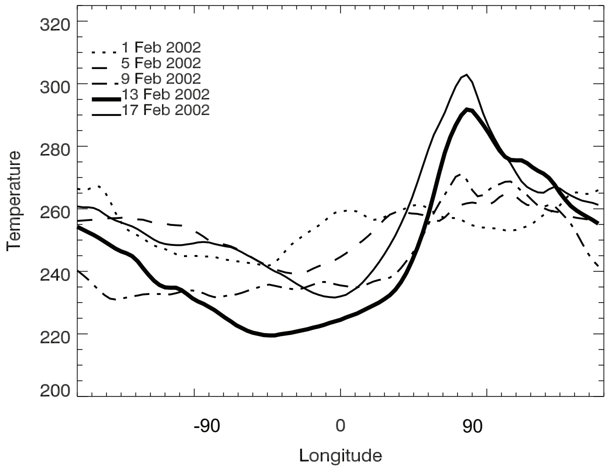

Figure 4.8: Temperatures on a common latitude circle containing the temperature high on the 2.154 hPa pressure surface from MetO assimilated temperature fields for select dates around the case study date of 13 February 2002 (solid line) [84].

In the days leading up to the identified event, the temperature minima and maxima on the 2.154 hPa pressure surface were determined for the closest latitude circle, predominantly near 70° N. These daily temperatures leading up to the event and including the beginning of the SSW are illustrated in Figure 4.8. In early February, the temperature varies by approximately 25 K around the latitude circle of maximum temperature variation. As the middle atmosphere becomes more perturbed by the S1 planetary wave leading up to our event (13 February 2002), the temperature difference between minima and maxima extrema increase to over 70 K. In addition, west of the longitude of the temperature maxima (approximately 80° E), the temperature gradients become increasingly steep, reminiscent of the temperature structures in the troposphere observed across a front. The phase of the temperature structures remains nearly constant, indicating a quasi-stationary planetary wave. As the event progresses into an event meeting the definitions of a major SSW (17 February 2002), the temperature maxima at this pressure surface continues to increase to over 300 K but the whole pressure surface warms so that the temperature differential is not significantly different than on 13 February 2002. The morphological study of the 2006 SSW by Manney et al. [2008] shows very similar behavior in synoptic-scale disturbances in the middle atmosphere prior to the SSW and they address the subsequent evolution of the middle atmosphere during and after an SSW.

From the aggregate observational evidence provided by the SABER and MetO data sets for this case study, a polar wintertime USLM disturbance is shown to be present and have a strong dynamical impact on the thermal structure and polar vortex in the middle atmosphere. Common characteristics of this disturbance are 1) strong vertical and horizontal temperature gradients on the east side of the polar low, 2) intermediate horizontal scale size, 3) poleward warm air advection below the polar high and cold advection below the polar low, and 4) differential (i.e. height dependent) thermal and vorticity advection.

4.1.1 Characteristics of USLM Events

This section is partially adapted from Greer, Thayer & Harvey [2013].

Based upon past observations(e.g., [90],[40],[84]), USLM disturbances were found to have the following characteristics:

- Strong baroclinic conditions near the stratopause
- Strong positive temperature gradient below 40 km
- Elevated stratopause temperatures in excess of 290 K
- Stratopause located at 41 km +/- 2 km
- Separated mesopause located between 65-85 km in altitude
- Concentrated latitudinal and longitudinal extent of temperature anomaly (synoptic scale) at stratopause
- Rapid development

4.2 USLM Climatology in MetO and WACCM

4.2.1 Identification Methodology of USLM events

USLM disturbances are tagged by searching for significant periods of deviation from the seasonal fit. Each day in the data sets (MetO and WACCM) is examined for the maximum temperatures at the 2 hPa level anywhere between 40° and the pole. Using regression, the following function is fit to the entire database of maximum daily temperatures using a least squares technique:

$$f(t) = b_1 + b_2 t + b_3 cos(2\pi t) + b_4 \sin(2\pi t) + b_5 \cos(4\pi t) + b_6 \sin(4\pi t) \tag{4.3}$$

Where t is time, and b are coefficients to be fit. This allows for an annual variation as well as a semi-annual variation. The following coefficients were determined for each hemisphere:

Table 4.1: Polynomial fit coefficients of the seasonal function for MetO and WACCM

	MetO		**WACCM**	
	NH	**SH**	**NH**	**SH**
b_1	264.30	266.28	264.37	268.38
b_2	0.22	0.08	0.01	-0.01
b_3	-5.51	18.29	-1.61	14.83
b_4	5.00	-4.75	7.33	-12.99
b_5	2.77	-1.27	3.79	2.19
b_6	7.14	0.80	1.79	-2.56

In equation (1), b_1 is the mean of the temperature data (units of K), b_2 is the linear trend component (units of K/year), the square root of the sum of the squared b_3 and b_4 coefficients give the annual amplitude while the square root of the sum of the squared b_5 and b_6 coefficients give the amplitude of the semi-annual variation. The MetO fit is significant at the 95% confidence level. The annual variation dominates in the Southern Hemisphere (SH) in both the assimilated data and the model, but the semi-annual variation dominates in the Northern Hemisphere (NH) due to the larger temperature variability during the Arctic winter. The model shows a stronger semi-annual variability in the SH than is seen in MetO.

From this analysis, temperatures in excess of 15 K from the fitted function were flagged and found to occur only in the winter months (November through March for the NH, April through October for the SH). The criteria of 15 K above the fitted temperature was selected due to this difference exceeding one standard deviation of winter temperatures in both hemispheres for MetO($\sigma_{NH} =$ 13.1 K, $\sigma_{SH} = 9.4$ K) and it is generally robust. If a day meets this requirement, it is designated as a candidate day for a USLM disturbance. If this condition persists for 2 or more days in any 4-day window, it is identified as a USLM event and is included in the climatology. The start and end dates of all USLM events are identified as the days over which these criteria are met. This methodology reduces the effects of abrupt but short-lived temperature enhancements due to transient waves.

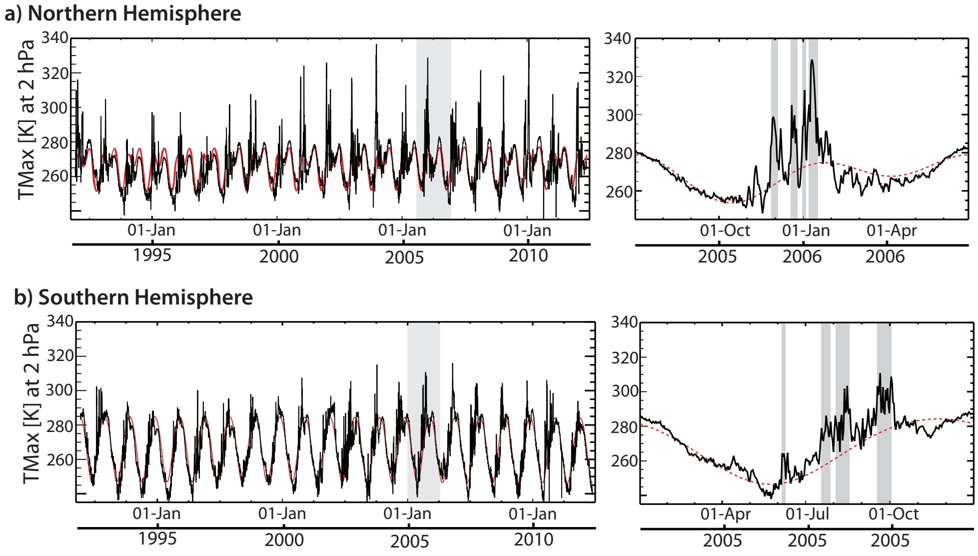

Figure 4.9: a) Time series of the daily maximum MetO temperature [K] poleward of 40N for 20.5 years (left) and for the 2005-2006 season (right). The red dashed line is the fitted seasonal function. The gray box in the left panel indicates the season shown on the right. During the 2005-2006 season, the vertical gray shading indicates periods when USLM conditions meet the established criteria. b) Time series for the Southern Hemisphere on the left and the 2005 winter season on the right, using the same notation as in the Northern Hemisphere.

Figure 4.9a shows the 20.5-year time series (1991-2012) of the MetO 2 hPa polar cap maximum temperature and an enlarged view of a single NH season. Figure 4.9b shows the same set of plots for the SH. In both panels, the solid black line is the daily maximum temperature between 40°N and the pole. The gray box in the left panels indicates the season shown in the right panels. The red dashed line in the single season panel is the fitted seasonal function. The mean seasonal cycle amplitude in the NH is approximately 20 K and the daily variation in maximum polar temperature exhibits 30 K to 50 K temperature spikes. The SH exhibits a larger mean seasonal cycle amplitude (approximately 30 K) but smaller daily variations in the maximum polar cap temperature. This difference between hemispheres is presumably due to the more stable polar vortex in the SH hemisphere. Shading in the right panels indicates USLM disturbances based on the established criteria.

a) Northern Hemisphere

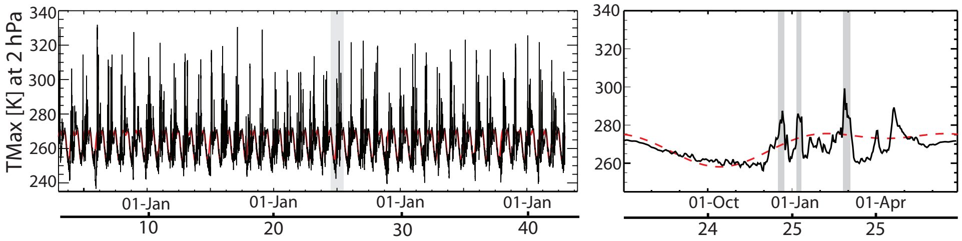

b) Southern Hemisphere

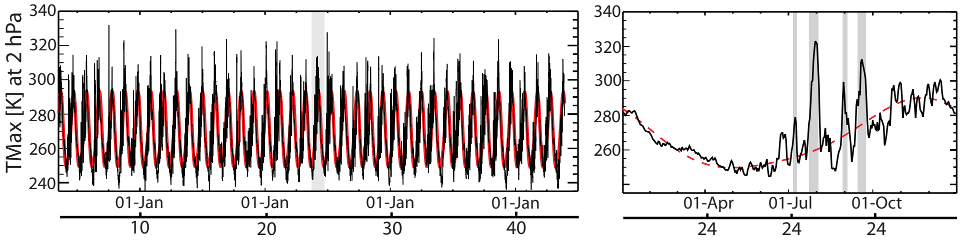

Figure 4.10: a) Time series of the daily maximum WACCM temperature [K] poleward of 40°N for the 40 year run (left) and for season 24–25 (right). The red dashed line is the fitted seasonal function. The gray box in the left panel indicates the season shown on the right. During season 24, the vertical gray shading indicates periods when USLM conditions meet the established criteria. b) Time series for the Southern Hemisphere on the left and winter season 24 on the right, using the same notation as in the Northern Hemisphere.

For comparison, the same analysis of time series using WACCM is shown in figure 4.10. Figure 4.10a shows the 40 year WACCM run of the 2 hPa polar cap maximum temperature and an enlarged view of a single NH season. Figure 4.10b shows the same set of plots for the SH. In both panels, the solid black line is the daily maximum temperature between 40 N and the pole. The gray box in the left panels indicates the season shown in the right panels. The red dashed line in the single season panel is the fitted seasonal function. The mean seasonal cycle amplitude in the NH is approximately 20 K and the daily variation in maximum polar temperature exhibits 40 K to 50 K temperature spikes (similar to the MetO analysis). The SH exhibits a larger mean seasonal cycle amplitude (approximately 40 K, which is approximately 10 K higher than the MetO analysis) but smaller daily variations in the maximum polar cap temperature. WACCM appears to be doing a reasonably good job of capturing the NH, but may be having some problems with the Southern hemisphere.

4.2.2 Summary of USLM Characteristics

For the MetO database of 20.5 years (1991 - 2012), a total of 49 USLM events are identified in the NH, and 31 USLM events are identified in the SH. These results are displayed in table 4.2 and table 4.3. Their onset dates are listed in Appendix A. On average, 2.3 USLM disturbances occur each NH season, while the frequency in the SH is 1.6 USLM events/year. The onset dates for major and minor SSWs are also cataloged for the data set. SSW dates are in agreement with Charlton and Polvani [2007] and extend their record to 2012. In the NH, 16 major SSWs and 72 minor SSWs are identified. The frequency of major SSWs is 0.76 per NH winter season. In the SH, 1 major SSW and 15 minor SSW's are identified. The one major SSW in the SH in 2002 has been examined extensively in the literature [e.g., Krüger et al., 2005; Simmons et al., 2005; Manney et al., 2005]. The seasonal average frequency of minor SSWs is 3.5 in the NH and 0.73 in the SH. Thus, the frequency of SH minor SSWs is similar to the frequency of major SSWs in the NH.

In the 40 year run of WACCM, a total of 118 USLM events were identified with a frequency of 2.95 events/ year in the Northern Hemisphere. In the Southern hemisphere, there were a total of 89 events with a frequency of 2.2 events per year. The seasonal average frequency of minor SSWs is 2.13 in the NH and 1.33 in the SH, somewhat different that those observed in MetO. Additionally, the model generated 27 major SSW events (0.67 events/year) in the Northern hemisphere. No major SSWs were generated in the Southern hemisphere.

One of the most striking characteristics of the USLM disturbance is its temperature profile. Figure 4.11 shows the temperature profiles of USLM events cataloged in MetO and the WACCM

Table 4.2: Northern Hemisphere Summary of MetO & WACCM Event Results

	MetO	WACCM
Data Set Length [yr]	20.5	40.0
Total USLM Occurrences [events]	49	106
USLM Frequency [events/yr]	2.4	2.65
Total Minor SSWs Occurrences [events]	72	127
Minor SSW Frequency [events/yr]	3.5	3.18
Total Major SSWs Occurrences [events]	16	23
Major SSW Frequency [events/yr]	0.78	0.58

Table 4.3: Southern Hemisphere Summary of MetO & WACCM Event Results

	MetO	WACCM
Data Set Length [yr]	20.5	40.0
Total USLM Occurrences [events]	31	89
USLM Frequency [events/yr]	1.5	2.2
Total Minor SSWs Occurrences [events]	15	53
Minor SSW Frequency [events/yr]	0.73	1.33
Total Major SSWs Occurrences [events]	1	0
Major SSW Frequency [events/yr]	n/a	n/a

run. Each black line is an individual profile of an event on the event's peak day through the warm anomaly found at the stratopause (this latitude/longitude location will vary with individual events). Red indicates is the average of all the identified USLM disturbances; the blue line is the climatological mean profile (DJF for the NH and JAS for the SH) at the location of USLM disturbances (63°N and 68°S). Figure 4.11 clearly illustrates the low altitude stratopause with anomalously high temperature; the temperature difference is less extreme in the SH. Also evident in Figure 4.11 is a mesosphere feature seen in both hemispheres near 0.01 hPa (approximately 70 km). This mesosphere cooling has also been observed in lidar profiles and TIMED/SABER observations of the NH[85][84], and is sometimes referred to as a "separated mesopause" because it is superimposed on the nominal mesopause at approximately 100 km (10^{-4} hPa). The minimum temperature in this mesosphere cooling is less than 190 K, some 30 K cooler than the winter season average profile. It is believed that this cooling is associated with the warm anomaly at 2.0 hPa. However, it should be noted that the associated cooling in the mesosphere may be out of phase with stratopause warming (due to the tilt of the polar vortex), and so a deeper cooling may be observed in location not directly above the stratopause warming. This figure also illustrates how during USLM events, the lower stratosphere remains relatively undisturbed and differentiates them from minor SSWs.

Figure 4.12 shows the annual cycle of the distribution of days per month per year that meet USLM criteria in each hemisphere for MetO (left) and WACCM (right). USLM disturbance days occur from November through March (although WACCM shows a few occurrences in October) in the NH and from May through September in the SH. The MetO data shows a pronounced preference for USLM disturbances during December in the NH and during July in the SH, while WACCM shows less of a preference for December.

Figure 4.13 shows USLM disturbance event duration in both hemispheres and data sets. The mean duration of a MetO USLM event in the NH is 8 days, while the mean duration of a USLM event in the SH is only 4 days. The duration of USLM events are not normally distributed. While MetO USLM disturbances can last as long as 3 weeks, events lasting one week or less comprise 57% of events in the NH and 58% in the SH. WACCM shows a pronounced preference for shorter lived events.

The warm temperature anomaly being located on the East side of the polar low suggests the possibility that baroclinic instability may be supported by the temperature anomaly. Figures 4.14 and 4.15 shows the geographic distribution of USLM disturbance frequency (in color) for all identified MetO and WACMM events in the NH and SH. Note the different frequency scales between the hemispheres. The black contour indicates the average position of the edge of the polar vortices during USLM days at the 1600 K potential surface (near 2 hPa) as defined by Harvey et al. [2002]. The warm anomaly associated with USLM disturbances preferentially occurs over Northeastern Russia and Scandinavia in the NH and south of Africa in the SH. In both hemispheres the warm anomaly occurs most frequently between 0° E and 90° E along the Eastern edge of the polar vortices. Thus, ground-based observation sites in Scandinavia and northern Russia in the NH and Davis Station or Dome Fuji Station in the SH have several opportunities per year to observe USLM events. The location of the thermal anomaly being on the east side of the low is also reminiscent of the structure of a developing tropospheric baroclinic wave [84].

Based on these results, the WACCM model does indeed spontaneously and internally generate USLM disturbances that satisfactorily match observed characteristics. With a comprehensive description of the phenomenology and climatology estblished, the dynamical mechanisms behind the evolution of USLM disturbances can now be developed.

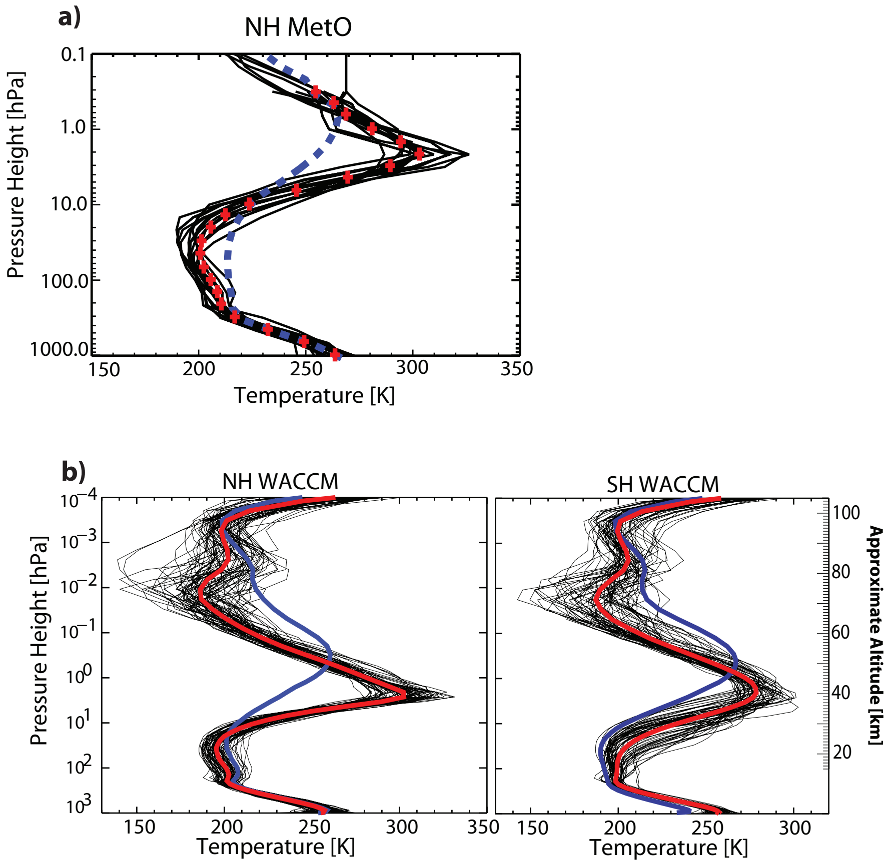

Figure 4.11: (a)MetO temperature profiles for the Northern Hemisphere; (b) WACCM temperature profiles for the Northern Hemisphere (left) and Southern Hemisphere (right) that intersect the 2 hPa warm anomaly on peak days during USLM disturbances. Individual daily temperature [K] profiles are black, the average profile is indicated in red. An average temperature profile at 63°N (68°S for WACCM) from December, January and February months for the entire MetO or WACCM databases are plotted for comparison as in blue.

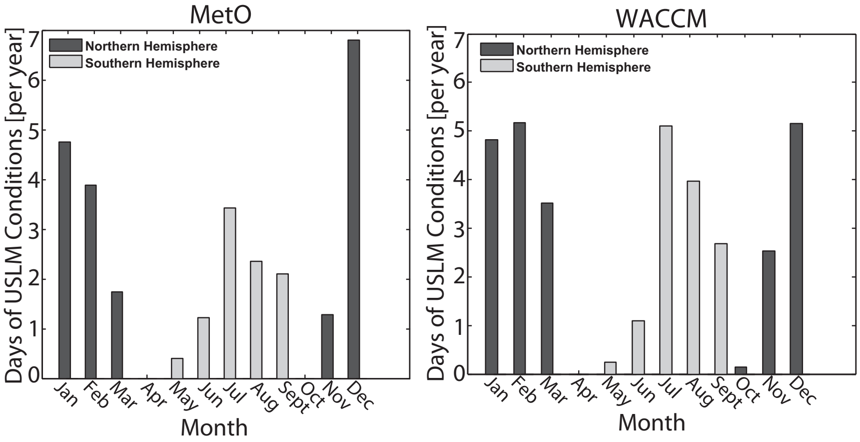

Figure 4.12: Average monthly frequency of USLM disturbance days per year; (left) MetO, (right) WACCM. Frequencies in the Northern (Southern) Hemisphere are in black (gray).

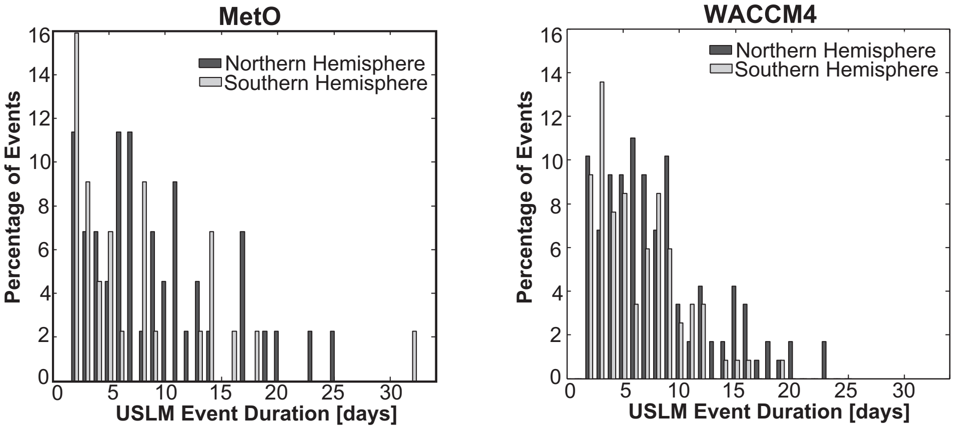

Figure 4.13: Bar plot of USLM duration; (left) MetO, (right) WACCM. Frequencies in the Northern (Southern) Hemisphere are in black (gray).

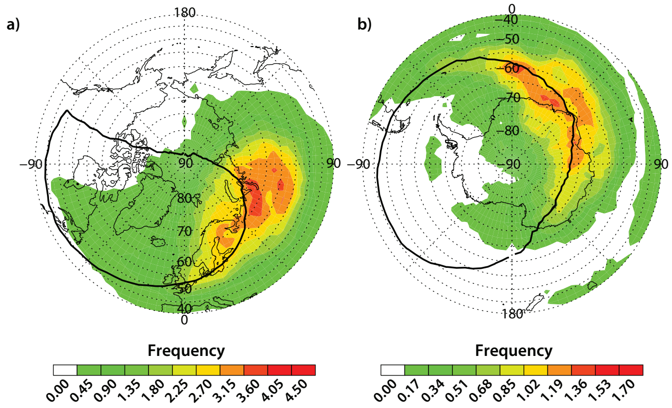

Figure 4.14: Polar stereographic projections of the geographical distribution of USLM event occurrence frequency in the Northern Hemisphere (a) and Southern Hemisphere (b). Frequency equals the number of days per year that a location satisfies USLM conditions. The average location of the boundary of the polar vortex for USLM days is indicated by the black contour at the 1600 K potential surface (near 2 hPa) as defined by Harvey et al. [2002]. Note the different frequency ranges between the hemispheres.

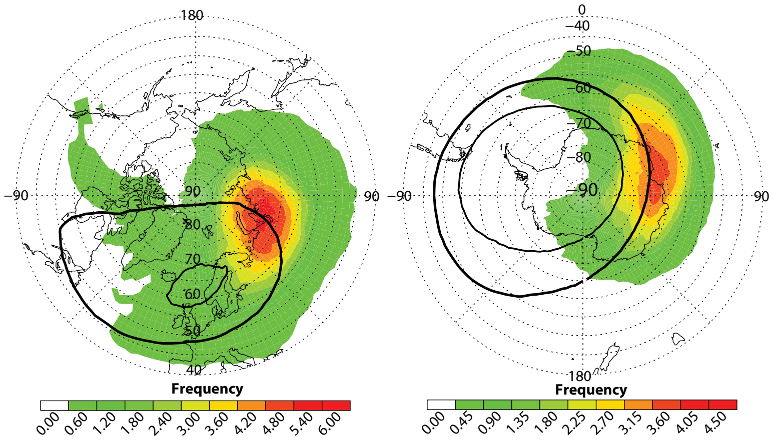

Figure 4.15: WACCM. Polar stereographic projections of the geographical distribution of USLM event occurrence frequency in the Northern Hemisphere (left) and Southern Hemisphere (right). Frequency equals the number of days per year that a location satisfies USLM conditions. The average location of the boundary of the polar vortex for USLM days is indicated by the black contour at the 1600 K potential surface (near 2 hPa) as defined by Harvey et al. [2002]. Note the different frequency ranges between hemispheres.

Chapter 5

Dynamical Mechanisms of USLM Events

This chapter is partially adapted from Greer, Thayer & Harvey [2013].

5.1 Introduction

Using the identification algorithm described in section 4.2.1, a composite analysis of the identified NH USLM events was created for both the MetO and WACCM data sets. USLM disturbances are regional phenomena that occur over a range of longitudes and latitudes (as shown by the colored region in Figure 4.14). For this composite analysis,a subset of all identified USLM disturbances wherein the center of the warm temperature anomaly is within +/-5 latitude of the mean location of all thermal anomalies at 2 hPa in the data set (52.5°E and 62.5°N for MetO, 53.1°E and 61.5°N for WACCM) were included. The fields of temperature and geopotential height are shifted in longitude so that all maximum thermal anomalies are in phase and located at the mean longitude location (52.5°E for MetO, 53.1°E for WACCM). In addition, vortex splitting events have eliminated for clarity. This results in a composite of 16 USLM events in this latitude / longitude region for MetO(the onset dates of these events are noted in Appendix A) and a total of 63 USLM events in WACCM (out of a total of 106 WACCM identified events).

Figures 5.1 and 5.2 illustrate the USLM life cycle over eight days with day 0 identified as the day when the temperature anomaly was warmest between 40° N and the pole at 2 hPa; the other days are noted in relation to day 0. The eight panels show the progression of 2 hPa temperature (filled color contours) and geopotential height (black contours) for days -4 through

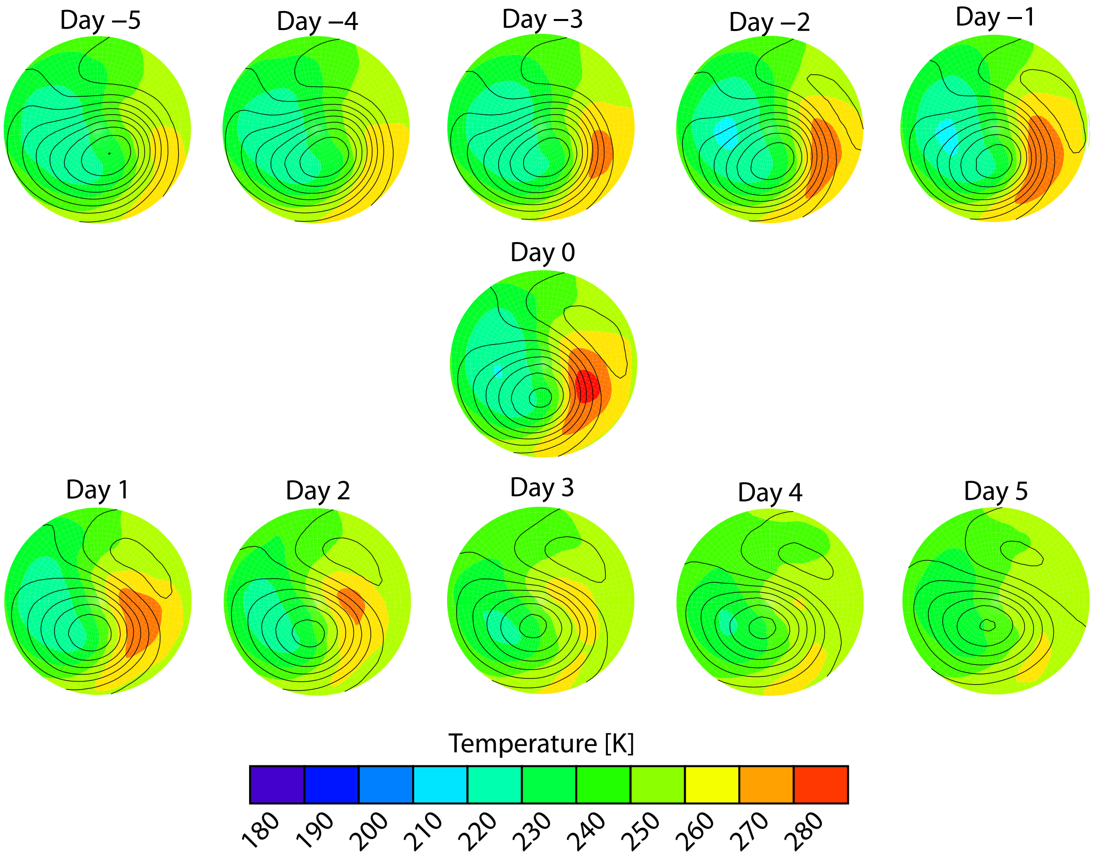

Figure 5.1: MetO. Northern Hemisphere composite maps of temperature [K] at 2 hPa in color on days surrounding USLM events. All events have been shifted in longitude such that the phase of the temperature maximum is aligned. Solid black lines are geopotential height; contour intervals are 400 m. The geopotential highs and lows are indicated by white "H" and "L" symbols, respectively [84].

day +3. During the onset of USLM events (days -4 to -1), the polar vortex (denoted with an "L") is increasingly displaced from the pole as the Aleutian high (denoted with an "H") strengthens and moves poleward. This synoptic development is displayed in the growth of planetary wave 1 (PW1) at 60° N. In the days leading up to day 0, the cold and warm anomalies are displaced from the core of the circulation systems such that large horizontal thermal advection occurs. This leads to strong baroclinic conditions and thermal gradients [see Thayer et al., 2010] that results in strong vertical wind shear through the thermal wind relation. A warm temperature anomaly develops on the east side of the polar low in the region of large geopotential height gradients (the polar night

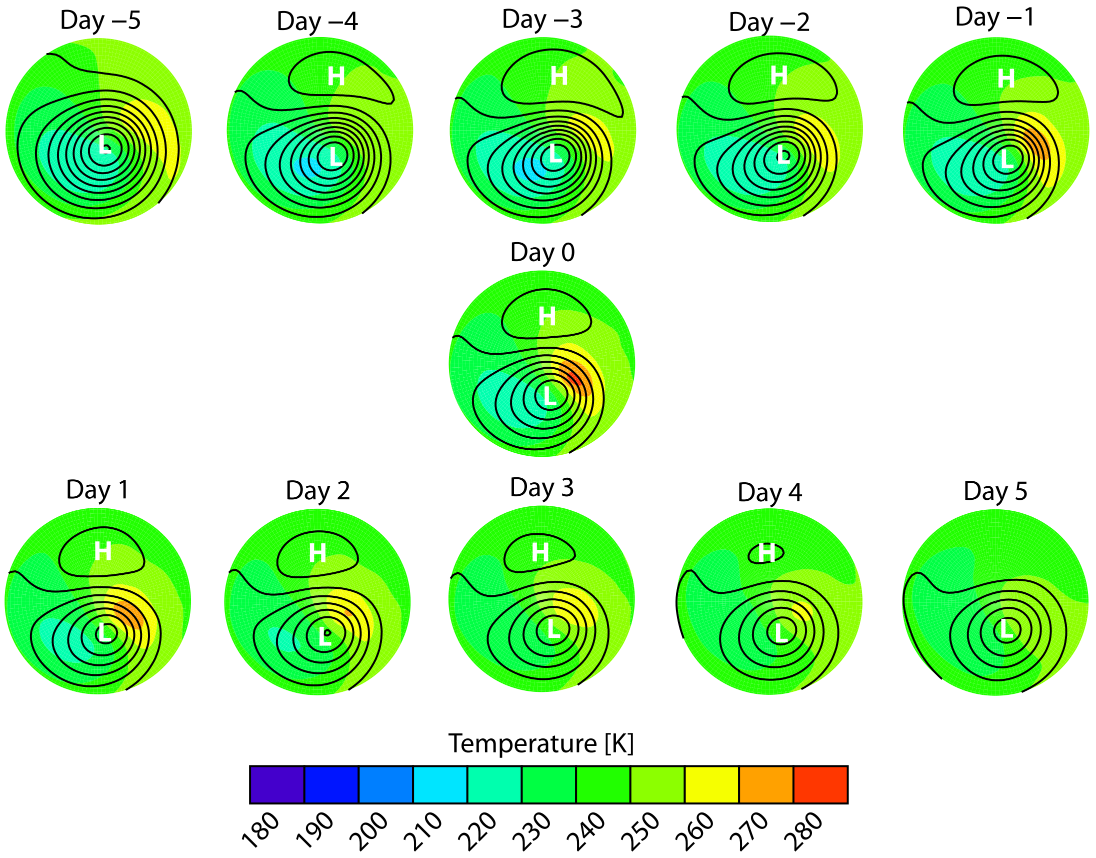

Figure 5.2: WACCM. Northern Hemisphere polar stereographic composite maps of temperature [K] at 2 hPa in color on days surrounding USLM events. All events have been shifted in longitude such that the phase of the temperature maximum is aligned. Solid black lines are geopotential height; contour intervals are 400 m. The geopotential highs and lows are indicated by white “H” and “L” symbols, respectively.

jet). The cool temperature anomaly near 90° W moves equator ward and warms over 10 K between day -4 and day 0. On day -2, PW1 amplitudes at the 2-hPa level at 65°N maximize; on day 0 the warm temperature anomaly maximizes. On day +1 the warm temperature anomaly is cooler compared to day 0, but the warm anomaly expands to cover a larger area. As the event continues, the warm temperature anomaly dissipates, conditions become less baroclinic and PW2 activity increases. After day +2, the variance of the temperature and geopotential height become much larger and the individual events begin to diverge in their development and structure (not shown). This is likely due to some USLM events dissipating and some events developing into SSWs. MetO and WACCM show remarkably similar development and these composites can be used for further analyses that may draw general conclusions about all USLM events.

Based on qualitative indications in Figures 5.1 and 5.2 that planetary wave breaking is driving USLM disturbances, further analyses of the WACCM output help to complete an understanding of the underlying dynamics. Through this analyses it is shown that planetary wave breaking at the 2000 K isentropic level causes a deceleration of the Westerlies through wave mean-flow interaction. By continuity, an ageostrophic vertical motion arises due to this deceleration, and adiabatic heating/cooling develops. This increases the horizontal temperature gradient at the 2 hPa level (approximately 1500 K isentropic level), leading to an increase in the thermal wind gradient, vertical shear and baroclinic conditions. These conditions support a baroclinic instability, which could feedback into the established primary disturbance and magnify the intensity of the thermal anomaly at 2 hPa. The action of these processes are shown in the following subsections.

5.2 Planetary Wave Breaking

The composite life cycles suggests that the growth phase of a USLM disturbance corresponds with increased PW1 and/or PW2 amplitudes. Figure 5.3 examines the PW amplitudes and phases of USLM events and compares them to “non-USLM event” winter days in MetO. Figure 5.3a illustrates the relationship between the maximum temperature during USLM events and the PW amplitudes (calculated from the geopotential height distribution at 65° N, 10 hPa) two days prior. For the entire MetO NH winter dataset (November through March, 21 seasons), we compute daily maximum polar cap temperatures at 2 hPa and PW amplitudes (the sum of PW1 and PW2) at 10 hPa from two days prior; PW amplitudes were seen to maximize two days prior to USLM events in the composite event. The black contours represent the 2-D frequency distribution of all 3354 winter days that do not meet USLM conditions. There is a concentration of days with low maximum polar cap temperatures (≈250 K) and low PW amplitudes (≈300 m); these are days in which the horizontal thermal structure is minimally baroclinic and a strong polar vortex is nearly pole-centered. As a subset of all NH winter days, the red crosses indicate days during

USLM disturbance life cycles (379 days). There is a cluster of USLM disturbance temperatures above ≈275 K (red crosses) with PW amplitudes larger than ≈800 m, indicating that strong PW amplitudes at 10 hPa are observed two days prior to USLM disturbances at 2 hPa. This suggests that increased PW amplitudes favor USLM event development, but large wave amplitudes do not always lead to USLM events. Figure 5.3b shows the PW1 and PW2 amplitude results for the SH. Overall, the non-USLM day (black contours) are concentrated in smaller PW amplitude ranges while USLM days represent events with a wide range of PW amplitudes. Despite having fewer USLM days in the SH, it is clear that (like the NH), these events are associated with stronger PW amplitudes.

Figure 5.3c shows the relationship between maximum polar cap temperature at 2 hPa and the differential zonal phase of PW1 geopotential height between the 10 hPa and 2 hPa levels at 65° N. The mean differential phase or vertical tilt for all non-USLM winter days is -19.3° of longitude (indicated by dashed back line). Negative phase changes with height are associated with westward tilting structures. Wintertime westward tilts are a sign of upward propagating planetary waves; when the phase becomes more vertical it signifies that the PW is breaking [73]. As in Figure 5.3a, all USLM days are plotted as red crosses. The mean westward tilt on these days is -37.9° (red dashed line), nearly double the value for days when USLM conditions are not met. The larger westward tilt is indicative of strong baroclinic conditions, a necessary condition for the onset of a USLM disturbance, and suggestive of the possibility of baroclinic type instabilities. Figure 5.3d shows the zonal phase analysis for the SH. For the population of all non-USLM winter days, the average phase difference between 10 hPa and 2 hPa is -17.7°, while the USLM days display a phase difference of -26.2°. This is not as strong as in the NH, but still a significant difference indicating propagating planetary waves and strong baroclinic conditions in the SH during USLM conditions. These results indicate the need for the propagation of large-amplitude PW to the upper levels of the stratosphere for USLM disturbances to occur. However, a large amplitude planetary wave propagating through the atmosphere does not necessarily mean that it is interacting with the mean flow, only that it has been amplified in some way from below.

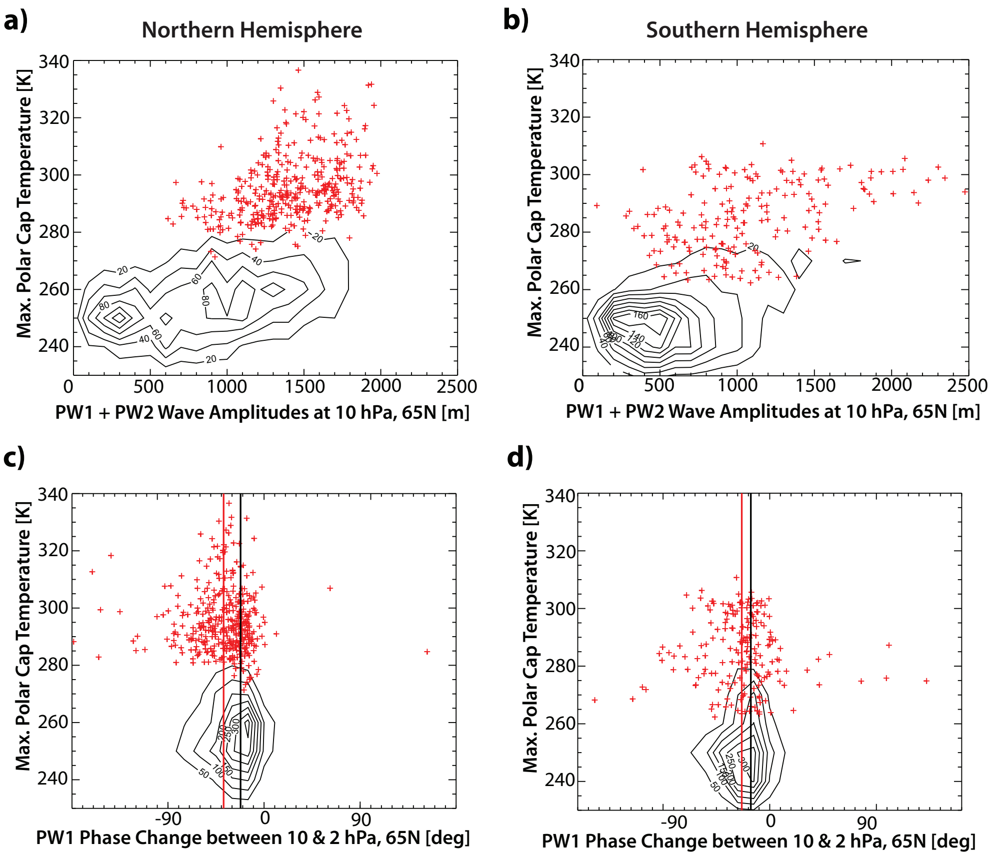

Figure 5.3: a) Comparison of maximum polar cap temperature [K] at 2 hPa with planetary wave amplitudes [m] (sum of PW1 and PW2) two days prior. All NH winter days that do not meet USLM criteria are indicated by the black contours. USLM days are plotted as red crosses. b) Same as a), but for the SH. c) Comparison of maximum polar cap temperature [K] at 2 hPa with the PW zonal phase change [degrees] (east-west tilt with altitude) between 10 hPa and 2 hPa two days prior. All NH winter days that do not meet USLM criteria are indicated by the black contours. d) Same as d), but for the SH. All USLM days are plotted as red crosses. [84]

In the middle atmosphere where planetary waves are described by potential vorticity (PV) contours on isentropic surfaces, a breaking wave occurs when a streamer, filament or blob of high PV is irreversibly pulled off the main bulk of high PV located within the polar vortex and mixed into the surrounding surf zone [6], see section 2.2.2. While planetary wave breaking is supposed to be occurring throughout the middle atmosphere during the winter season, it is likely that a specific planetary wave breaking regime is associated with USLM disturbances. The reversal of the meridional gradient of PV on an isentropic surface is the commonly accepted diagnostic of planetary wave breaking, although there are a variety of implementation methods. Once PV has been calculated on the isentropic surfaces of interest, a search is conducted for the PV reversals ($P_y < 0$). However, planetary waves generally break in layers spanning many isentropic surfaces and we are most interested in large-scale phenomenon. This has lead researchers such as Baldwin & Holton [1988] and Barnes & Hartmann [2012] to use spatial smoothing to focus on these breaking waves. In addition, many groups impose a reversal threshold to screen for significant features [1] [6][68]. However, as the isentropic surface increases, PV values also increase which requires new and arbitrary threshold values to be chosen for each isentropic surface. As we are interested in wide regions of the stratosphere and mesosphere, spanning isentropic surfaces between 300 K and 10000 K, it is too subjective to define threshold values at each isentropic surface. Here we will follow the simplest and most inclusive method of Knox & Harvey [2005] or Hitchman & Huesmann [2007] where $P_y < 0$.

To examine the properties of the planetary wave breaking during the period surrounding USLM events, we derived an index of planetary wave breaking strength S at each of 46 isentropic surfaces spanning the middle atmosphere for each day in the WACCM data set. The method is as follows: The WACCM output variables of temperature [K], zonal wind [m/s] and meridional wind [m/s] are first interpolated onto constant potential temperature surfaces (θ-surfaces: 30000K, 20000, 18000, 16000, 14000, 12000, 10000, 9000, 8000, 7000, 6000, 5000, 4500, 4000, 3500, 3000, 2800, 2600, 2400, 2200, 2000, 1900, 1800, 1700, 1600, 1500, 1400, 1300, 1200, 1100, 1000, 900, 800, 700, 650, 600, 550, 500, 475, 450, 425, 400, 375, 350, 325, 300K). Ertel's potential vorticity IPV and meridional gradient in potential vorticity P_y are then calculated on each surface as described in equation (2.27).

For each longitude, a search is conducted for $P_y < 0$ in latitudes outside the polar vortex boundary as defined by Harvey et al. [2002]. This is done to avoid counting a displaced polar vortex as planetary wave breaking and because we suppose that USLM disturbances are related to planetary wave breaking that occurs equator-ward of the polar vortex. The location of the largest reversal is designated as the arbitrary location of planetary wave breaking and $-P_y$ at that location is recorded as the strength S of planetary wave breaking; only one strongest location of planetary wave breaking is recorded for the polar cap for each day. S can be normalized by the value of the averaged polar cap IPV to account for seasonal and altitude variations. For each day a vertical profile of planetary wave breaking strength can be plotted from the lower stratosphere up through upper mesosphere.

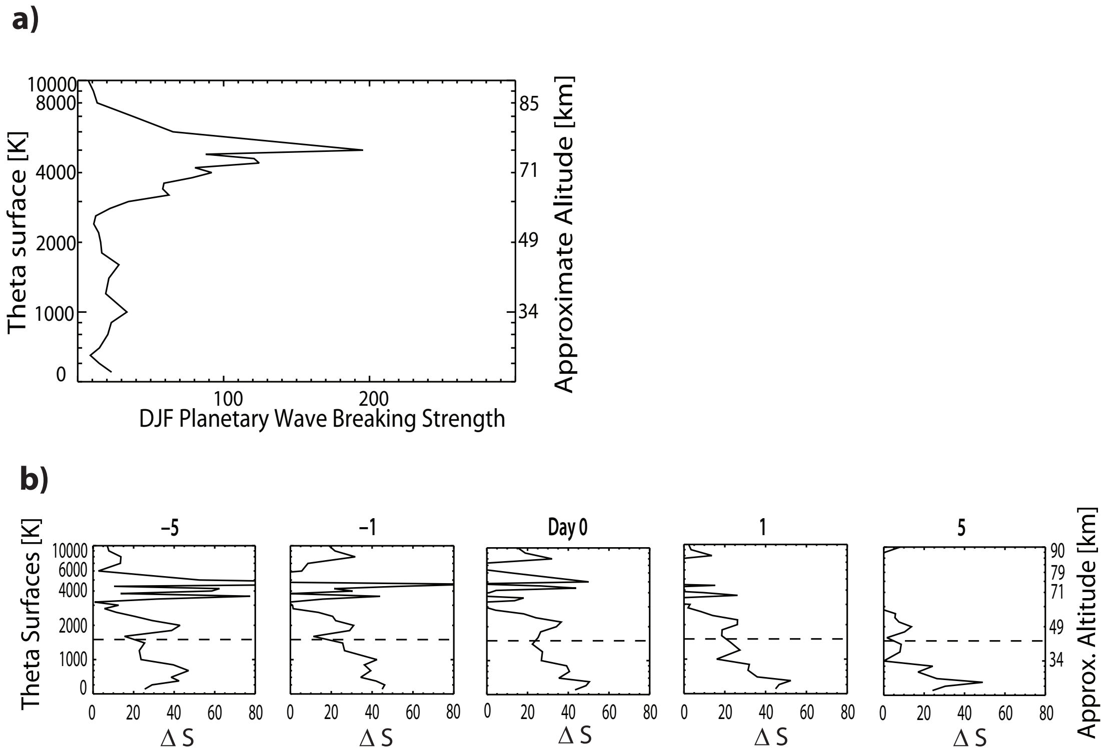

Figure 5.4: Profiles of normalized planetary wave breaking strength S equator ward of polar vortex on isentropic surfaces; a) DJF arctic winter profile; b) difference between composite days and DJF profiles ΔS for selected days of USLM composite described in section 5.1. The dashed line indicates the approximate altitude of the stratopause and thermal anomaly.

Using this methodology we created a series of profiles of planetary wave breaking in the polar winter middle atmosphere, shown in Figure 5.4. Since planetary wave breaking is an ubiquitous phenomenon in the polar winter middle atmosphere but USLM disturbances occur only intermittently, we examined the difference between a WACCM December-January-February (DJF) averaged climatology (without disturbed days that meet minor SSW, major SSW or USLM criteria) of planetary wave breaking and the wave breaking for the USLM composite event described in section 5.1. The DJF climatology profile shows that, on average, some level of wave breaking is occurring at all isentropic surfaces in the middle atmosphere. Since the algorithm looks outside the polar vortex and the zonal model resolution is 2.5° longitude, reversals in PV found are at least 275 km in size, which screens out small scale features such as gravity waves but retains larger phenomenon such as planetary wave breaking but also features of the surf zone. Figure 5.4a shows the DJF climatology planetary wave breaking strength profile where there is a main peak at 5000 K (76 km) in the upper mesosphere, which is the mesospheric surf zone as described by Oberheide et al. [2006]. A minimum in the strength of PWB occurs at 2600 K (58 km) in the lower mesosphere.

In Figure 5.4b, the USLM composite is centered around Day 0, the day of the peak thermal anomaly at 2 hPa. Each day surrounding Day 0 shows the difference between the composite profiles and the DJF climatology, ΔS. The horizontal dashed line indicates the level of the USLM thermal disturbance at 1500 K (2 hPa, 42 km). On day -5, there are three features of note: a large increase in the region of the mesospheric surf zone (approximately 5000 K), and peaks near 2000 K and 1000 K (in the troposphere) indicating stronger planetary wave breaking in these regions than the DJF average. On this day, a critical layer where the zonal mean zonal wind equals zero is located at 5000 K (approximately 75 km), which is likely influencing the increase in planetary wave breaking at this level. The increased breaking at the lower level of 2000 K interacts with the mean flow, which can lead to an alteration of the flow. This general pattern holds for the remaining days leading up to the peak in the composite event. After the peak of the USLM composite event, the strength of the breaking in the mesospheric surf zone begins to diminish on Day 1. Shortly thereafter, the additional planetary wave breaking seen at 2000 K also decreases and collapses to the DJF climatological average.

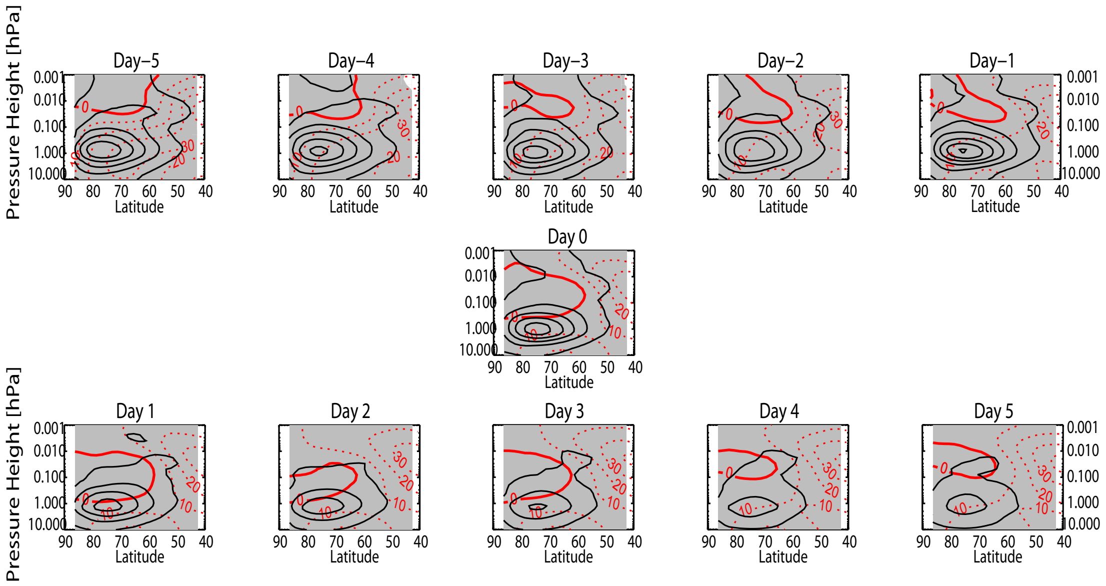

Figure 5.5: Calculations of Div$\mathcal{F}$ for each day of the composite USLM event shown in Figure 5.2. The peak day of the USLM event is designated Day 0, all other days are noted in relation to day 0. Red dashed lines are isolines of the zonal mean zonal wind [m/s]; the solid red line is the zero-wind line. Contours divergence of EP-flux are shown in solid black [0.5 m/s/day]. Regions of convergence of the EP-flux vector are shaded.

5.3 Wave Mean-Flow Interaction

Although the planetary wave breaking exhibited in figure 5.4 implies changes to the flow by momentum and energy arguments, the strength of breaking S, as it is used above, does not quantify how or where the flow is changed. However, the EP-flux is an excellent analysis tool (section 2.2) for examining the wave-mean flow interactions and changes. Figure 5.5 shows the divergence of the EP-flux vector for the WACCM composite USLM event in the meridional plane. The divergence in EP-flux (black solid contours), zonal mean zonal wind (dotted red lines) and the zero wind line (red solid line) indicate the locations of wave mean-flow interactions and the resulting influence on the zonal mean wind. Regions of convergence of the EP-flux vector (and deceleration of the zonal mean zonal wind) are shaded. The EP-flux convergence maximizes at the same level as the increased planetary wave breaking shown in Figure 5.4b near 0.8 hPa (2000 K isentropic surface), acting to decelerate the mean flow. The reversal is relatively shallow reaching only to 0.9 hPa, whereas the definition of a major SSW requires a reversal at 10 hPa or below. The zero wind line in the days before the peak of the disturbance descends from 0.05 hPa (68 km, 3500 K isentropic surface) down to near 1.0 hPa, which indicates that critical layer activity does not become important for the thermal anomaly at 2 hPa until near the peak of the disturbance and does not contribute to its onset. After the peak of the USLM disturbance, the EP-flux divergence diminishes and the zero wind line begins to return to an upper mesosphere height.

5.4 Vertical Motion and Adiabatic Heating

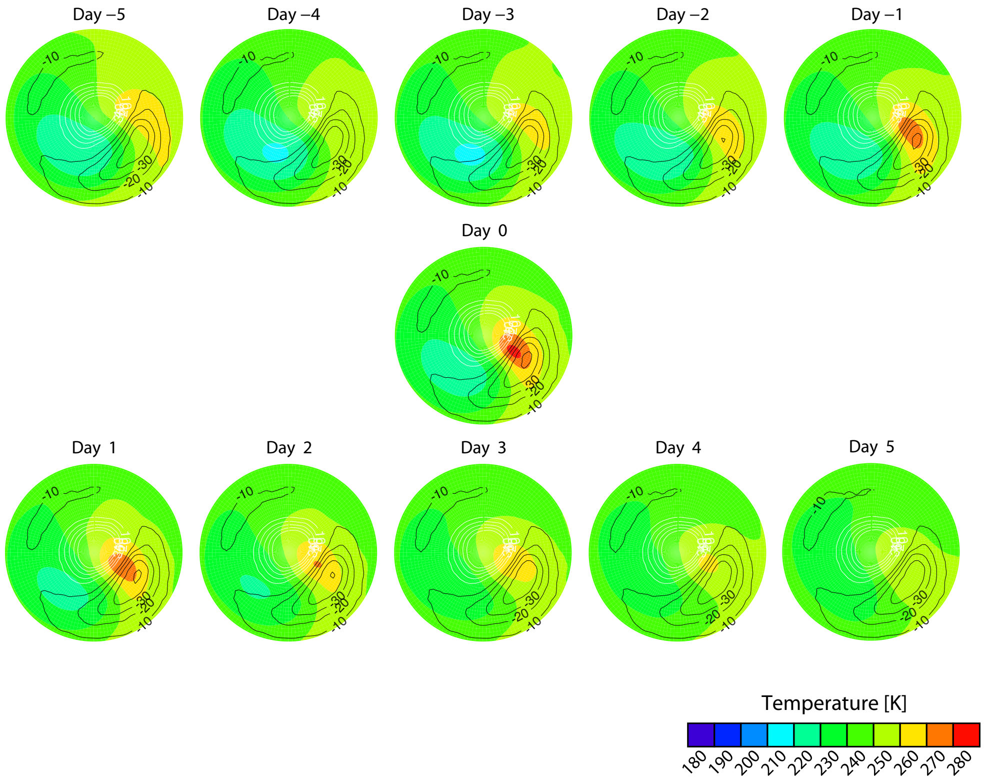

Figure 5.6: Derived $w = \frac{dz}{dt}$ [mm/s] for each day of the composite USLM event shown in Figure 5.2. Black contours indicate descent; each contour is 10 mm/s.

As the zonal mean wind decelerates, continuity requires that vertical air motion compensate for the horizontal convergence of air. Put another way, as the horizontal flux decreases, vertical flux must increase such that there is not an increase or decrease of mass. WACCM output is on pressure levels and the vertical motion is given as $\omega = \frac{dp}{dt}$. This can be converted to $w = \frac{dz}{dt}$ using the hydrostatic and ideal gas laws.

$$w = \omega\left(-\frac{RT}{gp}\right) \tag{5.1}$$

Figure 5.6 shows the evolution of the vertical motion at the 2 hPa level of the composite event from Figure 5.2. Descent is indicated in regions of warm temperature anomaly; it is also in roughly in the same region indicated by the Q-vector from the case study shown in Figure 4.5. On the days surrounding the peak of the composite event, the downward motion maximizes at a value of over 5 cm/s or approximately 4.3 km/day. Using the static stability parameter $S_p = -T\frac{\partial \ln \theta}{\partial p}$ results in $Sp \equiv 0.004$ [K m$^-$1] and a maximum diabatic heating rate of approximately 18 K/day. Including the diabatic cooling (output from WACCM model) results in a total maximum heating rates near $15K/day$.

As the air descends, it adiabatically heats and increases the temperature at the 2 hPa level. This limited region of heating also implies a strong and increasing temperature gradient at this level. Linked through the thermal wind relation, this stronger thermal gradient induces vertical shear in the horizontal wind. Instabilities are associated with horizontal and vertical shears.

5.5 Instabilities

This adiabatic heating accounts for the extreme temperature observed at the 2 hPa level, but the conditions may also support a secondary instability as the wave breaks at smaller and smaller scales. Both barotropic and baroclinic instabilities are candidates given the strong horizontal and vertical wind shears. An inertial instability is unlikely given that the PV for the region being observed (poleward of 40N) does not contain any negative PV blobs or streamers. To test whether an instability might be present at 2 hPa, the composite USLM event can be analyzed using the Charney-Stern criteria, which requires that there be a reversal in the meridional gradient of quasi-geostrophic potential vorticity q_y in the region of interest (see equation (2.51)).

Figure 5.7 shows the meridional gradient in quasi-geostrophic potential vorticity based on

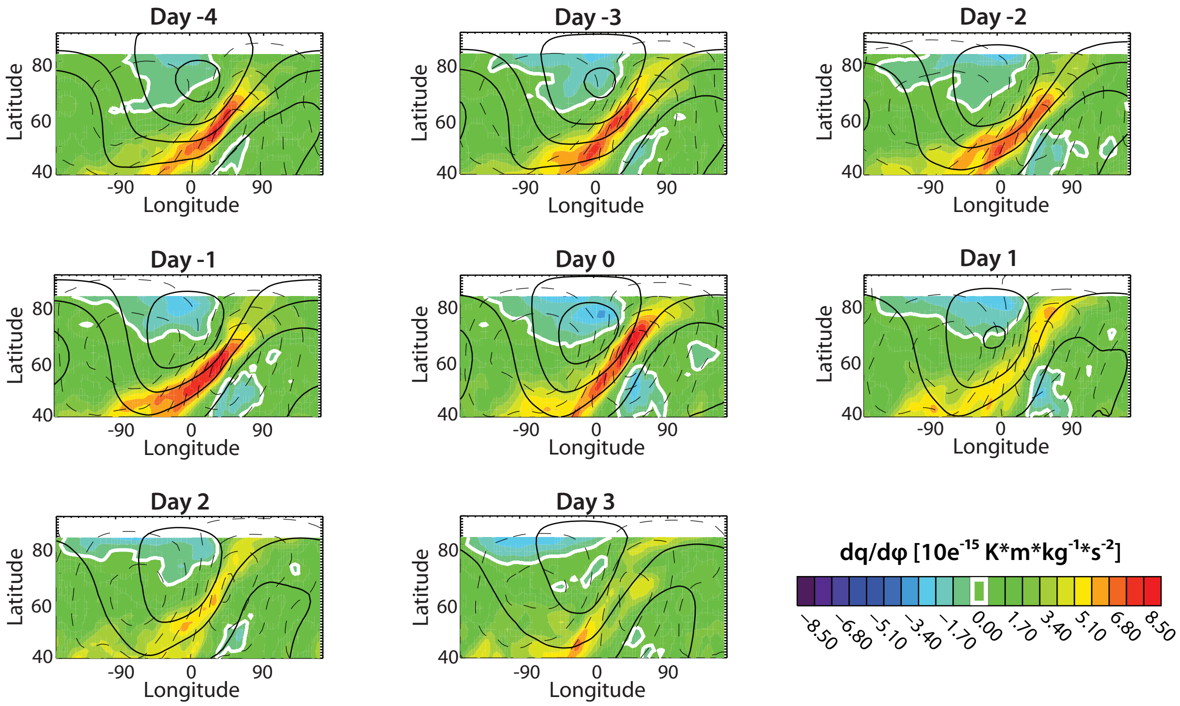

Figure 5.7: MetO. Same as Figure 5.1 but colored contours are the meridional gradient in quasi-geostrophic potential vorticity [10-9 PVU/m], the heavy white line indicates where $dq/dy = 0$, thin solid contours are lines of geopotential height (contour intervals at 750 m), dashed contours are isotherms (contour intervals at 10 K).

the composite life cycle temperature and geopotential height fields at 2 hPa shown in Figure 5.1. A term analysis of the barotropic and baroclinic components of the meridional gradient in quasi-geostrophic PV reveals that this diagnostic is dominated by the baroclinic component (see equation (2.28)) on USLM disturbance days by an order of magnitude, even though there are also strong horizontal wind gradients. Additionally, there is no negative quasi-geostrophic potential vorticity near the warm anomaly (not shown) which rules out inertial instability. The eight panels in Figure 5.7 show the progression of temperature (black dashed contours), geopotential height (black thin solid contours), and the meridional gradient in quasi-geostrophic PV (in color) for day -4 through day +3. A reversal in the meridional gradient in quasi-geostrophic PV is indicated by the thick white contour. The persistent region of negative q_y near the pole is due to the vortex being displaced off the pole (calculating the gradient in vortex-centric coordinates could avoid this polar condition,

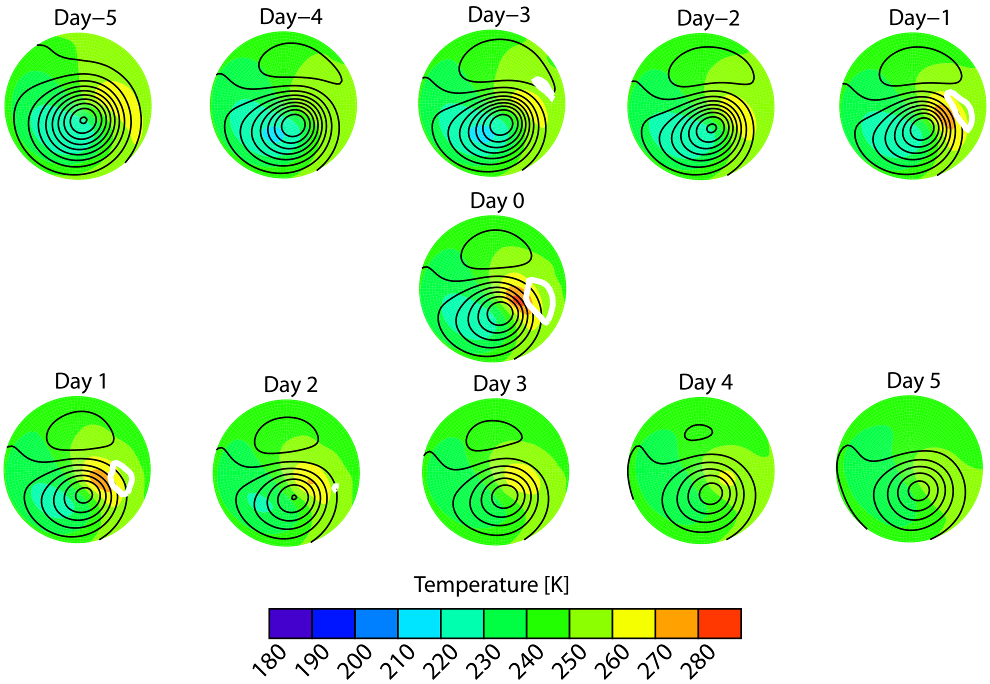

Figure 5.8: WACCM. Same as Figure 5.2 where colored contours are temperature, thin solid contours are lines of geopotential height (contour intervals at 750 m) and the heavy white line indicates where $dq/dy = 0$ and the Charney-Stern criteria is satisfied.

but is not necessary for this work). By day -3, a coherent region of negative q_y develops in a location southeast of the polar jet (between 30° E and 100° E) near the location of the stratopause warming. As the USLM event progresses to its peak on day 0, the region of negative q_y strengthens, grows, and then becomes less organized on the days following the peak warming. As the event dissipates, the area of negative q_y breaks up. This progression suggests that a local instability is intensifying the temperature gradient in the region of the flow. That the negative q_y becomes less organized after day 0 indicates that the source mechanism may already be diminishing. The variability among the individual USLM events begins to obscure the average q_y pattern beyond day +3.

Comparing this with figure 5.8, which is the WACCM composite event with reversal of q_y indicated by a thick white line, shows good agreement between the assimilated data set and the model (reversals due to vortex displacement off of the pole have been removed). The Charney-Stern criteria is met on the three days surrounding the peak of the USLM event in nearly the same location as in MetO. The regions are somewhat more smoothed in WACCM, due to the large number of events composited.

As the baroclinic instability acts to extract energy from the breaking planetary wave, it diminishes as IPV is irreversibly mixed into the surf zone. Results shown here suggest that USLM disturbances require baroclinic conditions embedded in a larger region of planetary wave breaking. When baroclinic conditions are not present, large amplitude planetary waves may manifest as a minor SSW event that is associated with neither a USLM event nor a major SSW event. In these cases, the vortex is displaced but remains barotropic.

However, the Charney-Stern criteria is only a necessary condition and possibly not a sufficient condition, meaning that while the condition is met it does not guarantee that a baroclinic instability is there. An additional complication is that the diagnostics for identifying breaking planetary waves and baroclinic instability both rely on potential vorticity. While planetary wave breaking uses Ertel's potential vorticity and the Charney-Stern criteria uses quasi-geostrophic potential vorticity, which are not the same quantity, they are closely related [34]. Even though the planetary wave breaking is identified approximately 90° E of the identified baroclinic instability, a secondary analysis would be constructive in determining whether there is more going on than just planetary wave breaking while USLM conditions are occurring.

By definition, planetary waves that break in the middle atmosphere are large-scale waves with low wave numbers, S1 and S2. However, a baroclinic instability is expected to be of a smaller scale, which could be of higher wave numbers between S3 and S7. By diagnosing which wave numbers are interacting with the mean-flow, the dynamical effect of breaking planetary waves and secondary instabilities can be separated. Here we examine a WACCM case study of an independent USLM from November of model year 0013. A case study is used because the averaging required in the composite USLM suppresses the higher wave numbers that may be present in individual events. This particular USLM event is an early winter event that dissipated without developing into a minor SSW or major SSW. The EP-flux for the day of USLM onset is shown in Figure 5.9 and is separated by wave number. The center panel shows the EP-flux divergence using fields composed of only S1 and S2, low planetary scale waves. The right hand panel shows the EP-flux divergence of higher wave numbers, S3 through S7, which are expected to be associated with a baroclinic instability. The sum of the low and high wave number divergences should equal the divergence calculated using fields composed of S1 through S7 (S0 is not necessary since the EP-flux is calculated using perturbations from the mean state (S0)). In this figure, most of the convergence in EP-flux is due to low wave numbers, although there is some convergence in the upper mesosphere due to the higher wave numbers; the zero wind line is also located in the upper mesosphere at this time.

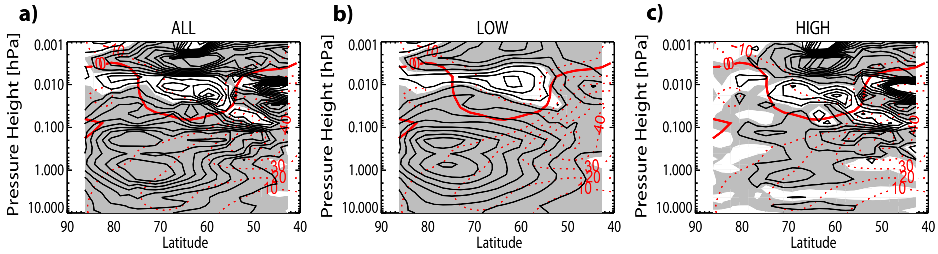

Figure 5.9: WACCM case study date of 17 November 0013, the onset of an independent USLM event. a) The divergence in the EP-flux $\nabla \circ \mathcal{F}$ for wave numbers S1 through S7; b) low wave numbers S1 and S2; and c) high wave numbers S3 through S7.Red dashed lines are isolines of the zonal mean zonal wind [m/s]; the solid red line is the zero-wind line. Contours divergence of EP-flux are shown in solid black [0.5 m/s/day]. Regions of convergence of the EP-flux vector are shaded. The green arrow indicates the onset of USLM conditions, the black arrow indicates the peak of the USLM disturbance and the red arrow indicates the termination of USLM conditions.

Since the thermal disturbance is located at a latitude near 63.5° N and the planetary wave breaking strength shown in Figure 5.4 has a local maximum near 0.8hPa, a plot of the divergence in EP-flux at this point following the evolution will help confirm the action of a baroclinic instability. Figure 5.10 shows a time series of the $\nabla \circ \mathcal{F}$ for wave all numbers S1 through S7 (solid black line), low wave numbers S1 and S2 (dotted line), and high wave numbers S3 through S7 (dashed line). The zonal-mean zonal wind is also shown (red line). USLM criteria is first met on 17 November, indicated by the green arrow. The peak and end of the USLM event are indicated by black and red arrows, respectively. The sum of the divergence due to low wave numbers and high wave numbers, again, equals the divergence due to all seven wave numbers. Where the divergence is mostly due to the low wave numbers, the all wave numbers line and the low wave numbers line are nearly the same. However, between November 15 and 21 there is significant contribution from low wave numbers. This timing agrees with the Charney-Stern criteria being satisfied and is strong evidence of a secondary baroclinic instability acting to intensify the thermal anomaly at the stratopause.

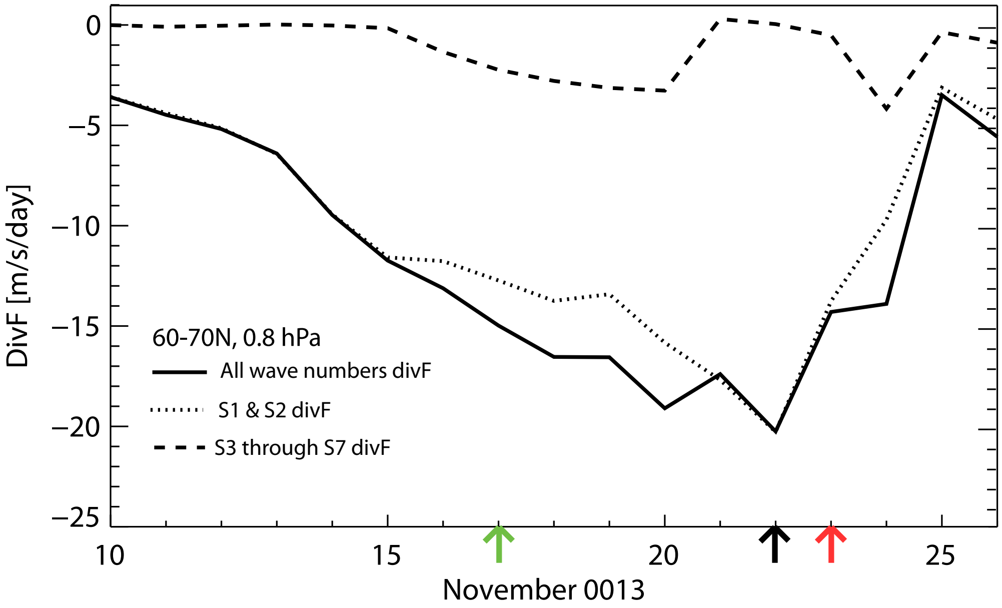

Figure 5.10: WACCM case study for November 0013. The divergence in the EP-flux $\nabla \circ \mathcal{F}$ for wave numbers S1 through S7 (solid black line), low wave numbers S1 and S2 (dotted black line), high wave numbers S3 through S7 (dashed black line) at 63.5°N and 0.8 hPa. Green arrow indicates USLM onset; red arrow indicates USLM end.

A further example using the MetO assimilated data set showing the same wave number separated EP-flux analysis is shown in Figure 5.11. This case study supports the results found in WACCM and shows repeatability of the high wave number feature associated with the divergence of the EP-flux.

These secondary baroclinic instabilities may be harbingers of further disruption to the structure of the polar vortex. USLM events significantly disturb the polar winter middle atmosphere and as regularly occurring events are part of a family of disturbances to the polar winter middle atmosphere. As such, they should be placed into context within this family of disturbances.

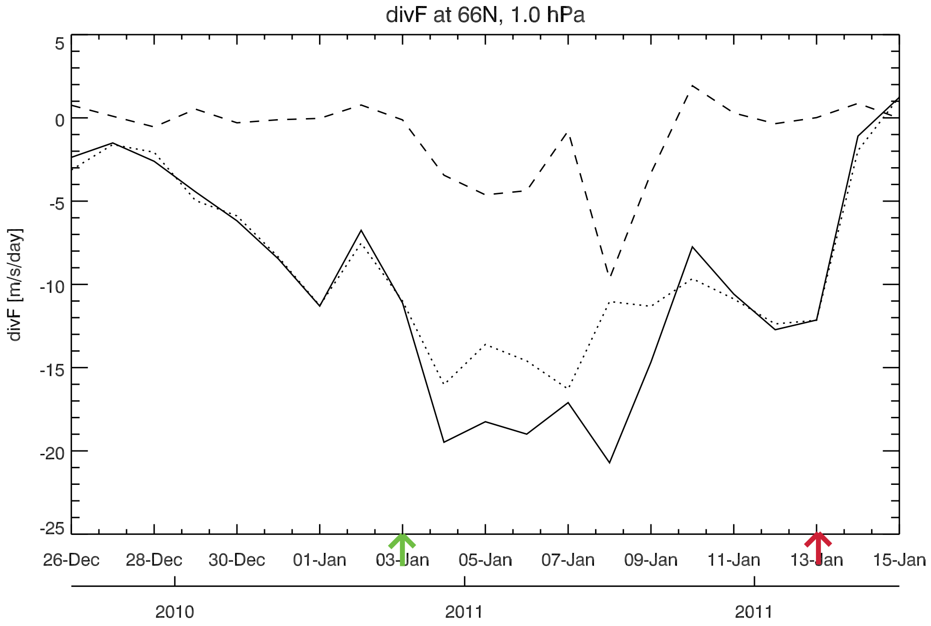

Figure 5.11: MetO case study for January 2011. The divergence in the EP-flux $\nabla \circ \mathcal{F}$ for wave numbers S1 through S7 (solid black line), low wave numbers S1 and S2 (dotted black line), high wave numbers S3 through S7 (dashed black line) at 66°N and 1.0 hPa. Green arrow indicates USLM onset; red arrow indicates USLM end.

Chapter 6

Relationship Between USLM events, Minor SSWs & Major SSWs

6.1 A Family of Middle Atmospheric Disturbances

Just as the mid-latitude troposphere experiences a related group of weather events in the wintertime (cold fronts, blizzards, ice storms, foehn winds, etc), the polar winter middle atmosphere experiences its own family of weather phenomena. Although most of this study has focused on establishing USLM disturbances as regularly occurring polar wintertime events and describing the dynamical mechanisms responsible for their development, here we seek to put them into context within the family of polar winter middle atmospheric events. Of most importance (and great interest) are major SSWs (defined in Chapter 2), because of the impact on the entire atmospheric column, extreme disruption to the polar vortex and only modest ability to currently predict major SSWs[82].

6.2 Venn Diagrams of Events

As regularly occurring weather events in the middle atmosphere, USLM disturbances are associated with SSWs by contributing to the preconditioned state for major SSWs to evolve. Starting with the MetO data set, Figure 6.1 shows two Venn diagrams, one for each hemisphere, which illustrates four possible groupings among USLM events, minor SSW events, and major SSW events. All of the USLM events that were identified in the MetO database are contained within the green ovals, while all minor SSW events are contained in the blue ovals. Red circles denote major SSW events. Where the ovals overlap suggests a relationship between events. A relationship is defined to exist if different events occur within 14 days of each other. This time period allows for the extended development of a USLM (see Figure 4.13), minor SSW and major SSW; the specific criterion is relatively insensitive to periods of 14 days +/- 2 days. Most notable in Figure 6.1 is that every major SSW is associated with (and preceded by) a minor SSW and a USLM event (as indicated by the red major SSW circle being fully contained within the green USLM oval and the blue minor SSW oval). For these occurrences, the time progression begins with a USLM event followed by a minor warming and then a major warming. This suggests that the development of USLM disturbances is a necessary pre-condition for major SSWs and may be a useful tool to forecast major SSWs.

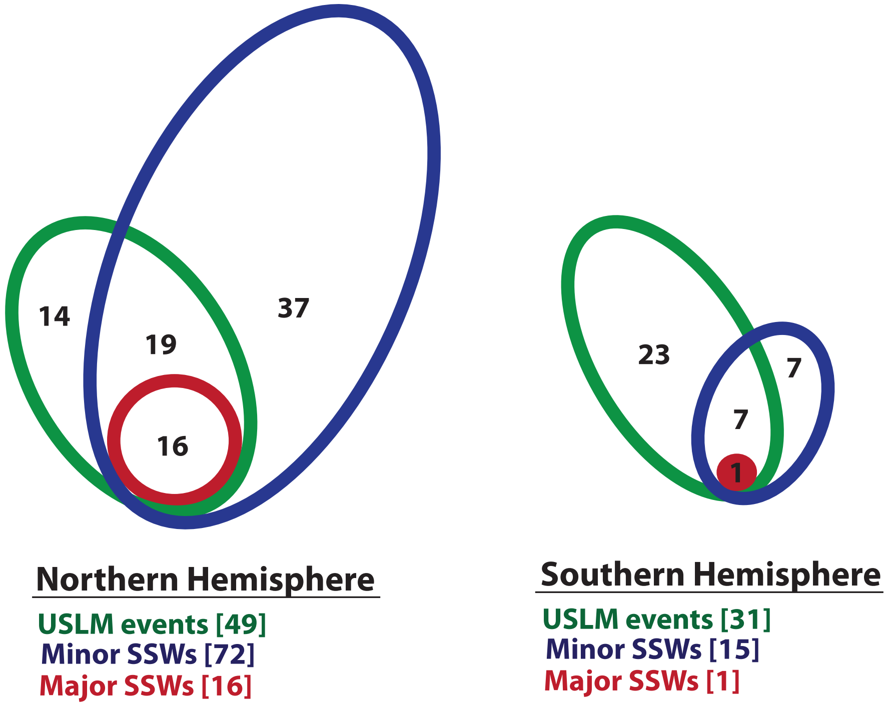

Figure 6.1: MetO Venn diagram illustrating the various relationships between USLM events (green ovals), minor SSWs (blue ovals), and major SSWs (red ovals) for each hemisphere.

The 19 NH events found where the USLM (green) and minor SSW (blue) ovals overlap are events when both minor SSW and USLM criteria are satisfied within a two-week period but did not develop into a major SSW. In the SH, the Venn diagram shows that there are 7 events in the overlapping green and blue ovals. Inspection of these occurrences indicates that the minor warming criteria are typically met after the USLM criteria. This is indicative of the later stages of the USLM life cycle, shown in Figure 5.1, where the enhanced temperatures are spread over a greater area such that zonally averaged temperatures meet the minor warming criteria at 10 hPa. The proportion of USLM events that are associated with minor SSWs is approximately 50% in both hemispheres for the MetO data set.

The region inside the blue minor SSW oval that does not overlap the green USLM oval represents minor SSWs that occur independently of USLM and major SSW events. This suggests that the WMO criteria for identifying minor SSWs represent a diversity of wintertime middle atmospheric thermal disturbances that do not result in major warmings. For example, Canadian warmings are characterized by an amplification of PW1 resulting in a displacement of the vortex from the pole and can satisfy the minor warming criteria. These events do not evolve into major warmings [41][61] and are not associated with USLM events because they are largely confined to the lower stratosphere. In both hemispheres, approximately 50% of all minor SSWs occur independently of USLM events and in the NH 78% of minor warmings occur independent of major SSWs.

There are also USLM events that occur and dissipate without developing into a minor or major SSW (14 out of 49 events in the NH, 23 out of 31 events in the SH for MetO). Furthermore, 67% of NH USLM events do not evolve into major SSWs. A significant difference between the hemispheres is the relative number of independently occurring USLM events. Because the SH vortex is more stable than in the NH at 2 hPa, there are twice as many independent USLM events in the SH.

A similar analysis was undertaken using the WACCM model data. Only the Northern Hemisphere was analyzed due to the earlier mentioned ‘cold pole’ problem with accurately representing the Southern Hemisphere. The results are shown in Figure 6.2; comparing with Figure 6.1, the numbers are larger due mostly to the longer data set (40 years versus 21 years). In this WACCM run approximately 35% of all minor SSW events evolved independently and did not contribute to the development of major SSWs. All major SSWs (23 events) were preceeded by both USLM and minor SSW conditions. The trend seen in the MetO Venn diagram of more minor SSWs being

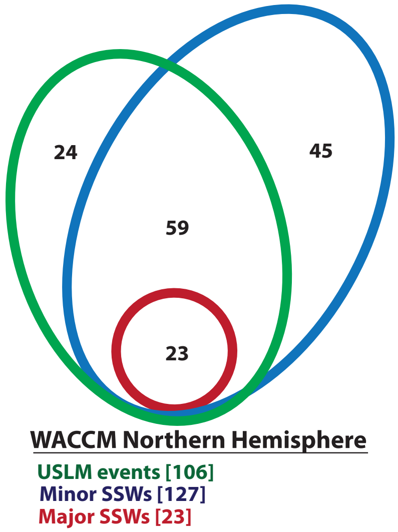

Figure 6.2: WACCM Venn diagram illustrating the various relationships between USLM events (green oval), minor SSWs (blue oval), and major SSWs (red oval) for the Northern hemisphere.

identified than USLMs is continued here, but a larger proportion of minor SSWs are associated with USLM conditions. Only 23% of USLM events in WACCM developed independently and nearly 30% of all events that meet both USLM and minor SSW criteria eventually develop into major SSWs, which may help to improve prediction of major SSWs.

To further examine the relationships between USLM events, minor SSWs and major SSWs, four case studies are shown in Figure 6.3 that displays IPV (black contours) on the 1600 K isentropic surfaces (approximately 2 hPa) superimposed on the temperature field (colored contours). The white dashed contour is the edge of the Arctic vortex. Figure 6.3(a) is a USLM event on 5 January 2011 that dissipated without further disruptions to the temperature gradient or zonal wind direction at 10 hPa; Figure 6.3(b) is a USLM event on 21 January 2008 that resulted in a minor SSW; Figure 6.3(c) is a USLM event on 20 February 2005 that evolved into a displacement type major SSW; and Figure 6.3(d) is a USLM event on 19 January 2009 that culminated into a vortex splitting type major SSW. These examples represent different regions in the Venn diagram shown in Figure 6.1. The shape of the Arctic vortex suggests planetary wave breaking in all cases. Planetary wave breaking is further demonstrated by IPV filaments and nodules that have been irreversibly

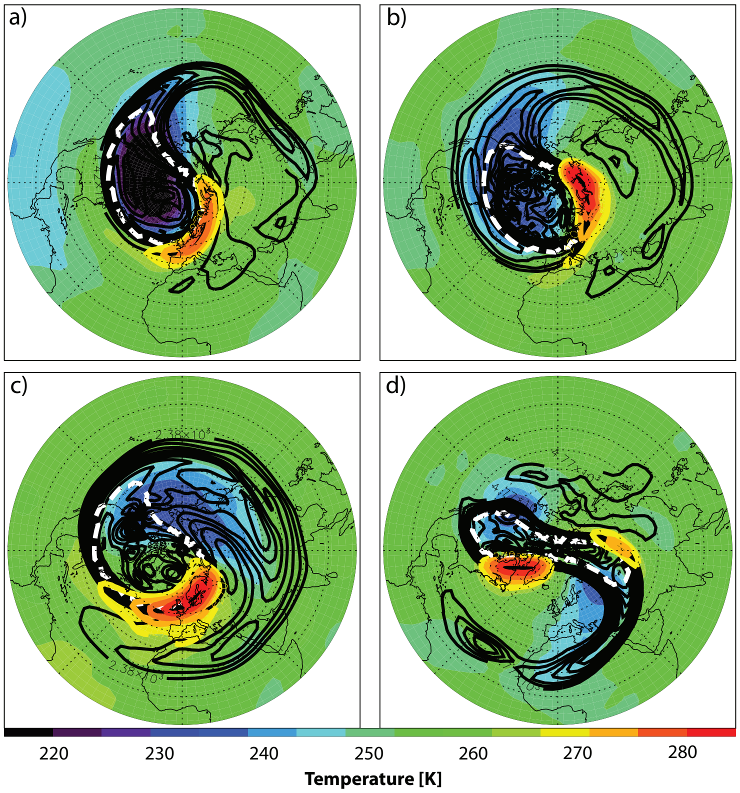

Figure 6.3: Polar stereographic plot on the 1600 K isentropic surface (approximately 2 hPa) for for (a) 5 January 2011, (b) 21 January 2008, (c) 20 February 2005, and (d) 19 January 2009 of potential vorticity [$10^{-6} K m^2 kg^{-1} s^{-2}$ (PVU)] contours (black). The white dashed contour indicates the edge of the Arctic vortex. Shading denotes temperature with superimposed colored contours at 270 K, 275 K, and 280 K to emphasize the location of the warm pool(s).

contorted or separated from the high IPV region inside the vortex[56]. Figure 6.3 indicates the presence of strong gradients in potential vorticity in the vicinity of the stratopause warmings. High IPV air that has been detrained from the polar vortex will be mixed into the stratospheric surf zone. The spatial size of the detrained IPV filament appears to increase from panel (a) to panel (b) and from panel (b) to panel (c). This is revealing in that the USLM event in panel (a) did not evolve into a SSW, the USLM event in panel (b) evolved into a minor SSW, and the USLM event in panel (c) evolved into a major SSW. A review of all NH USLM disturbances showed that PWB occurred during all events (not shown). However, PWB is a 'ubiquitous' process in the winter polar regions[57][29], and not all PWB events are accompanied by USLM disturbances.

While USLM disturbances appear to require additional dynamical circumstances (such as strong baroclinic conditions at the stratopause level and differential thermal advection between the levels), PWB likely provides the necessary energy for further development mechanisms of USLM formation.

Returning to the Venn diagram in Figure 6.2 of the categorized WACCM events, we can also examine common characteristics of the events grouped into the different regions of the Venn diagram. Figure 6.4 shows the seasonal distribution of the different areas of the Venn digram; the frequency is the cumulative number of events in each month for the entire 40 year WACCM run and the month is noted by the onset date of the USLM event (or minor SSW event in the case of independent minor SSWs). Independent USLM events are displayed as black bars and are the only type of event identified in October as well as all of the winter months. Independent minor SSWs are shown in dark gray. Independent minor SSW events have a strong concentration of events in the very late winter, in March. Many of these independent minor SSWs are actually associated with the change of the season, increasing solar insolation at the poles which eventually leads to the breakdown of the polar vortex in March or April. The events in the red circle of the Venn diagram in Figure 6.2, are all shown as white bars indicating major SSWs tend to develop in mid to late winter, likely after an independent USLM event or USLM/minor SSW event. This distribution, while certainly not conclusive, is suggestive of a preconditioning relationship between USLM events and major SSW events.

Using the methodology described in section 5.1 for creating composite events, the WACCM data set contains enough events in each region of the Venn diagram (Figure 6.2) to explore the general characteristics of 'Independent USLM' events, 'Independent minor SSW' events, and events that satisfy both 'USLM + minor SSW' criteria within a 14 day period; this is shown in Figure 6.5.

Figure 6.5 compares the composites for the different groups of interest. The upper left panel are the independent USLM events, the upper right panel are the independent minor SSW events, the lower left panel are events that meet both USLM and minor SSW event criteria within a 14 day period, and the lower right panel are events that meet USLM, minor SSW and major SSW criteria within a 14 day period. Although composites for days -5 through +5 were computed, only

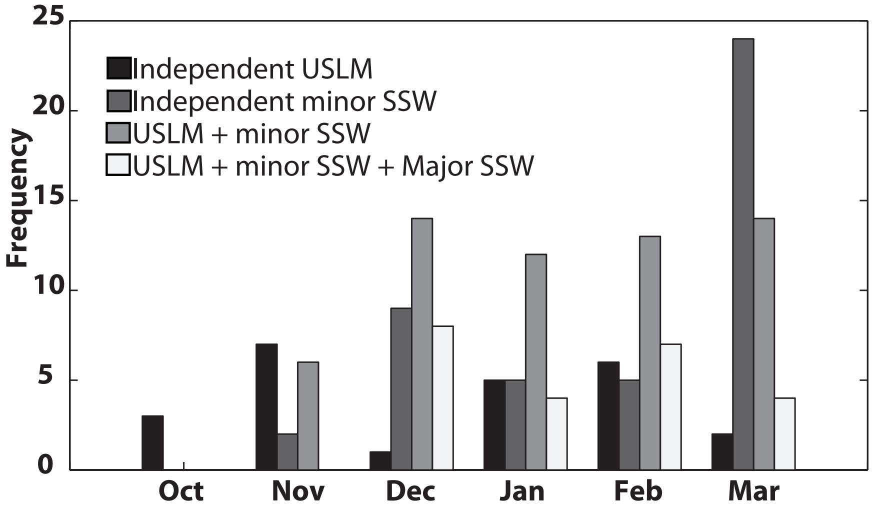

Figure 6.4: Bar plot of the seasonal distribution, by month, of the different groupings in the WACCM Venn diagram.

day 0 and day -2 are included for examining conditions leading to the development of the events. Although the USLM events are aligned in time by the peak of the thermal disturbance at 2 hPa as day 0, the independent minor SSWs are aligned in time by the onset of the reversal of the temperature gradient at 10 hPa as day 0.

The first row (a) displays temperature (colored contours) and geopotential heights (solid lines at intervals of 400 m) as in Figure 5.2. The center of the warm thermal anomaly at 2 hPa is located at 84°E, 69°N for the independent USLM composite, while there is very little warm thermal anomaly at 2 hPa for the independent minor SSW events. The lower left panel, showing events that meet both USLM and minor SSW criteria, shows a warm thermal anomaly located at 71°N, 69°E that is somewhat more intense than independent USLM composite. The lower right hand panel, showing USLM events related to major SSWs shows a significant thermal anomaly at 63°N 41°E. All of the composites share the feature of a polar vortex disturbed off of the pole, although the Aleutian high in the composites containing USLM events is larger and stronger. Qualitatively, this is indicative of planetary wave activity, potentially amplifying planetary wave 1. Additionally, the polar vortex seems to be stronger in independent USLM events than in USLM events related

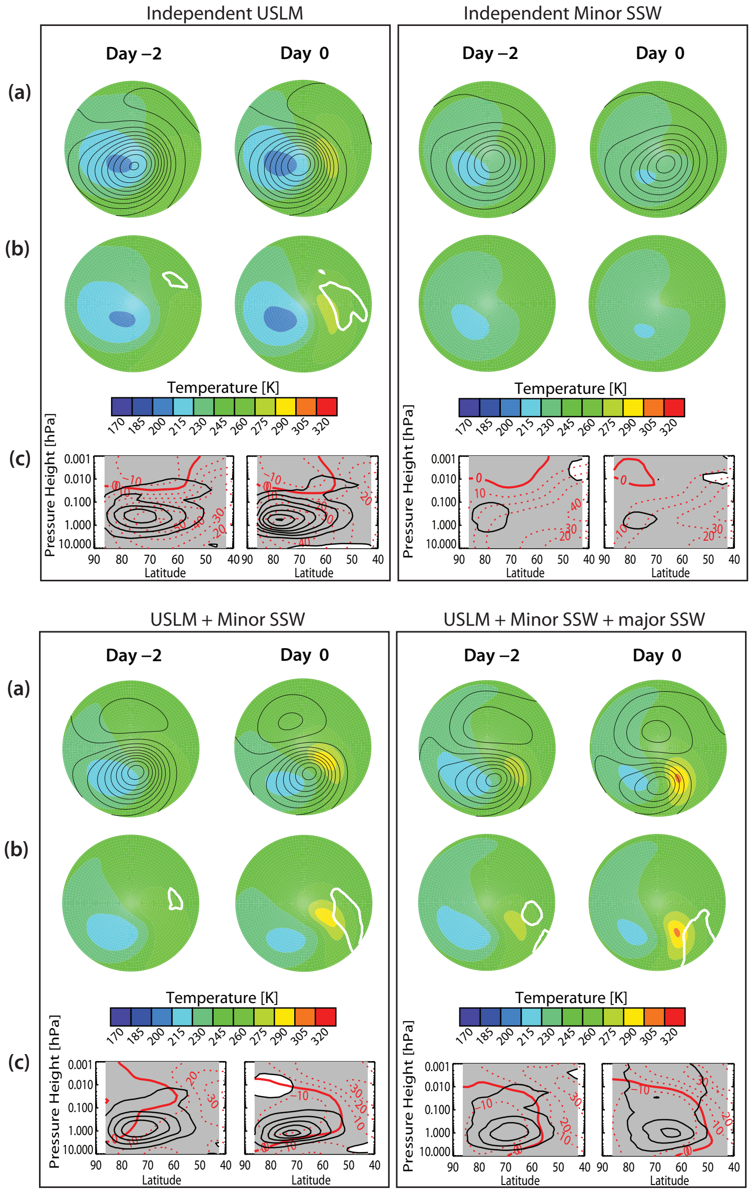

Figure 6.5: The events that were grouped into the different regions of the Venn Diagram in Figure 6.2 have been composited and analyzed. The upper left panel are independent USLM events; the upper right panel are independent minor SSW events; the lower left panel are events that meet both USLM and minor SSW event criteria within a 14 day period; and the lower right panel are events that meet USLM, minor SSW and major SSW event criteria with a 14 day period. Two days for each composite have been included: Day 0 and Day -2. (a)As in Figure 5.2, filled color contours are temperature and black contours are geopotential heights on the 2 hPa pressure surface; (b) as in Figure 5.8, thick white contours outline regions that meet the Charney-Stern criteria for baroclinic instability; and (c) as in Figure 5.5, black contours are $\nabla \circ \mathcal{F}$, convergence is indicated in gray shading, the zero zonal mean zonal wind is indicated as a solid red contour.

to major SSWs.

The second row (b) is as Figure 5.8, and examines whether a baroclinic instability could be acting in these events. At the 2 hPa pressure surface, the filled color contours are temperature and the thick solid white lines indicate the boundary of regions that satisfy the Charney-Stern criteria: a reversal in the meridional gradient of quasi-geostrophic potential vorticity. All composites that are made of USLM events (independent USLM, USLM + minor SSW, USLM + minor SSW + major SSW) show large regions that satisfy this criteria on the days surrounding the peak of the disturbance. Crucially, the independent minor SSW composite shows no regions (on any day) that satisfy the Charney-Stern criteria; no baroclinic instability is acting at this level.

In the third row (c) the divergence of the EP-flux (black contours with intervals of 2.5 m/s/day and zonal-mean zonal wind (red contours)) illustrates the waves' interaction with the mean flow (as in Figure 5.5). All of the composites show some convergence (gray shading) of the EP-flux vector between heights of 10.0 hPa and 0.1 hPa (approximately 30 km and 63 km) indicating a wave transience (wave breaking or amplification/decay), interaction with the mean flow and deceleration of the zonal-mean zonal wind. However, the independent USLM composite shows a more focused convergence of the EP-flux, with the convergence concentrating in a region near 1 hPa by day 0, likely the region of maximum wave breaking. Two days prior to the peak of the event (day -2), there is a significant region of weakly reversed winds, but it only extends to about 0.05 hPa. The lower left panel of USLM + minor SSW also shows significant convergence in this region, but spread over a deeper range of the atmosphere; again, there is a weak reversal of zonal winds, but they extend to a depth of only about 5 hPa. The lower right panel, showing USLM events related to both a minor and major SSW event, indicates a broad region of convergence of EP-flux, which is sustained for more than 15 days before the peak of the event, as shown in Figure 6.6. The zonal wind is reversed in the upper stratosphere, but does not reverse at 60°N and 10 hPa until 2 days after the peak of the USLM event. In these three cases, there is strong evidence that planetary waves are breaking in the region of EP-flux divergence, depositing momentum and making energy available for the growth of a secondary baroclinic instability. The zero wind line descends in altitude over the course of 15 days until reaching its lowest location on day 0, forming a critical layer for vertically propagating planetary waves, contributing to even more planetary wave breaking. In contrast, the independent minor SSW composite shows the zero wind line high in the mesosphere and little convergence between 70°N and 80°N. After the major SSW dissipates, the upper mesosphere zonal winds begin to recover first.

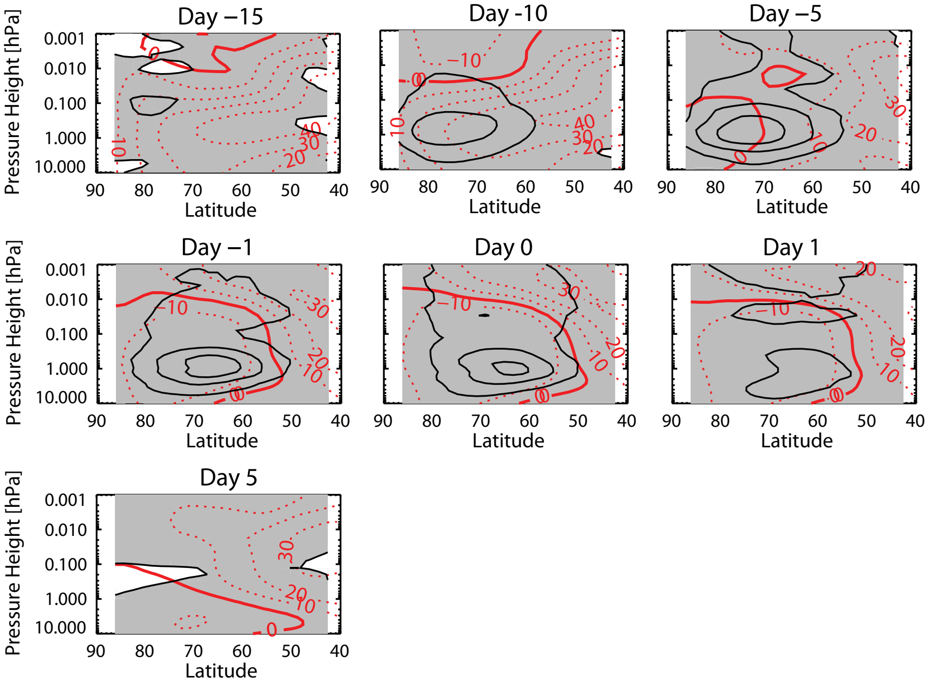

Figure 6.6: Calculations of Div$\mathcal{F}$ for selected days of the composite USLM + minor SSW + major SSW event shown in the lower right panel of Figure 6.5. The peak day of the USLM event is designated Day 0, all other days are noted in relation to day 0. Red dashed lines are isolines of the zonal mean zonal wind [m/s]; the solid red line is the zero-wind line. Contours divergence of EP-flux are shown in solid black [2.5 m/s/day]. Regions of convergence of the EP-flux vector are shaded.

6.3 Significance of Venn Diagram Results & A New Family of Dynamically Defined Disturbances

These results bring into question the standard understanding that minor SSWs are precursors and related disturbances to major SSWs. In fact, the current definition of minor SSWs encompasses a variety of winter middle atmospheric disturbances. Minor SSWs that are not related to USLM disturbances (or major SSWs) are a result of transient planetary waves that displace the polar vortex off the pole far enough at the 10 hPa level to induce a reversal of the zonal mean temperature gradient. When the planetary wave pulse from the troposphere dissipates, there is no further evolution in the anomaly and the middle atmosphere returns to nominal conditions. In addition, it is debatable that these independent minor SSWs lessen the strength of the polar vortex or precondition the polar vortex[57] to be more susceptible to major SSWs as more planetary wave pulses interact with the middle atmosphere.

Given the results of the Venn diagrams and Figure 6.5, we propose that USLM conditions are a harbinger for the development of major SSWs. Independent USLM composites may also act as a preconditioning event when the initiating planetary wave breaks and pulls high PV air off of the core of the polar vortex, it shrinks and weakens the polar vortex making it more susceptible to further planetary wave pulses that are the key mechanism of major SSWs. The baroclinic instability that is embedded in the planetary wave breaking of USLM disturbances mark significant disruption to the middle atmosphere, always accompany major SSWs and may be used to help identify conditions which may spawn a major SSW.

Recently there have been efforts to adjust the definitions of the various winter middle atmospheric disturbances or to build a new classification system all together[14][27] for the family of polar winter middle atmospheric disturbances, and this study contributes another commonly occurring, distinctive event. This study does not specifically endorse the proposed ‘continuum’ of disturbed middle atmosphere states or the classification based on planetary wave number. Current definitions of wintertime polar middle atmospheric disturbances are based on wind and temperature criteria at the 10 hPa level, however a more fitting methodology may involve diagnostics of the dynamics that are responsible for the disturbances, such as specific planetary wave activity or instability at the appropriate dynamically active level. Using temperature and winds (and zonally averaged ones at that) result in attempting to diagnose the manifestations of the underlying dynamical mechanisms instead of dynamical mechanisms driving the disturbance themselves. For example, this study shows that the current definition of minor SSWs captures a diverse group of dynamical conditions, some of which are not related to the development of major SSWs because the zonally averaged temperature structure at 10 hPa looks similar in both cases. Here we propose an initial attempt at composing amended definitions incorporating dynamical diagnostics based on the results of this study:

USLM disturbance occurs when planetary wave breaking in the layer surrounding the 2000K (approximately 0.8 hPa) isentropic surface (indicated by a reversal in isentropic potential vorticity) causes focused convergence of EP-flux surrounding the layer around 1 hPa to exceed a given threshold at 65N on any winter day.

Minor Sudden Stratospheric Warming occurs when planetary wave breaking in the layer surrounding the 2000K (approximately 0.8 hPa) isentropic surface (indicated by a reversal in isentropic potential vorticity) causes a time-integrated convergence of the EP-flux vector to exceed a given threshold over the depth of the atmosphere between 10 hPa and 1 hPa at 65N.

Major Sudden Stratospheric Warming occurs when planetary wave breaking in the layer surrounding the 2000K (approximately 0.8 hPa) isentropic surface (indicated by a reversal in isentropic potential vorticity) causes a time-integrated convergence of the EP-flux vector to exceed a given threshold over the depth of the atmosphere between 10 hPa and 0.01 hPa (approximately 30 km to 75 km) at 65N.

Although the computational complexity required in these definitions is greater than zonal mean temperature and wind based definitions, modern computers make this manageable and straightforward. It is hoped that defining polar winter middle atmospheric disturbances using dynamical diagnostics will clarify the driving mechanisms of active polar winters and aid in improving the forecast ability of major SSWs.

Chapter 7

Related Phenomena

7.1 Separated Mesopause

Observations of mesospheric coolings associated with major SSWs have been found in studies by Gregory & Manson [1975], Myrabøet al. [1984], Whiteway & Carswell [1994], and Waltersheid et al. [2000], among others. Mesospheric coolings have been seen to accompany major SSW since Matsuno's 1971 modeling study, but have been also seen in more comprehensive and complex models. More recently, Liu et al. [2002] used TIME-CGM/CCM3 to internally generate major SSWs, which showed an alternating pattern of warming and coolings, including a mesospheric cooling and lower thermospheric warming that is due to a secondary downward circulation induced by equator ward mesospheric circulation. Other groups have investigated Mesospheric Inversion Layers (MILs) which are not thought to be caused by major SSWs and most of these MIL features are located at low and mid-latitudes[59].

A co-incident feature of USLM disturbances is a mesospheric cooling, or a 'separated mesopause.' This is a region of anomalous cooling in the mesosphere between 65 km and 85 km in altitude. High power Rayleigh lidar has observed this feature in the December 2000 event over Sondrestrom Greenland, as shown in Figure 7.1. This figure has been reproduced from Thayer & Livingston [2008], and was also shown in Chapter 2. Of particular interest here is the part of the lidar profile that is some 20 K colder than the MSIS profile near 65 km in altitude. Although this event is not associated with any identified major SSW events, 11 December 2000 was classified as a USLM and minor SSW day for the polar middle atmosphere.

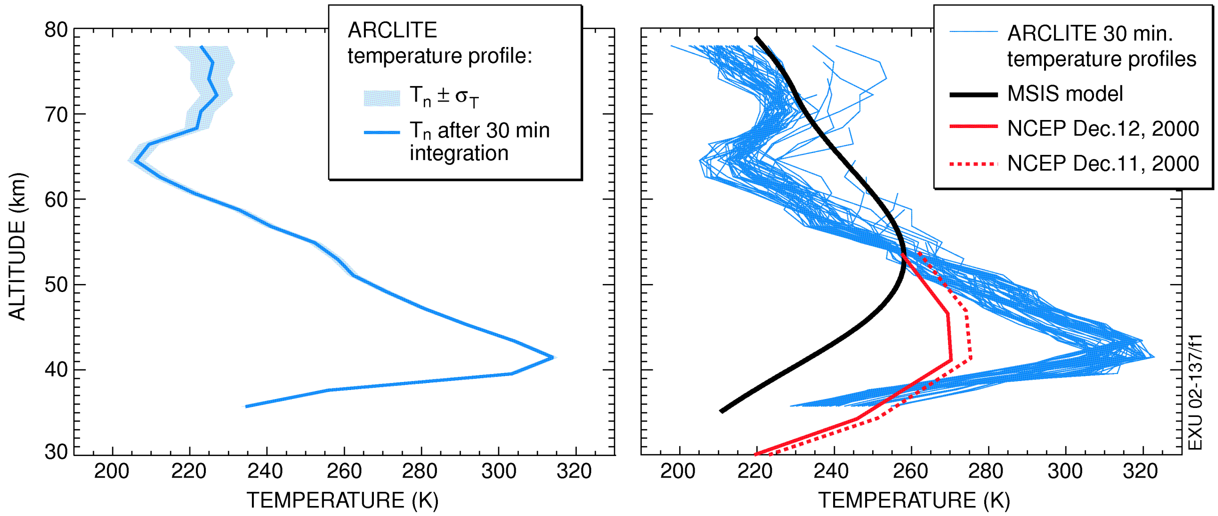

Figure 7.1: The left panel shows an average temperature profile and its error derived from the ARCLITE lidar in Sondrestrom, Greenland on 11 December 2000. The right panel shows each 30 minute integration. The black line is the MSIS profile for this date and location. The lidar profiles deviate from standard models and NCEP fields with the stratopause 50 K warmer and located at approximately 42 km in altitude.[85]

Another example of an observation of a USLM with vertical coverage through the upper mesosphere was captured by the TIMED/SABER instrument. Figure 7.2 shows the temperature structure in longitude and altitude (pressure height) around the 70°N latitude circle during the peak of a USLM event in February 2002. A zonal average of this event might have obscured the extreme temperatures during the event and missed important temperature structures dependent on longitude and the position of the polar vortex. Below 10 hPa the stratosphere remains cool and relatively undisturbed. A nominal mesopause can be seen near 0.002 hPa as the coldest part of the atmosphere. However, the stratopause is highly disturbed, the altitude varying with longitude, and near 75°E the stratopause is located low at 2 hPa with unusually warm temperatures over 305 K (defining features of a USLM event). In addition to this stratopause feature, which has been discussed thoroughly throughout this work, there is a cooling in the mesosphere near 0.02 hPa (approximately 75 km in altitude), extending some 100° of longitude, located roughly in phase with the stratopause warming.

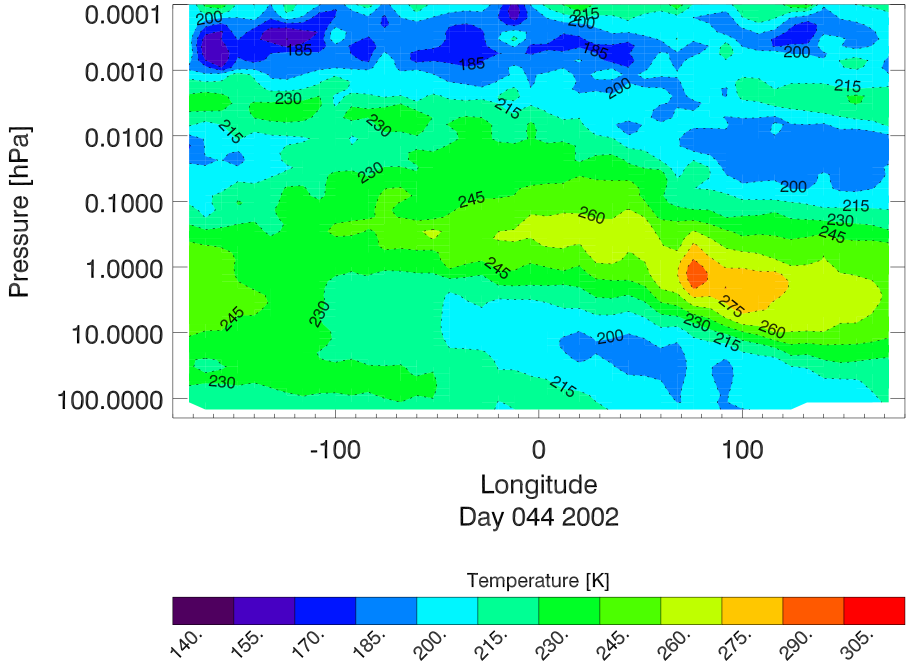

Figure 7.2: Longitude-Pressure Height plot around the 70°N latitude circle of temperature during the peak of the USLM event from February 2002.

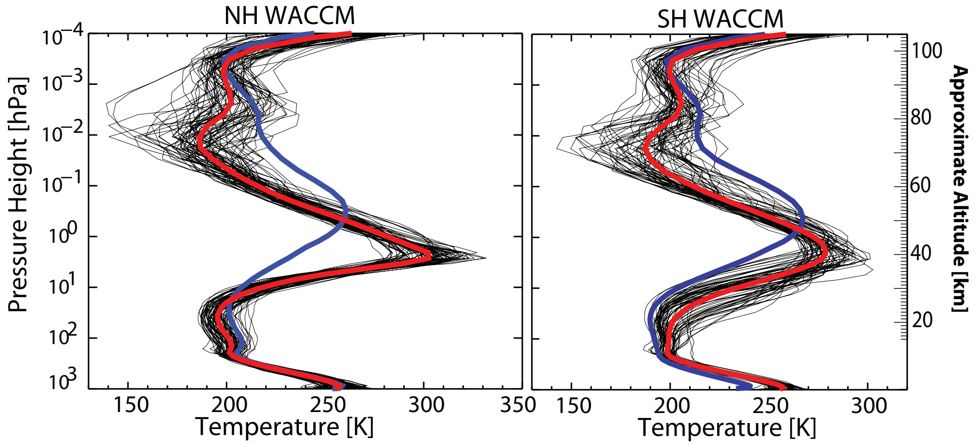

Figure 7.3: WACCM temperature profiles for the Northern Hemisphere (left) and Southern Hemisphere (right) that intersect the 2 hPa warm anomaly on peak days during USLM disturbances. Individual daily temperature [K] profiles are black, the average profile is indicated in red. An average temperature profile at 63°N (68°S) from December, January and February (July, August and September) months for the entire WACCM databases are plotted for comparison as in blue.

This mesospheric cooling is also associated with the identified USLM disturbances in the WACCM model run. Figure 7.3 is repeated from Chapter 4 and displays the temperature profiles of all identified USLM events (peak day) for both hemispheres as thin black lines; the thick red line is the average profile. For reference, the climatological winter mean profile is shown in blue. Above the sharp stratopause feature near 2 hPa (approximately 42 km), there is negative static stability until the upper mesosphere. In this region, both hemispheres see the average USLM profile as significantly cooler than the climatological mean, by approximately 30 K, although individual profiles may exhibit anomalous cooling in excess of 60 K. The variability of profiles increases above 50 km. The warm anomaly at 42 km is intimately connected to the position and tilt of the polar vortex with height; it is likely that this feature is also sensitive to the structure of the polar vortex with height. For example, a strongly tilted vortex may result in a mesospheric cooling that is not directly overhead of the stratopause warming, but may be located 10-20° degrees West. A vertical profile through the stratopause anomaly may not capture the maximum anomaly in the mesosphere.

Using the composite method described in Chapter 5, a composite event can be examined for the thermal structure in longitude and height, as shown in Figure 7.4. The peak day of the thermal disturbance at 2 hPa along with 5 days before and after are shown. In this plot, the altitude

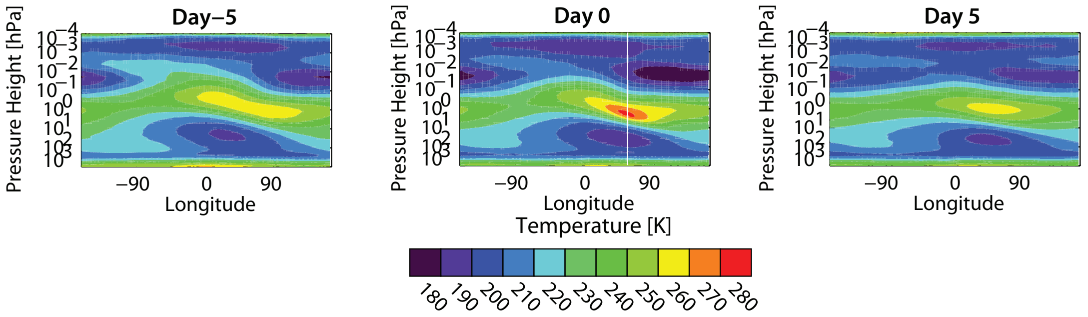

Figure 7.4: Northern Hemisphere composite maps of temperature [K] around the 61° latitude circle on selected days surrounding USLM events. All events have been shifted in longitude such that the phase of the temperature maximum at 2 hPa is aligned.

range covers the cool lower stratosphere to the very bottom of the thermosphere. The mesospheric cooling is located roughly between 0.1 hPa and 0.01 hPa on all days. The mesospheric cooling also peaks on the same day as the stratopause warming, but onsets more than 5 days before the peak. In longitude, this composite mesospheric cooling is centered some 65° longitude East of the stratopause cooling, which explains why a single vertical temperature profile may fail to capture the associated thermal features and thermal extremes (white line on Day 0).

The key mechanism that initiates the USLM thermal disturbance at the stratopause is also responsible for the mesosphere cooling. As a growing wave propagates up from the troposphere and interacts with the mean flow, the mean flow is decelerated in the stratosphere. This induces a downward circulation in the stratosphere and an upward circulation in the mesosphere causing adiabatic heating and cooling[44].

7.2 Stratopause Folds and Front-like Behavior

The observational evidence suggests that synoptic-scale disturbances embedded in planetary wave breaking in the middle atmosphere are amplified through baroclinic instability similar to front-like behavior in the troposphere. Numerical simulations of stratospheric warmings by Fairlie et al. [1990] and Manney et al. [1994] have reproduced these narrow baroclinic zones in the stratosphere and suggest that these synoptic-scale features may play an integral part in the overall onset and evolution of stratospheric warmings. Fairlie et al. [1990] likened these synoptic-scale disturbances to surface fronts in the troposphere and provide a comparison among frontogenesis in the stratosphere, upper tropospheric folds, and surface fronts. In the troposphere, baroclinic instability is associated with warm air advected poleward and cold air advected equator ward that, in terms of perturbation energetics, leads to a conversion from available potential energy in the mean flow to kinetic energy of the perturbation, i.e. growth. The available potential energy in the troposphere is provided and replenished by the maintenance of the radiatively generated meridional thermal gradient. In the tropospheric case of a growing disturbance, the vertical wind is in phase with the temperature such that warm air rises and cools and cold air descends and warms, thus completing a thermally driven, direct ageostrophic circulation. A distinguishing feature between stratospheric synoptic-scale disturbances and tropospheric disturbances is that the ageostrophic circulation in the stratosphere is indirect, i.e. cold air rises and further cools while warm air descends and warms. Thus, in contrast to the troposphere, the vertical ageostrophic motions provide a positive feedback that act to amplify the disturbance. Fairlie et al. [1990] also simulate multiple cell indirect circulations about the stratospheric baroclinic zones, although their indirect circulations are more confined to the region near the disturbance.

An indirect circulation, such as associated with USLM disturbances, is not thermally driven but is dynamically driven by eddy momentum convergence occurring in the polar winter middle atmosphere. Due to the eddy momentum transfer to the mean flow, a secondary indirect ageostrophic circulation is induced in order to maintain quasi-geostrophy and hydrostasis. This eddy momentum transfer is due to planetary wave transience and interaction in the polar middle atmosphere. Analogous to the troposphere, the eddy fluxes provide the available potential energy which is then converted to kinetic energy to drive the indirect ageostrophic circulation. The vertical motions lead to adiabatic heating and cooling in the middle atmosphere which then lead to the poleward advection of warm air and equator ward advection of cold air by the horizontal geostrophic wind. This is precisely what is observed in USLM disturbances, giving the similarity to tropospheric fronts, but the middle atmosphere disturbance is dynamically driven rather than thermally driven. Once the dynamically driven circulation is established, the perturbation may grow through baroclinic instability. As the perturbation extracts energy from the mean flow, the available potential energy in the mean flow decreases and the disturbance begins to decay. However, if the available potential energy in the mean flow is renewed, such as by continuous planetary wave forcing from below, the perturbation can continue to grow. Further amplification of the perturbation can lead to highly ageostrophic flow and strong baroclinic zones in the USLM.

A USLM event that peaked on 13 February 2002 is shown in Figure 7.5a and displays the calculated values of IPV (colored contours) and the boundary of the polar vortex (solid black contour) on two isentropic surfaces at 1400 K and 1800 K (approximately 2 hPa and 1 hPa,

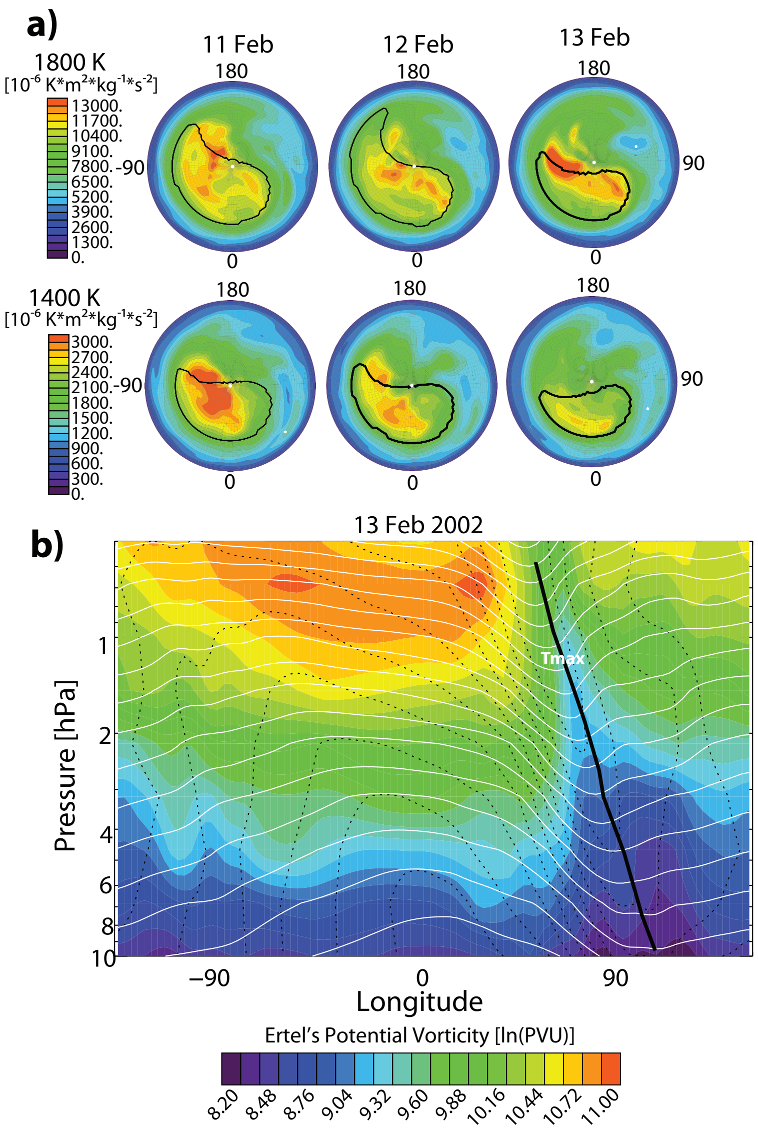

Figure 7.5: (a)Calculated values of Ertel's IPV (color contours) on two isentropic surfaces at 1400 K and 1800 K for three days leading up to the USLM event in February 2002. Solid black contours are the calculated boundary of the polar vortex [Harvey et al.,2002]. (b) Cross-sectional view of the peak of the February 2002 event around the 67°N latitude circle, color contours are Ertel's IPV, white contours are surfaces of constant potential temperature, and dashed contours are temperature [K]. The peak of the temperature anomaly at 2 hPa is marked as 'Tmax'.

respectively) for three days in February 2002. In the upper stratosphere, radiative cooling reduces the period for which IPV can be conserved to less than a week; so here the IPV distribution will be followed for no more than about 5 days. The disturbance meets USLM criteria on 12 February and the thermal anomaly peaks on 13 February 2002. A westward tilt is evident in many of the IPV structures and the vortex boundary, indicative of planetary wave activity. The two levels interact as anomalies embedded in the background IPV, inducing cyclonic (anti-cyclonic) motion around positive (negative) synoptic scale IPV anomalies. Using the 'gentle vacuum cleaner' idea expressed by Hoskins [1985], upper level negative anomalies pull air upward behind it and pushes air downward ahead of it (air is traveling roughly cyclonically around the polar vortex boundary), as is required to close continuity. This is confirmed by the Q-vector analysis of the event shown in Figure 4.5, which qualitatively shows air sinking in this region west of the USLM thermal anomaly at 2hPa, acting to tighten the horizontal temperature gradient. In the days leading up to the peak, a high IPV streamer is pulled off of the main source of high IPV; this is qualitatively planetary wave breaking.

The Fairlie et al. [1990] model of the stratospheric warming of the winter of 1984-1985 produced narrow baroclinic zones and elevated temperatures near the 2 hPa level. The cross-section of isentropes and IPV suggested stratopause analogy to tropopause folding where high IPV stratospheric air may be injected into the troposphere by riding downward sloping isentropes. The assimilated data from MetO for the 13 February 2002 event is strikingly similar to the numerical model produced by Fairlie et al. Figure 7.5b is a cross-section of longitude and pressure height around the 67 N latitude circle (through the warm temperature anomaly at 2 hPa). Isotherms are indicated by dashed contours at 10 K intervals; isentropes are indicated by solid contours at 100 K intervals and isopleths of IPV are colored contours at intervals of 3000 PVU. Between 25 E and 100 E, a region of high IPV gently dips down to lower levels while a narrow tongue of low IPV stretches into the mesosphere; in between is a region of strong zonal IPV gradients. Here, again, is the westward tilt of IPV, θ, and T. In the absence of frictional or diabatic effects (which can be assumed for a couple days at the 2 hPa level), it is expected that IPV is advected on isentropic surfaces. The smaller downward pointing tongue of high IPV contours are co-aligned with the isentropes suggestive of downward air motion, which leads to adiabatic heating and intensification of the horizontal temperature gradient. However, it is apparent in Figure 7.5b that there are no sources of low IPV on the 67 N latitude circle isentropes that could produce the upward pointing tongue of low IPV. The isentropes in the region of the upward pointing low IPV tongue dip in pressure height and are nearly perpendicular to the isopleths of IPV; this is an indication of three-dimensional advection of low IPV into the region. Figure 7.5a shows that a streamer of low IPV has been advected into this region from the lower latitude sources of low IPV outside of the polar vortex. Because of the short-term conservation of IPV in the upper stratosphere, there is no stratopause analogy to the dynamically defined tropopause. However, this structure can still be considered to be a type of stratopause folding, wherein high IPV air from the mesosphere may advect down the isentropes into the stratosphere. Advection along the jet in a region of baroclinic flow is also required for the fold's development [19]. Given the invertibility principle of potential vorticity, this fold-like structure in the IPV is therefore required to produce the observed temperature and geopotential height fields observed as part of a USLM event's development.

The analogous dynamical construction between tropospheric fronts and USLM phenomena suggests that the baroclinic instability of the USLM may act to amplify the disturbance. The USLM is subject to conditions of baroclinic instability but its free energy comes from planetary wave propagation/absorption as opposed to the meridional thermal gradient in the troposphere case. Consequently, using energy arguments, perturbation kinetic energy drawn from the planetary waves drives an ageostrophic circulation that is indirect in the USLM disturbance. This circulation produces the necessary temperature distributions that promote baroclinic instability and the disturbance grows by feeding off of the available potential energy provided by the vertically propagating planetary waves.

Chapter 8

Conclusions

This research set out to establish the nature of observed Upper Stratosphere Lower Mesosphere *USLM* disturbances in observations, assimilated data and models, to characterize the coupled thermal and dynamical mechanisms responsible for its formation, and determine their relationship with other types of middle atmospheric disturbances. Central to polar winter middle atmosphere dynamics is the polar vortex and the large-scale restructuring of it during dynamically active winters. USLM disturbances dramatically alter the thermal structure in the middle atmosphere and are enmeshed in planetary wave breaking at the edge of the polar vortex. Middle atmospheric weather disturbances, such as major SSWs, may impact the entire atmospheric column of the polar vortex, from alteration of storm tracks in the troposphere to warming anomalies in the thermosphere. USLM disturbances appear to be more confined to the middle atmosphere but have associated dynamics and occur prior to SSW events such that they may be a prognosticator of a more extensive disturbance. This research sought to address the following topics:

- Establish criteria for identifying USLM events in observations, assimilated data sets and models; determine whether the Whole Atmosphere Community Climate Model (WACCM) spontaneously and internally generates USLMs that match the observed characteristics
- Identification of the USLM thermal structure as a synoptic-scale feature of polar wintertime disturbances; determine their dynamical forcing mechanisms
- Develop climatologies detailing frequency of occurrence, duration, geographical preference,

composited structure and morphology in assimilated data and the WACCM model for both hemispheres

- Determine the characteristics of planetary wave activity that produce conditions to support the characteristic USLM baroclinic instability on the East side of the polar vortex; discern whether this is the likely mechanism leading to front-like behavior in the polar middle atmosphere
- Identify critical relationships of USLM disturbances with minor and major SSWs which may assist in the prediction of major SSWs
- Connect the co-incident phenomenon of mesosphere coolings (separated mesopause) and in-situ generated gravity waves with USLM events

8.1 Summary of Findings

Beginning with Labtizke [1972], USLM disturbances have been intermittently observed in temperature profiles by lidar and rockets. The most striking feature of these disturbances was a low altitude stratopause near 42 km and exceptional temperatures in excess of 50 K above nominal conditions. With the advent of global assimilated data sets and global satellite measurements of the middle atmosphere, this research was able to put these anomalous USLM disturbances into the context of polar dynamics. By developing criteria that depends on the unique state of the winter polar stratopause during USLM disturbances, a search of the MetO assimilated data was conducted that identified 49 USLM events in the Northern Hemisphere and 31 USLM events in the Southern Hemisphere between 1991 and 2011. Using one of these events as a case study, it was found that the USLM event displayed strong baroclinic conditions at the stratopause, involved planetary wave activity, invoked vertical ageostrophic motion and was suggested amplification through baroclinic instability.

Following this case study, a climatology of USLM events was undertaken to establish the general characteristics of USLM disturbances. Phenomenological characteristics included: strong baroclinic conditions near the stratopause, strong positive temperature gradients below 40 km, elevated stratopause temperatures in excess of 290 K, lowered stratopause locations repeatedly occurring at 41 km +/- 2 km (approximately 2 hPa), separated mesopause located between 65-85 km in altitude, concentrated latitudinal and longitudinal extent of the temperature anomaly (synoptic scale) at the stratopause, and rapid development over the course of 2 to 5 days. The frequency and duration of USLM events in MetO showed them to be common wintertime events, frequently with episodes in the early winter. Tracking the geographic location of the stratopause thermal anomaly for all identified events showed a distinct preference for the longitude sector between 10°E and 110°E in both hemispheres. When the location of the polar vortex was overlaid on the thermal anomaly field, a strong correlation was implied between the polar vortex displaced off of the pole and the thermal anomaly located on the East side of the polar low, which is reminiscent the of a developing tropospheric front, amplifying by baroclinic instability.

Using the same methodology for identifying USLM events and building climatologies of these events, the Whole Atmosphere Community Climate Model *WACCM* version 4 was established to spontaneously and internally generate USLM disturbances that matched the observations and many of its phenomenological characteristics. Since WACCM satisfactorily reproduced USLM disturbances, the power of the model (such as the availability of vertical winds and extended vertical range) could be used to further interrogate the structure and dynamics of USLM disturbances.

Composites of USLM disturbances were constructed by aligning in space each thermal disturbance within a 10 latitude at an average longitude and correlating in time by the peak of each thermal disturbance at 2 hPa. Both MetO and WACCM composites showed coherent composite patterns with time by a strengthening of the Aleutian High, a displacement of the polar vortex off of the pole, and an increase of temperatures at the 2 hPa level. As the composite patterns dissipated, they became less coherent with larger statistical variances due to some of the events dissipating, others developing into minor SSWs and yet others developing into major SSWs.

Given the case study's indication of strong baroclinic conditions, vertical ageostrophic flow and structure suggestive of baroclinic instability, the composite USLM events were used to further elucidate the dynamical mechanisms responsible for the thermal structure observed in the USLM disturbances. The case study also indicated that planetary wave activity was intimately involved with the development of the USLM disturbance, and as wave transience is required for wave mean-flow interactions, both planetary wave amplification/decay and planetary wave breaking were investigated as potential energy sources. Although USLM disturbances are correlated with large amplitude planetary waves, it does not appear that planetary waves are being amplified as they propagate vertically through the stratosphere (although the amplitude of the wave does grow exponentially with height as the density of the atmosphere decays exponentially with height). An investigation of planetary wave breaking qualitatively and quantitatively indicated that planetary waves were breaking at a level just above the stratopause and depositing their momentum. An EP-flux analysis confirmed that planetary wave transience (breaking) through convergence of the EP-flux vector was occurring in this region. Convergence of EP-flux decelerates the eastward zonal-mean wind (by depositing westward momentum) and induces ageostrophic vertical motion to maintain mass continuity. Air below the breaking region descends and heats adiabatically while air above the breaking region rises and cools adiabatically. The descending air increases the horizontal temperature gradient at 2 hPa and is responsible for the stratopause warming.

Embedded in this planetary wave breaking process is the potential to support an instability. As the horizontal temperature gradient at 2 hPa is increased, the vertical shear is also increased through the thermal wind relation. However, merely having baroclinic conditions, vertical motion and vertical shear is not enough to indicate a baroclinic instability. The Charney-Stern criteria for baroclinic instability can be used to test whether a region of interest is able to support a baroclinic instability; the most relevant criteria is that associated with the reversals in the meridional gradient of quasi-geostrophic potential vorticity. Applying this analysis to the composite USLM events reveals the Charney-Stern criteria is indeed met in both the MetO and WACCM composites on the days surrounding the peak of the event.

A complication of using the Charney-Stern criteria to identify baroclinic instability may be that planetary wave breaking diagnostics also depend on gradients of potential vorticity, although strictly speaking quasi-geostrophic potential vorticity and Ertel's isentropic potential vorticity are not the same quantity. To disentangle baroclinic instability from planetary wave breaking, a case study was Fourier decomposed by wave number through fitting to a Fourier series. Low wave numbers (wave 1 and wave 2) are considered to be planetary waves, higher wave numbers (waves 3-7) are synoptic scale in the polar winter middle atmosphere; baroclinic instabilities are expected to be of synoptic scale. When analyzed using EP-flux it was seen that planetary wave breaking dominated the convergence in EP-flux early in the onset of the USLM event, but as the event progressed toward the peak of the event a significant portion of the convergence in EP-flux was contributed by the higher wave number synoptic scale features of the USLM event, again implicating the action of baroclinic instability in USLM events.

It is recognized that USLM events are part of a family of disturbances that occur in the polar winter middle atmosphere which have the potential to impact the entire atmospheric column. Some events are perceived to contribute or precondition the polar vortex for more stronger events. Relationships between USLM events, minor SSWs and major SSWs were examined and displayed through a Venn diagram which looked for events that were linked to each other (or not) by temporal evolution of the polar vortex within 14 days. Crucially, every identified major SSW (in both MetO and WACCM) were preceded by a USLM disturbance, indicating that USLM conditions are a necessary (but perhaps insufficient) condition for development of major SSWs. Additionally, identified minor SSWs consist of a variety of dynamical disturbances to the polar winter atmosphere, many which are not related to the development of major SSWs and may be poor indicators of whether a major SSW will subsequently develop.

Using the WACCM Venn diagram to identify relationships amongst these types of winter events, composites were created for different regions of the Venn diagram consisting of independent USLM events (not related to any minor or major SSW event that occurred), independent minor SSWs and USLM events that were related to an identified minor SSW event. The independent minor events (which did not develop into a major SSW) indicated that dynamical conditions could not support baroclinic instability. These independent, so-called 'minor' SSW events are dynamically divergent from the dynamical mechanisms responsible for major SSWs (and USLM events). The independent USLM disturbances supported baroclinic instability as the mechanism responsible for the formation of independent USLM events and are due to planetary wave breaking. Conditions that support baroclinic instability are essential for identifying and forecasting conditions that may develop into major SSWs.

Related phenomena give further insight into the consequences of USLM disturbances and potential similarities with the Upper Troposphere Lower Stratosphere (UTLS) region of the atmosphere. In conjunction with the stratopause warming at 42 km, a cooling in the mesosphere between 65 km and 85 km was observed in instrument observations (lidar, SABER) and the WACCM model. The composite event showed that the cooling developed several days in advance of the stratopause warming. The cooling is due to ascending and adiabatically cooling air that is obliged to move vertically due to the same breaking waves near 50 km that initiates the stratopause warming characteristic of USLM events. Mesospheric coolings are also observed in conjunction with major SSWs. As the planetary wave breaks below and the zonal wind properties are altered, propagation of gravity waves may also be altered and contribute to the cooling observed. Although true ‘fronts’ cannot be formed in the middle atmosphere due to the lack of a rigid lower boundary, ‘front-like’ conditions may develop in the stratopause region. Just as the UTLS may develop fronts with characteristic tropopause folds, case studies of USLM events indicate stratopause fold structures in the potential temperature surfaces, in conjunction with the identified baroclinic instability that exists near the stratopause. As air flows along these distorted potential temperature surfaces, gravity waves may be generated in-situ similarly to gravity waves generated by orography.

It should also be noted again that since baroclinic instability is active at the stratopause region and important for the evolution of the thermal structure and polar vortex, models wishing to produce an accurate representation of the middle atmosphere must be of sufficient horizontal resolution to capture baroclinic instability.

8.2 Future Work & Conclusion

The importance of planetary wave driven circulations to the dynamical evolution of the polar winter stratosphere raises several possibilities for extension of this work, particularly of USLM disturbances on other regions and phenomena in the atmosphere. Major SSWs have been shown to have influences reaching into the thermosphere and affecting the ionosphere; USLM events may also have impacts on these regions, although observational evidence have yet to be obtained. Studies of the forecast ability for major SSWs incorporating information about USLM may show additional usefulness of identifying USLMs and their embedded secondary instabilities. The wave-driven indirect circulation of USLM events may also redistribute chemical tracers and chemically active species that could impact studies of middle atmospheric chemistry. While this research established that USLMs are driven by planetary waves propagating from below, the types and genesis of these waves has not been examined. Lastly, given the multitude of interacting waves and tides in the middle atmosphere, generation, propagation, interaction and dissipation of waves involved with USLM events may also be a fruitful region of study for a deeper understanding of the structure and dynamics of disturbances to the polar winter vortex.

As more comprehensive observations and sophisticated models have allowed more detailed investigations of the middle atmosphere, it has become ever more apparent that this region is a dynamically active part of our atmosphere displaying its own ‘weather’ and coupling the troposphere to the outermost extensions of our atmosphere. This study aimed to orient USLM disturbances within the established classifications of polar winter middle atmospheric dynamical disturbances to the vortex and thermal structures. Its contribution to the field of aeronomy may help future research to improve the prediction of large scale polar vortex restructuring and its accompanying impacts on other atmospheric phenomena.

Bibliography

[1] J. T. Abatzoglou and G. Magnusdottir. Wave breaking along the stratospheric polar vortex as seen in era-40 data. Geophysical Research Letters, 34(L08812), 2007.

[2] D. R. Allen, R. M. Bevilacqua, G. E. Nedoluha, C. E. Randall, and G. L. Manney. Unusual stratospheric transport and mixing during the 2002 antarctic winter. Geophysical Research Letters, 30(1599), 2003.

[3] David G. Andrews, Conway B. Leovy, and James R. Holton. Middle Atmosphere Dynamics, Volume 40. Academic Press, October 1987.

[4] M. P. Baldwin and T. J. Dunkerton. Propagation of the arctic oscillation from the stratosphere to the troposphere. Journal of Geophyical Research, 104(D24):30937–30946, 1999.

[5] M. P. Baldwin, T. Hirooka, A. ONeill, and S. Yoden. Major stratospheric warming in the southern hemisphere in 2002: Dynamical aspects of the ozone hole split. SPARC Newsletter, 20:24–26, 2003.

[6] M. P. Baldwin and J. R. Holton. Climatology of the stratospheric polar vortex and planetary wave breaking. Journal of Atmospheric Science, 45:1124–1142, 1988.

[7] E. A. Barnes and D. L. Hartmann. Detection of rossby wave breaking and its response to shifts of the midlatitude jet with climate change. Journal of Geophysical Research, 117(D09117), 2012.

[8] P. Braesicke and U. Langematz. On the occurrence and evolution of extremely high temperatures at the polar winter straopause: A gcm study. Geophysical Research Letters, 27(10):1467–1470, 2000.

[9] N. Butchart, S. A. Clough, T. N. Palmer, and P. J. Trevelyan. Simulations of an observed stratospheric warming with quasigeostrophic refractive index as a model diagnostic. Quart. J. Roy. Meteor. Soc, 108:475–502, 1982.

[10] A. J Charlton and L. M Polvani. A new look at stratospheric sudden warmings. part i: Climatology and modeling benchmarks. Journal of Climate, 20(3):449–469, 2007.

[11] J. G. Charney and P. G. Drazin. Propagation of planetary-scale disturbances from the lower into the upper atmosphere. Journal of Geophysical Research, 66(1):83–109, 1961.

[12] J. G. Charney and M. E. Stern. On the stability of internal baroclinic jets in a rotating atmosphere. Journal of Atmosheric Science, 19:159–172, 1962.

[13] J. L. Chau, B. G. Fejer, and L. P. Goncharenko. Quiet variability of equatorial e b drifts during a sudden stratospheric warming event. Geophysical Research Letters, 36(L05101), 2009.

[14] K. Coughlin and L. J. Gray. A continuum of sudden stratospheric warmings. Journal of Atmosheric Science, 66:531–540, 2009.

[15] T. Davies, M. J. Cullen, A. J. Malcolm, M. H. Mawson, A. Staniforth, A. A. White, and N. Wood. A new dynamical core for the met office's global and regional modelling of the atmosphere. Quarterly Journal of the Royal Meteorological Society, 131:1759–1782, 2005.

[16] D. G. Dritschel and R. Saravanan. Three-dimensional quasigeostrophic contour dynamics, with an application to stratospheric vortex dynamics. Quarterly Journal of the Royal Meteorological Society, 120:1267–1298, 1994.

[17] T. J. Duck, J. A. Whiteway, and A. I. Carswell. Sudden stratospheric and stratopause warmings: observations of temperatures in the middle atmosphere above eureka. Geophysical Monographs Series, 123, 2000.

[18] P. R. Gent et al. The community climate system model version 4. Journal of Climate, 24:4973–4991, 2011.

[19] T. D. A. Fairlie, M. Fisher, and A. O'Neill. The development of narrow baroclinic zones and other small-scale structure in the stratosphere during simulated major warmings. Q. J. R. Meteorol. Soc., 116:287–315, 1990.

[20] Ben Foster. Thermosphere, Ionosphere, Electrodynamic General Circulation Models TIEGCM: A User's Guide to the Models and Post-processors. High Altitude Observatory: NCAR, 2009.

[21] R. R. Garcia, D. R. Marsh, D. E. Kinnison, B. A. Boville, and F. Sassi. Simulation of secular trends in the middle atmosphere 1950–2003. Journal of Geophysical Researh, 112(D09301), 2007.

[22] Adrian E. Gill. Atmosphere-Ocean Dynamics, Volume 30. Academic Press, December 1982.

[23] L. P. Goncharenko and S-R Zhang. Ionosphere signatures of sudden stratospheric warming: Ion temperature at middle latitude. Geophysical Research Letters, 35(L21103), 2008.

[24] K. Greer, J. P. Thayer, and V. L. Harvey. Winds and wave motions to 110 km at mid-latitudes. iii. response of mesospheric and thermospheric winds to major stratospheric warmings. Journal of Atmsopheric Science, 32:1676–1682, 1975.

[25] K. Greer, J. P. Thayer, and V. L. Harvey. A climatology of polar winter stratopause warmings and associated planetary wave breaking. Journal of Geophysical Research Atmospheres, 118:4168–4180, 2013.

[26] K. Greer, J. P. Thayer, V. L. Harvey, H.-L. Liu, E. Peck, and C. E. Randall. Waccm climotology of polar wintertime middle atmospheric disturbances. Journal of Geophysical Research Atmospheres, *in preparation.*

[27] A. Hannachi, D. Mitchell, L. Gray, and A. Charlton-Pere. On the use of geometric moments to examine the continuum of sudden stratospheric warmings. Journal of Atmospheric Science, 68:657–674, 2011.

[28] V. L. Harvey, R. B. Pierce, T. D. Fairlie, and M. H. Hitchman. A climatology of stratospheric polar vortices and anticyclones. Journal of Geophysical Research, 107(D20), 2002.

[29] M. H. Hitchman and A. S. Huesmann. A seasonal climatology of rossby wave breaking in the 320–2000 k layer. Journal of Atmospheric Science, 64:1922–1940, 2007.

[30] P. Hoffmann, W. Singer, and D. Keuer. Variability of the mesospheric wind field at middle and arctic latitudes in winter and its relation to stratospheric circulation disturbances. Journal of Atmospheric and Solar-Terrestrial Physics, 64:1229–1240, 2002.

[31] James R. Holton. The Dynamic Meteorology of the Stratosphere and Mesosphere. Meteorological Monographs Number 37 American Meteorological Society, 1975.

[32] James R. Holton. An Introduction to Dynamic Meteorology, Fourth Edition. Academic Press, 4 edition, 2004.

[33] B. J. Hoskins, I. Draghici, and H. C. Davies. A new look at the ω-equation. Quarterly Journal of the Royal Meteorological Society, 104(439):31–38, 1978.

[34] B. J. Hoskins, M. E. McIntyre, and A. W. Robertson. On the use and significance of isentropic potential vorticity maps. Quarterly Journal of the Royal Meteorological Society, 111:877–947, 1985.

[35] J. M. Russell III, M. G. Mlynczak, L. L. Gordley, C. J. Mertens, E. E. Remsberg, B. T. Marshall, G. Paxton, P. McMichael, J. G. Wells, M. Lopez-Puertas, et al. SABER experiment 2003 annual report. SPIE Conference on Optical Spectroscopic Techniques and Instrumentation for Atmsopheric and Space Research, 3, 1999.

[36] D. E. Kinnison and et al. Sensitivity of chemical tracers to meteorological parameters in the mozart-3 chemical transport model. Journal of Geophysical Research, 112(D20302), 2007.

[37] J. A. Knox and V. L. Harvey. Global climatology of inertial instability and rossby wave breaking in the stratosphere. Journal of Geophysical Research, 110, 2005.

[38] K. Krüger, B. Naujokat, and K. Labitzke. The unusual midwinter warming in the southern hemisphere stratosphere 2002: A comparison to northern hemisphere phenomen. Journal of Atmospheric Science, 62:603–613, 2005.

[39] Pijush K. Kundu and Ira M. Cohen. Fluid Mechanics with Multimedia DVD, Fourth Edition. Academic Press, 4 edition, 2010.

[40] K. Labitzke. Temperature changes in the mesosphere and stratosphere connected with circulation changes in winter. Journal of Atmospheric Science, 29:756–766, 1972.

[41] Karin Labitzke. On the interannual variability of the middle stratosphere during the northern winters. Journal of the Meteorological Society of Japan, 60(1), 1982.

[42] S. J. Lin. A vertically lagrangian finite-volume dynamical core for global models. Monthly Weather Review, 132:2293–2307, 2004.

[43] R. S. Lindzen. Turbulence and stress owing to gravity wave and tidal breakdown. Journal of Geophysical Research, 86:9707–9714, 1981.

[44] H.-L. Liu and R. G. Roble. A study of a self-generated stratospheric sudden warming and its mesosphericlower thermospheric impacts using the coupled time-gcm/ccm3. Journal of Geophysical Research, 107(D23), 2002.

[45] H. L Liu and R. G. Roble. A study of a self-generated stratospheric sudden warming and its mesospheric–lower thermospheric impacts using the coupled TIME-GCM/CCM3. Journal of Geophysical Research, 107(D23):4695, 2002.

[46] A. C. Lorenc, S. P. Ballard, R. S. Bell, N. B. Ingleby, P. L. F. Andrews, D. M. Barker, J. R. Bray, A. M. Clayton, T. Dalby, D. Li, et al. The met. office global three-dimensional variational data assimilation scheme. Quarterly Journal of the Royal Meteorological Society, 126(570):2991–3012, 2000.

[47] A. C. Lorenc, R. S. Bell, and B. Macpherson. The meteorological office analysis correction data assimilation scheme. Quarterly Journal of the Royal Meteorological Society, 117:59–89, 1991.

[48] G. L. Manney. Simulation of the december 1998 stratospheric major warming. Geophysical Research Letters, 26(17):2733–2736, 1999.

[49] G. L. Manney. The evolution of the stratopause during the 2006 major warming: Satellite data and assimilated meteorological analyses. Journal of Geophysical Research, 113(D11115), 2008.

[50] G. L. Manney, R. W. Zurek, A. O'Neill, and R. Swinbank. On the motion of air through the stratospheric polar vortex. Journal of Atmospheric Sciences, 1994.

[51] Gloria L. Manney, Joseph L. Sabutis, Douglas R. Allen, William A. Lahoz, Adam A. Scaife, Cora E. Randall, Steven Pawson, Barbara Naujokat, and Richard Swinbank. Simulations of dynamics and transport during the september 2002 antarctic major warming. Journal of the Atmospheric Sciences, 62(3):690–707, March 2005.

[52] D. R. Marsh, R. R. Garcia, D. E. Kinnison, B. A. Boville, F. Sassi, S. C. Solomon, and K. Matthes. Modeling the whole atmosphere response to solar cycle changes in radiative and geomagnetic forcing. Journal of Geophysical Research, 112(D23306), 2007.

[53] T. Matsuno. A dynamical model of the stratospheric sudden warming. Journal of Atmospheric Sciences, 28:1479–1494, 1971.

[54] N. A. McFarlane. The effect of orographically excited wave drag on the general circulation of the lower stratosphere and troposphere. Journal of Atmospheric Science, 44:1775–1800, 1987.

[55] R. M. McInturff. Stratospheric warmings: Synoptic, dynamic and general-circulation aspects. NASA Ref. Publ., 1017, 1978.

[56] M. E. McIntyre and T. N. Palmer. Breaking waves in the stratosphere. Nature, 305:593–600, 1983.

[57] M. E. McIntyre and T. N. Palmer. A note on the general concept of wave breaking for rossby and gravity waves. Pure and Applied Geophysics, 123(6):964–975, 1985.

[58] Michael E. McIntyre. How well do we understand the dynamics of stratospheric warmings? Journal of the Meteorological Society of Japan, 60(1), 1982.

[59] J. W. Meriwether and A. J. Gerrard. Mesosphere inversion layers and stratosphere temperature enhancements. Review of Geophysics, 42(RG3003), 2004.

[60] H. K. Myrabø, C. S. Deehr, and B. Lybekk. Polar cap oh airglow rotational temperatures at the mesopuase during a stratospheric warming event. Planet. Space Sci., 32:853–856, 1984.

[61] B. Naujokat, K. Krger, K. Matthes, J. Hoffmann, M. Kunze, and K. Labitzke. The early major warming in december 2001 - exceptional? Geophysical Research Letters, 49(21), 2002.

[62] R. B. Neale, C-C Chen, A. Gettleman, P. Lauritzen, S. Park, D. Williamson, A. Conley, R. R. Garcia, D. Kinnison, J-F Lamarque, D. Marsh, M. Mills, Anne K. Smith, S. Tilmes, F. Vitt, P. Cameron-Smith, W. Collins, M. Iacono, R. Easter, Xiaohong Liu, and M. A. Taylor. Description of the NCAR community atmosphere model (CAM 5.0). NCAR Technical Note, 2010.

[63] K.P. Nielsen, C.S. Deehr, E. Raustein, Y. Gjessing, and F Sigernes. Polar oh-airglow temperature variations in the 87/88 winter. Physics and Chemistry of the Earth, Part C: Solar, Terrestrial & Planetary Science, 26:405–410, 2001.

[64] T. N. Palmer. Diagnostic study of a wavenumber-2 stratospheric sudden warming in a transformed eulerian-mean formalism. Journal of Amtospheric Science, 38:844–855, 1981.

[65] Joseph Pedlosky. The stability of currents in the atmosphere and the ocean: Part ii. Journal of Atmospheric Science, 21:342–353, 1964.

[66] Joseph Pedlosky. Geophysical Fluid Dynamics. Springer, 2nd edition, January 1990.

[67] Alan Plumb. On the three-dimensional propagation of stationary waves. Journal of Atmospheric Sciences, 42(3), 1985.

[68] A. G. Postel and M. H. Hitchman. A climatology of rossby wave breaking along the subtropical tropopause. Journal of Atmospheric Sciences, 56, 1999.

[69] E. E. Remsberg and et al. Assessment of the quality of the version 1.07 temperature-versus-pressure profiles of the middle atmosphere from timed/saber. Journal of Geophsyical Research, 113(D17101), 2008.

[70] J. H. Richter, F. Sassi, and R.R. Garcia. Toward a physically based gravity wave source parameterization in a general circulation model. Journal of Atmospheric Science, 67:136–156, 2010.

[71] Walter Robinson. The application of the Quasi-Geostrophic Eliassen-Palm flux to the analysis fo stratospheric data. Journal of Atmospheric Sciences, 43(10):1017–1024, 1986.

[72] K. H. Rosenlof and James R. Holton. Estimates of the stratospheric residual circulation using the downward control principle. Journal of Geophysical Research, 98(D6):10465–10479, 1993.

[73] Murry Salby, Fabrizio Sassi, Patrick Callaghan, Dong Wu, Philippe Keckhut, and Alain Hauchecorne. Mesospheric inversions and their relationship to planetary wave structure. Journal of Geophysical Research, 107(D4), 2002.

[74] F. Sanders and B. J. Hoskins. An easy method for estimation of q-vectors from weather maps. Weather Forecasting, 5:346–353, 1990.

[75] S. Sathishkumar, S. Sridharan, and C. Jacobi. Dynamical response of low-latitude middle atmosphere to major sudden stratospheric warming events. Journal of Atmospheric Solar–Terrestrial Physics, 71:857–865, 2009.

[76] R. Scherhag. Die explosionsartigen stratosphrenerwrmungen des sptwinters 1952. Berichte des Deutschen Wetterdienstes in der US-Zone 6, 38:51–63, 1952.

[77] Richard Scherhag. Stratospheric temerature changes and the associated changes in pressure distribution. Journal of Meteorology, 17(6), 1960.

[78] M. L. Schoeberl, L. R. Lait, P. A. Newman, and J. E. Rosenfield. The structure of the polar vortex. Journal of Geophysical Research, 97:7859textendash7882, 1992.

[79] A. Simmons. Baroclinic instability at the winter stratopause. Q.J.R. Meteorol. Soc., page 531–540, 1974.

[80] A. Simmons, M. Hortal, G. Kelly, A. McNally, A. Untch, and S. Uppal. Ecmwf analyses and forecasts of stratospheric winter polar vortex breakup: September 2002 in the southern hemisphere and related events. Journal of Atmospheric Science, page 668–689, 2005.

[81] A. K. Smith. Preconditioning for stratospheric sudden warmings: Sensitivity studies with a numerical model. Journal of Atmospheric Sciences, 49:1003–1019, 1992.

[82] C. Stan and D. M. Straus. Stratospheric predictability and sudden stratospheric warming events. Journal of Geophysical Research, 114(D12103), 2009.

[83] R. Swinbank and A. O'Neill. A stratosphere–troposphere data assimilation system. Monthly Weather Review, 122:686–702, 1994.

[84] J. P. Thayer, K. Greer, and V. L. Harvey. Front-like behavior in the arctic wintertime upper stratosphere and lower mesosphere. Journal of Geophysical Research, 115(D00N04), 2010.

[85] J. P. Thayer and J. M. Livingston. Observations of wintertime arctic mesosphere cooling associated with stratosphere baroclinic zones. Geophysical Research Letters, 35(18):L18803, 2008.

[86] J. P. Thayer, N. B. Nielsen, R. E. Warren, C. J. Heinselman, and J. Sohn. Rayleigh lidar system for middle atmosphere research in the arctic. Optical Engineering, 36(7):2045–2061, 1997.

[87] K. K. Tung and R. S. Lindzen. A theory of stationary long waves. part ii: Resonant rossby waves in the presence of realistic vertical shears. Monthly Weather Review, 107:735–750, 1979.

[88] Geoffrey K. Vallis. Atmospheric and Oceanic Fluid Dynamics: Fundamentals and Large-scale Circulation. Cambridge University Press, November 2006.

[89] C. Varotsos. The southern hemisphere ozone hole split in 2002. Environ. Sci. Pollut. Res., 9:375 – 376, 2002.

[90] U. von Zahn, J. Fiedler, B. Naujokat, U. Langematz, and K. Krüger. A note on record-high temperatures at the northern polar stratopause in winter 1997/98. Geophysical Research Letters, 25(22):4169 – 4172, 1998.

[91] R. L. Walterscheid, G. G. Sivjee, and R. G. Roble. Mesospheric and lower thermospheric manifestation of a stratospheric warming event over eureka. Geophysical Research Letters, 27:2897 2900, 2000.

[92] D. W. Waugh and D. G. Dritschel. Vertical structure of rossby wave breaking: Dependence on polar vortex vertical structure. Journal of Atmospheric Science, 56:2359–2375, 1999.

[93] D. W. Waugh and L. M. Polvani. Upward wave activity flux as a precursor to extreme stratospheric events and subsequent anomalous surface weather regimes. Journal of Climate, 17:3548–3554, 2004.

[94] D. W. Waugh and L. M. Polvani. Stratospheric polar vorticies. Geophysical Mongraph Series: The Stroapshere Dynamics Transport and Chemistry, 190(43), 2010.

[95] Charles Welch. The ozone hole: Atmosphere. http://www.theozonehole.com/atmosphere.htm, 2013.

[96] J. A. Whiteway and A. I. Carswell. Stratospheric polar vorticies. Rayleigh lidar observations of thermal structure and gravity wave activity in the high Arctic during a stratospheric warming, 51(21), 1994.

[97] C. Yamashita, H.-L. Liu, and X. Chu. Gravity wave variations during the 2009 stratospheric sudden warming as revealed by ecmwf-t799 and observations. Geophysical Research Letters, 37(L22806), 2010.

Appendix A

List of Symbols

Primed quantities (e.g. u', v', Φ') denote perturbations of atmospheric variables such as wind, temperature, and geopotential, while barred quantities (e.g. $\bar{u}, \bar{v}$), denote the zonal mean. Time means are indicated by $\langle\rangle$ (e.g. $\langle\bar{u}\rangle, \langle\bar{u}\rangle$)such as a time mean of the zonal mean wind and the time mean of the meridional mean wind.

a	Radius of the Earth
f	Coriolis parameter $= 2\Omega \sin\phi$
p	Pressure
q	Quasi-geostrophic potential vorticity
u	Zonal wind velocity
v	Meridional wind velocity
w	Vertical wind in log-pressure coordinates $w = \frac{dz}{dt}$
J	Diabatic heating rate
H	Scale height
N	Bouyancy frequency
R	Gas constant for dry air
S	Planetary zonal wavenumber
T	Temperature
V_g	Geostrophic wind vector

β	Variation of Coriolis parameter with latitude $\equiv \frac{\partial f}{\partial y}$
κ	Ratio of gas constant to specific at constant pressure
λ	Longitude
ρ	Density
σ	Standard atmospheric stability parameter$ORwavefreqency$
θ	Potential temperature
ϕ	Latitude
ψ	Streamfunction; $u = -\frac{\partial \psi}{\partial y}$, $v = \frac{\partial \psi}{\partial x}$
ω	Vertical wind velocity in isobaric coordinates $\equiv \frac{\partial p}{\partial t}$ or Angular frequency
Φ	Geopotential
Ω	Rotation rate of the Earth

Appendix B

Approximate Conversions of Vertical Coordinates

These are only approximate conversions between the different vertical coordinate systems used. The actual conversions depend on the exact temperature and pressure, which may vary from day to day. In addition, constant surfaces (of pressure, potential temperature, altitude) may not be parallel to each other, especially in front-like conditions.

Pressure [hPa]	**Theta [K]**	**Altitude [km]**
0.0014	10000	90
0.0021	9000	87
0.0032	8000	85
0.0050	7000	82
0.0077	6000	79
0.0134	5000	76
0.0200	4500	74
0.0300	4000	71
0.0530	3500	68
0.11	3000	63
0.16	2800	61
0.24	2600	58

Pressure [hPa]	**Theta** [K]	**Altitude** [km]
0.35	2400	55
0.53	2200	52
0.80	2000	49
0.95	1900	48
1.15	1800	46
1.39	1700	45
1.68	1600	43
2.04	1500	42
2.50	1400	40
3.06	1300	39
3.81	1200	37
4.86	1100	36
6.38	1000	34
8.71	900	32
12.4	800	29
18.8	700	27
23.8	650	25
30.8	600	23
40.6	550	22
54.7	500	20
63.5	475	19
73.9	450	18
86.8	425	17
104	400	16

Appendix C

Event Onset Dates in MetO

NH USLM

15-Dec-91
8-Jan-92
10-Mar-92
13-Dec-92
17-Feb-93
28-Dec-94
24-Jan-95
16-Feb-96
13-Mar-97
2-Feb-98
10-Nov-98
1-Dec-98
18-Feb-99
9-Mar-00
25-Nov-00
2-Dec-00
26-Jan-01
16-Feb-01
18-Dec-01
18-Jan-02
12-Feb-02
18-Dec-02
21-Mar-03
1-Jan-04
20-Feb-05
26-Nov-05
6-Dec-05
19-Dec-05
31-Dec-05
25-Jan-06
13-Dec-06
25-Dec-06
7-Jan-07
8-Feb-07
20-Feb-07
26-Dec-07
21-Jan-08
14-Feb-08
19-Feb-08
12-Mar-08
19-Jan-09
18-Nov-09
14-Jan-10
11-Dec-10
5-Jan-11
24-Dec-11
14-Jan-12

NH Minor SSW

11-Jan-92
3-Feb-92
10-Feb-92
19-Feb-92
17-Mar-92
19-Feb-93
30-Dec-93
7-Mar-94
25-Mar-94
27-Jan-95
22-Mar-95
30-Mar-95
27-Jan-96
17-Feb-96
26-Feb-96
8-Dec-97
19-Dec-97
7-Jan-98
1-Feb-98
18-Feb-98
5-Mar-98
27-Mar-98
14-Dec-98
23-Feb-99
26-Jan-00
3-Feb-00
8-Feb-00
14-Feb-00
29-Feb-00
11-Mar-00
20-Nov-00
11-Dec-00
19-Dec-00
30-Jan-01
17-Feb-01
23-Dec-01
22-Jan-02
13-Feb-02
29-Dec-02
15-Jan-03
1-Feb-03
12-Feb-03
6-Mar-03
30-Mar-03
19-Dec-03
22-Jan-04
2-Feb-05
22-Feb-05
9-Mar-05
28-Mar-05
3-Jan-06
9-Jan-06
5-Jan-07
4-Feb-07
21-Feb-07
23-Jan-08
6-Feb-08
13-Feb-08
14-Mar-08
22-Mar-08
21-Jan-09
10-Feb-09
15-Nov-09
21-Jan-10
17-Feb-10
26-Feb-10
14-Mar-10
22-Mar-10
31-Jan-11
16-Mar-11
12-Jan-12
14-Feb-12

NH Major SSW

22-Mar-92
15-Dec-98
25-Feb-99
20-Mar-00
11-Feb-01
29-Dec-01
17-Feb-02
5-Jan-04
12-Mar-05
21-Jan-06
24-Feb-07
22-Feb-08
14-Mar-08
24-Jan-09
10-Feb-09

SH USLM

26-Jul-92
3-Sep-92
28-Sep-92
3-Jul-96
29-Jul-96
9-Aug-96
22-Aug-97
16-Aug-01
17-May-02
11-Jun-02
26-Jun-02
8-Jul-02
20-Aug-02
13-Sep-02
24-Sep-02
5-Jun-04
18-Jul-04
20-Aug-04
8-Sep-04
27-Sep-04
5-Jun-05
17-Jul-05
1-Aug-05
17-Sep-05
5-Jul-07
12-Jul-07
16-Sep-07
25-Sep-08
28-Jun-10
18-Jul-10
13-Sep-10

SH Minor SSW

22-Sep-96
27-Sep-96
5-Aug-01
22-Aug-02
31-Aug-02
12-Sep-02
21-Sep-02
9-Aug-04
25-Sep-04
21-Sep-05
12-Jul-06
21-Jul-06
26-Jul-06
19-Sep-07
27-Sep-07

SH Major SSW

25-Sep-02